Technology Integration (Task 20) Aeroservoelastic Modeling and Design Studies (Subtask 15)

Part A

Evaluation of Aeroservoelastic Effects on Flutter and Dynamic Gust Response

WBS 2.1.15
Deliverable No. TI4D1502

September 30, 1999

Prepared for
NASA LaRC Research Center
Hampton, Virginia 23665

[redacted]D[redacted]E[redacted]E

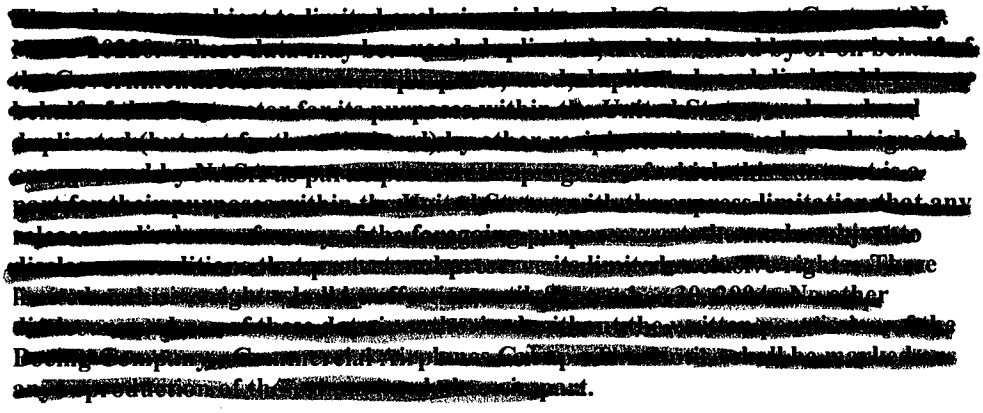

BOEING®

Task 20 - Technology Integration

Sub Task 15: Aeroservoelastic Modeling and Design Studies

Evaluation of Aeroservoelastic Effects on Flutter and Dynamic Gust Response

September 30, 1999

Prepared by: K.S. Nagaraja

MS 67-HW 234-0158

Prepared by: Raymond H Kraft

MS 6H-FA 965-2015

Reviewed by: Kumar G. Bhatia

MS 67-HL 965-0899

Reviewed by: Chris Borland

MS 6H-FK 965-0336

Approved by: Steven Precup

MS 67-HM 234-3171

Approved by Peter Radloff

MS 6H-FM 237-4038

BOEING®

Boeing Commercial Airplane Group
Technology and Product Development
P.O. Box 3707
Center
Seattle, Washington 98124-2207

Under Contract: NAS1-20220
Prepared for: National Aeronautics and Space Administration, Langley Research
Hampton, Virginia 23665-5225

Foreword

This document is being submitted to satisfy the deliverable "Aeroservoelastic Design Studies" for WBS 2.1.15.2 under the High Speed Research II – Airframe Technologies Contract NAS1-20220. The document reports work being performed for aeroservoelasticity (2.1.15) tasks under the Technology Integration (2.1) effort. Boeing personnel performed the analysis work reported in this document.

Acknowledgments

The following Aeroservoelasticity (ASE) Working Group members contributed to the work reported in this document:

William N Boyd
Kumar G Bhatia
Chris J Borland
Frode Engelsen
John Kim
Raymond H Kraft
Wei-Lin Li
K.S. Nagaraja
Steven R Precup
Steven C Stone
Payam Rowhani
Russ D Rausch
Skip Short
Eli Livine
Edward E Meyer
Larry Felt

William N. Boyd and Steven C Stone provided the modified DITS dynamic models and the reference open-loop flutter solutions for validation purposes.

[redacted]

Table of Contents

List of Figures

List of References

1. NASA Contract NAS1-20220 - Task Assignment No. 20, (NAS1-20220/RGB), Recv. 2/7/95.
2. Task 20 Subtask 7, DTF TI8004, Evaluation of Aeroservoelastic Effects on Dynamic Gust Response, December 23, 1998.
3. Task 20 Subtask 7, DTF 20-7-02, Evaluation of Aeroservoelastic Effects on Symmetric Flutter, March 31, 1998.
4. Task 28 Report - Design Integration Trade Studies, DTF28, September 30,1998,
5. Apex (Aeroelastic Program Executive) Boeing In-house Program.

1.0 Summary

The HSCT Flight Controls Group has developed longitudinal control laws, utilizing PTC aeroelastic flexible models to minimize aeroservoelastic interaction effects, for a number of flight conditions. The control law design process resulted in a higher order controller and utilized a large number of sensors distributed along the body for minimizing the flexibility effects. Processes were developed to implement these higher order control laws for performing the dynamic gust loads and flutter analyses. The processes and its validation were documented in Reference 2, for selected flight condition. The analytical results for additional flight conditions are presented in this document for further validation.

The conclusions based on this study are:

1) The common FEM model and common modal EOM for control law design, flutter and dynamic gust loads analyses have been used in an integrated fashion.

2) The control law design process using Multiple-Input Multiple-Output (MIMO) design strategy has been established.

3) The PSD gust loads using the modal approach correlated well with the ELFINI loads basis approach for the open loop system.

4) Reduction in responses at the pilot station is observed due to the active control system for the selected conditions.

5) The PSD gust loads analysis for three of the four selected conditions showed that the control laws reduced the gust loads on the wing. However, the loads increased on the fore body, aft body and on the horizontal tail due to increased activity of the active controls. The impact of the control laws on the overall loads (combined static and dynamic) on the design loads was not examined at this time.

6) The p-k based flutter analysis, frequency domain based PSD gust loads analysis and state-space based time domain loads analysis methods should be used concurrently for design verification and validation of control laws.

7) The closed loop differences between the eight lags Roger and P-transform models is relatively insignificant in comparison with the open loop responses.

As part of ASE methodology development and to support the ASE flutter model design, flutter analysis was performed to study the effect of mounting springs on flutter, for the TCA scaled airplane analytical model, in Langley TDT wind-tunnel conditions. The parameter sensitivities of the mounting springs revealed a 4.5 to 6.5 Hz spring mount flutter mode, in addition to the basic flutter mode of 18 Hz mode, for the tentatively selected nominal spring rate of 68 LB/in. The nominal mounting spring rate has been changed to 100 LB/in at this time to eliminate the presence of mount flutter mode mechanism.

The P-transform process used for the control law design was examined and compared with the traditional Rogers method. A summary of these findings is documented in this part of the report. A more complete description of the P-transform method is found in Part B of this report.

2.0 Introduction

This report presents work performed by The Boeing Company to satisfy the deliverable "Evaluation of Aeroservoelastic Effects on Dynamic Gust Response" for sub task 15 of Reference 1. The objective of this report is to present symmetric gust loads and response analysis methods, with control system included, developed under NASA HSR technical Integration Task 20 work. Also, the effects of control laws on the gust loads and flutter are presented for selected conditions of the PTC configuration. However, the primary goal has been to develop an improved modeling methodology for gust loads and flutter and then perform design studies that account for the aero-structures-systems interaction effects early in the design process.

During the early phases of the HSR II Program, it was recognized that the topic of Aeroservoelasticity (ASE) would be important to the successful development of an HSCT airplane. Aeroservoelasticity describes the interaction between the structure of a flexible aircraft, the aerodynamics, and the control system. In most aircraft development projects, although the aerodynamic/structural interactions (aeroelasticity) are considered as early as possible, the initial control system development design process does not use a fully dynamic structural representation of the aircraft. The usual representation is called Quasi-Static Aeroelastic (QSAE) which accounts for the static stiffness, but not the dynamic, characteristics. Often, control system "fixes" need to be accomplished at later stages of the design, sometimes after the initial vehicle design is complete. This process leads to additional expense, schedule delays, and high risk. Until 1997, the HSCT flight controls development was based on QSAE model.

Under the Technology Integration Task, efforts were undertaken to develop and evaluate the development of tools and methods which could be employed by all the affected disciplines to address ASE interactions, and use those tools and methods to examine the ASE effects on specific configurations under consideration. An ASE Working Group was established to address specific tool development and design study activities. The group concentrated on longitudinal control/symmetric flutter and gust loads interactions, control effects on lateral-directional control / antisymmetric flutter interactions and dynamic maneuver loads. The activities of the Working Group are described in this report.

The TCA configuration flight control laws (gamma-dot/V) were designed based on the rigid airplane dynamics (QSAE models) and using "mean axis ideal sensors" for the TCA configuration. Closed loop flutter analysis showed that the airplane flexibility would drastically destabilize the airplane in the entire speed spectrum. This was also confirmed by the flight controls ASE analysis process, utilizing the real sensors that had the dynamic structural modes feed back effects. These findings and the ASE method validations and descriptions were

published in the March 1998 Level IV report, "Evaluation of Aeroservoelastic Effects on Symmetric Flutter" (Reference 3). Also, the airplane flexibility effects were later observed in the lateral axis ASE flutter analyses while making the assessment of the p-beta control laws.

The above findings changed the direction of the control law design process and later effort was directed towards developing the control laws for pitch axis control and stability augmentation system using the flexible dynamic aeroelastic models and real sensors to reflect correct structural feedback effects. The control law design process used the Multiple-Input and Multiple-Output strategy known as Linear Quadratic Gaussian (LQG) regulation and estimation. Also, the effort was directed in developing processes using the common model approach and common equations of motion for control law design, flutter and dynamics gust loads analyses. These new processes were developed and validated using the dynamic aeroelastic models that became available for the PTC airplane configuration. The results for selected conditions were published in the 1998 Level IV report, " Evaluation of Aeroservoelastic Effects on Dynamic Gust Response" (Reference 2). The complexity of the higher order control laws led to extensive and detailed process validation across multiple disciplines including flutter, gust loads and flight controls. The processes utilized various software tools including Apex, Easy5_Mat, Matlab, Perl and Elfini. Method improvements were made to handle high order control laws and automate the control laws implementation into the p-k flutter and gust loads analyses. Also computation time reduction, by as much as 33% relative to traditional approach, was achieved while performing the flutter analysis. Results for several conditions showing further validation of the processes are presented in this report.

As part of ASE methodology development and to support the ASE flutter model design, flutter analysis was performed to study the effect of mounting springs and Mach number on flutter. The analysis was based on the TCA scaled airplane model in the TDT tunnel environment. Several observations were made during the investigation and these results are presented in this document.

One of many ways to generate aeroelastic models for use in control law design and dynamic gust loads is to use the P-transform method. This method transforms the frequency or k domain modal based open loop equations to s-domain equations. The control system can then be designed, based on the s-domain equations, to account for aeroelastic effects and minimize the adverse coupling between the structures and flight control system. This approach has been used for HSCT configurations for designing stability augmentation systems, structural mode control, and to improve handling and ride qualities of the airplane. However, the above process makes the basic assumption that the aeroelastic characteristics do not change by the inclusion of the augmentation systems. The validity of this assumption is examined and the results are

documented in this report. A more complete description of the P-transform method is given in Part B.

3.0 Approach

The control law design strategy used has been described in detail in Reference 2 for minimizing the structures/systems interaction effects. The methodology is extended to additional mass / flight conditions for further validations of processes used for multidisciplinary environment including flutter and dynamic gust loads. Additional improvements are made to the flutter process for minimizing the computational time required for closed loop analysis, by use of complex A,B,C,D matrices to generate the system transfer functions and eliminate the need for inverting the (sI-A) matrix in the iterative process. This process is described in Section 5.4.

APEX p-k flutter process was used to support the ASE model design, for evaluating the effect of mounting spring rates and Mach number on flutter characteristics of the ASM flutter model. This was done as part of the ASE methodology development. Some interesting trends were identified and these results are discussed in Section 8.3.

To evaluate the underlying assumption in the P-transform process use for control law design, the MATLAB tool is used to represent the EOM in state-space form by use of Rogers aerodynamic approximation and the P-transform process. The responses at the pilot station were calculated, using the two aero representations, for nominal control laws for a selected mass/flight condition. The two processes and the comparison between the two are presented in Section 5.1 and the p-transform process is described briefly in Appendix A.

4.0 Aeroelastic Models

Aeroelastic models developed for the PTC configuration are used for the control law design, flutter and dynamic gust loads analyses are described in Reference 4. The description of the Elfini based finite element model, the linear unsteady aerodynamic theories used for the aeroelastic analysis have been described in Reference 2. The math model utilized 60 flexible modes, 3 symmetric rigid body modes, and three partial rigid degrees of freedom for the canard, stabilizer and elevator rotation modes required for control system closed loop representation.

It may be noted that the PTC configuration has a critical flutter problem and the stiffness design closure was not established. PTC variant configurations were examined to improve the flutter stability of the airplane with minimum weight penalty. Therefore, the strength design model (PTSD) of Reference 3 is used to establish the gust loads analysis process and incorporate the control effects into

the analysis process. Four flight conditions are considered for establishing the analysis process. They are,

1) M=0.65 at an altitude of 35000' (Veas=208.56) for mass case M1 (light weight)
2) M=0.65 at an altitude of 35000' (Veas=208.56) for mass case MT1 (maximum weight, forward c.g.)
3) M=2.4 at an altitude of 66000' (Veas=365.64) for mass case M1 (light weight)
4) M=2.4 at an altitude of 66000' (Veas=365.64) for mass case MT1 (maximum weight, forward c.g.)

5 Control Law Design Process

Control law development efforts occurred in close cooperation with the HSCT Structures. The primary goal of this effort, as mentioned earlier in this report, was to validate analysis and design processes used by the Structures and Flight Controls communities.

As the main emphasis for this stage was not to provide a mature control law design, the development of a detailed set of control law requirements was postponed. The simplified control law design goals were:

1. Augment damping of structural modes, primarily low frequency.
2. Provide rigid body stability augmentation.
3. Provide flight path angle control performance comparable to current HSR baseline $\dot{\gamma}V$ design.[1]
4. Use only "real" sensors for feedback (i.e. no use of mean-axis sensors).
5. Ensure closed loop stability for high order, high fidelity, state-space vehicle representations.

5.1 State-Space Vehicle Models and Actuator Modeling

The first step in any control law design process is to develop a model of the system to be controlled. Flight Controls obtained Elfini file 41 data descriptions of the PTC vehicle for two mass cases (M1 and MT1) and two Mach numbers (Mach 0.65 and Mach 2.40). These four flight conditions and their designations are shown in Table 5.1.1. State space models for each of the

Flight Conditions			
Mass Case	Mach	Altitude	Designation
M1	0.65	35 kft	FA165
M1	2.40	66 kft	FA124
MT1	0.65	35 kft	FA865
MT1	2.40	66 kft	FA824

Table 5.1.1: Analyzed Flight Conditions

four flight conditions were developed and combined with simple third order actuator representations. The resulting vehicle plus actuator systems were then used for control law design. The previous release of this report in December of 1998 [2] described the results for only the FA865 flight condition. This report presents data for the remaining three flight conditions. Results are presented in Section 7.2 and Appendix A.1.

[1]The current $\dot{\gamma}V$ design is a combination of a QSAE control law providing stability augmentation and maneuver control, and a structural mode control law providing augmentation of flexible mode damping. This QSAE control law makes use of mean-axis sensor measurements.

Actuator Modeling

The symmetric FEM model data received from Structures contained eight (8) actuator degrees of freedom: stabilizer, elevator, canard, and the five right wing trailing edge surfaces (DTE6–10). The functional allocation for these surfaces currently being assumed is that the canard, elevator, and trailing edge surfaces are used to provide active structural damping, and that the stabilizer and canard are used for mean-axis stability augmentation and maneuver control. As such, the canard, elevator, and trailing edge surfaces are viewed as high bandwidth devices (fast actuators), and the stabilizer is viewed as a low bandwidth device (slow actuator). As described in Reference [2], simple, linear, third order actuator models were used.

Airframe Modeling

State-space models were generated for each of the four described flight conditions (see Table 5.1.1). The general process for creating these state space models involves the well known Roger Rational Function Approximation (RFA). This process is described in greater detail in Reference [2] and includes actuator modeling descriptions.

In an effort to minimize the order of the resulting control law (LQG control designs have as many states as the vehicle design model), design models were constructed for each of the four flight conditions using *no* additional lag states. This keeps the control law order at roughly twice the number of modes in the vehicle, but sacrifices accuracy. One of the findings of last years report was that great care needed to be taken when using these less accurate models for control design, else stability could be significantly compromised. There are several solutions to this dilemma of wanting low control law order and high model fidelity. One is to use a high order, high fidelity vehicle model, and reduce the control law order later. Another is to use a reduced order vehicle model to keep the control law order manageable.

A more high fidelity means of generating open loop vehicle models of low order is the P-transform method. The methodology was developed at McDonnell Douglas in the 1980's, and is based on the PK flutter solution process (see Appendix A.2). From the standpoint of capturing dynamic vehicle motions, models produced using the p-transform method have high accuracy open loop, and generally have acceptable accuracy closed loop[2]. In the open loop case, p-transform models exactly match the results of traditional PK flutter analysis. In the closed loop case, model accuracy is somewhat degraded, but appears more than adequate for most flight controls work.

Figure 5.1.1 depicts a comparison of 8-lag Roger and P-transform model accuracy in an open loop setting. This comparison was conducted for the Mach 0.65 MT1 flight condition at 35,000 feet. Note that lightly damped poles show excellent agreement, and more damped poles show still show very good agreement.

Figure 5.1.2 depicts a comparison of 8-lag Roger and P-transform model accuracy in a closed loop setting. This comparison was conducted for the same Mach 0.65 MT1 flight condition at 35,000 feet. The control law, in this case, was a very aggressive, LQG-derived γ controller using output feedback. Again, the lightly damped poles show reasonably good agreement, but the more

[2]The accuracy of the P-transform method for estimating dynamic loads is discussed in Part B.

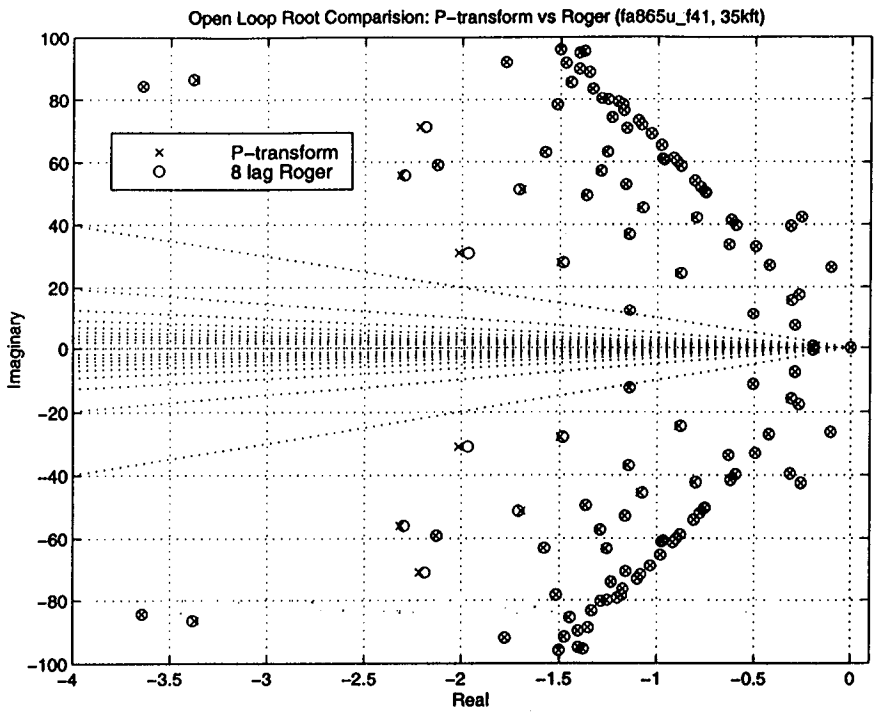

Figure 5.1.1: Open Loop Comparison: P-transform vs. 8-lag Roger Model

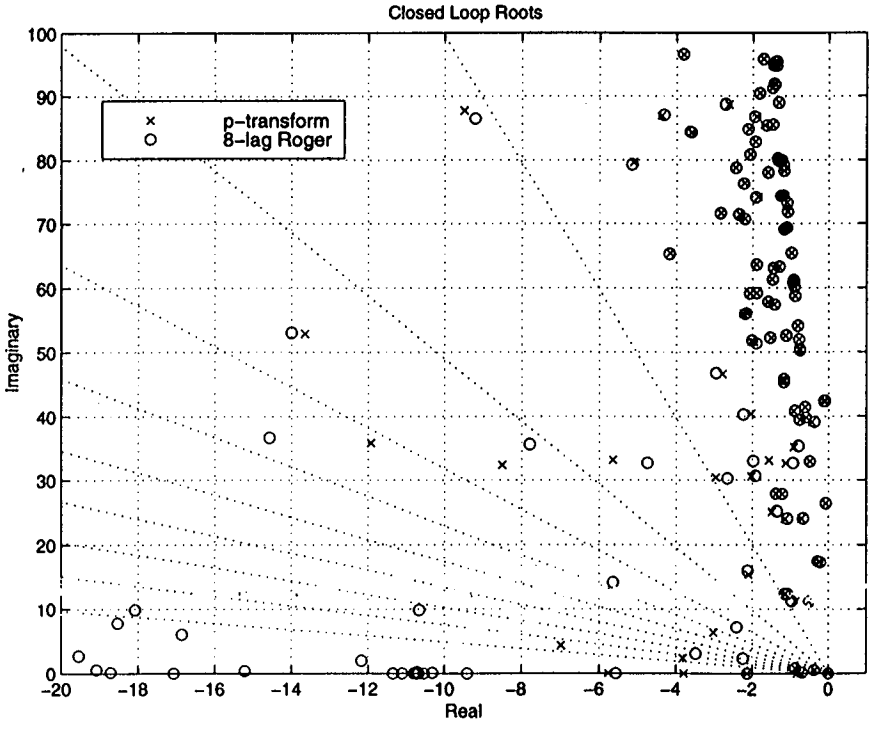

Figure 5.1.2: Open Loop Comparison: P-transform vs. 8-lag Roger Model

heavily damped poles are more suspect. As poles alone do not tell the entire story, it is valuable to also examine the frequency response. Figure 5.1.3 shows a closed loop frequency response comparison of the Roger and P-transform models. The open loop response is also shown to cast

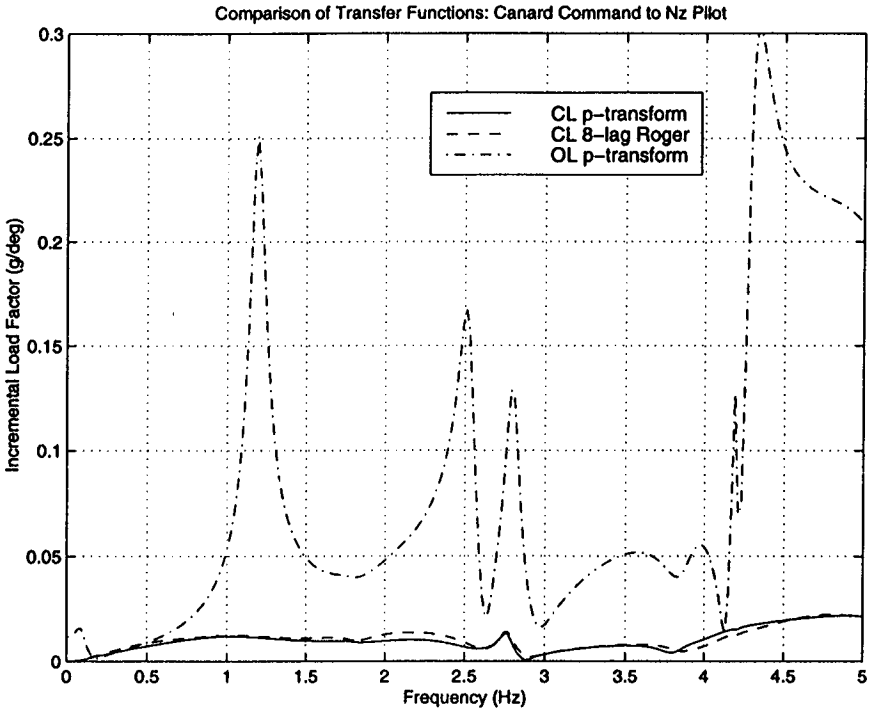

Figure 5.1.3: Open Loop Comparison: P-transform vs. 8-lag Roger Model

differences between the two closed loop responses into proper perspective. This frequency response is from canard command input to pilot station load factor. Comparing with the open loop response, it is clear that the control law is very effective at reducing modal excitation. Furthermore, in comparison with the open loop response, the closed loop differences between the 8 lag Roger and P-transform models is relatively insignificant.

5.2 Control Law Design Method: LQG

The control design methodology adopted in this report is a Linear Quadratic Gaussian (LQG) approach, and is identical to that reported previously in Reference [2]. The LQG control design consists of an "optimal" full state feedback regulator and an "optimal" state estimator. For further details on this control design approach, please see last year's report [2].

5.3 Control Law Diagonalization for Computational Efficiency

Any control law may be described by a set of state space equations as

$$\dot{x}_c = Ax_c + By \tag{5.1}$$

$$u = Cx_c + Dy, \tag{5.2}$$

where x_c are the nominal control states, y is the measurement vector, and u is the control law output.

Calculating the frequency response function for a high order control law involves computing the quantity

$$F(\omega) = C\left(j\omega I - A\right)^{-1} B + D. \tag{5.3}$$

For a high order control law, or for a large number of frequency evaluation points, the matrix inverse calculation in Eq.(5.3) can be costly. One approach for significantly reducing the computational burden of generating frequency response data is to diagonalize the control law. The matrix inverse in Eq.(5.3) then reduces to the trivial problem of n scalar inverse calculations, where n is the order of the control law.

The process for diagonalizing the control law and its system A matrix is to transform coordinates to the orthogonal normal modes given by the control law eigenvectors. In the event of repeated roots it will not be possible to fully diagonalize the control law, but computational savings can still be obtained by block diagonalizing the control law into a Jordan canonical form.

If the control law eigenvector matrix or Jordan form transformation is given by Φ, then the diagonalized control law may be written as

$$\dot{x}_{cd} = \Phi^{-1}A\Phi x_{cd} + \Phi^{-1}By \tag{5.4}$$

$$u = C\Phi x_{cd} + Dy. \tag{5.5}$$

The diagonal (or block diagonal) matrix $(j\omega - \Phi^{-1}A\Phi)$ is then much easier to invert than $(j\omega - A)$. It should be noted that the state-space descriptors of the diagonalized system are in general complex.

6.0 Flutter and Gust Loads Analysis Processes

The common model approach used for the present study is based on the CATIA FEM model and Elfini aeroelastic model described in earlier Section 4.0 of Reference 2. The aeroelastic models described in Section 4.0 and the control laws of Section 5.0 are used for incorporating the higher order control laws into the flutter analysis process. The analytical results would be used as a basis for validating the stability characteristics with the other tools. Also, the frequency response analysis results generated using the APEX analysis process (Reference 5) are used for correlation purposes. A summary of the approach and the equations solved are reported in Reference 2.

The open loop dynamic gust loads is based on the loads basis approach used in the Elfini aeroelasticity Module. This approach is selected so as to have a common basis with the static loads method. However, the common model modal approach is used for validation purposes, with other processes, as well as to assess the closed loop control effects, in the frequency and time domains, on dynamic gust loads. Reference 2 describes in detail the processes used for the gust analyses, continuous turbulence and discrete gust. The processes included Elfini loads basis approach, common model modal approach, the discrete gust analysis using FFT analysis and state-space analysis approach for open and closed loop systems.

7.0 Results

7.1 Validation Process

To ensure that various analysis processes use consistent aeroelastic models and control laws, frequency response analysis validation is carried out separately for each of the components such as structures/plant model, control laws plant model and then obtain overall loop transfer functions. This was done in detail for M=0.65, altitude=35000' condition. The various programs including APEX, EASY5_MAT and Elfini are used for this validation process. The implementation verification of the structures/plant validation and control laws was performed for the above condition and is reported in Reference 2. The correlation was found to be excellent. The process has not changed for other mass / flight conditions and therefore the comparisons were not performed.

Validation of the second order model and the force summation approach were performed in detail and the results are reported in Reference 2. The comparison verified that the common model approach using the modal basis and the force summation approach resulted in reliable results using a lesser number of elastic models.

7.2 Control Laws Performance Assessment

7.2.1 Open Loop Model Analysis

This section presents frequency response comparisons that illustrate the effect of certain model generation parameters. The key parameters that were varied were the number of retained structural degrees of freedom, and the number of aerodynamic lag states used in the RFA process.

Figures 7.2.1.1–7.2.1.3 depict the open loop frequency responses from commanded stabilizer, elevator, and canard, respectively, to vertical load factor response at the pilot station for mass case M1, Mach 0.65, and 35,000 feet. These responses incorporate the characteristics of the

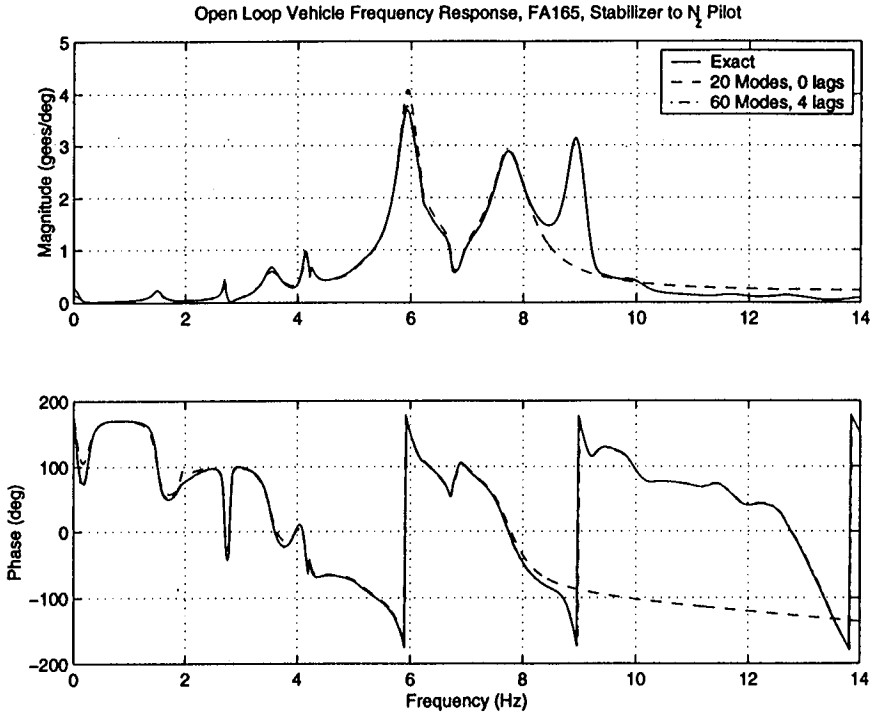

Figure 7.2.1.1: Open Loop Frequency Response, FA165, Stabilizer to N_z Pilot

third order actuator model. Results are shown for an "exact" solution, a 60 flexible mode 4 lag solution, and a 20 flexible mode 0 lag solution. The "exact" solution was constructed from purely frequency domain model analysis using linear interpolation of the unsteady aerodynamic data. The 60 mode 4 lag solution retained all the flexible modes included in the data from Structures, and used 4 aerodynamic lag states in the RFA process. Finally, the 20 mode 0 lag solution truncated all but 20 lowest frequency in-vacuo modes and used 0 lag states in the RFA process.

Overall, below roughly 7 Hz, there is good agreement between the 60 mode, 20 mode, and "exact" solutions, both in terms of magnitude and phase characteristics. Beyond 7 Hz, however, the 20 mode model begins to lose fidelity, but the 60 mode model continues to closely follow the "exact" solution.

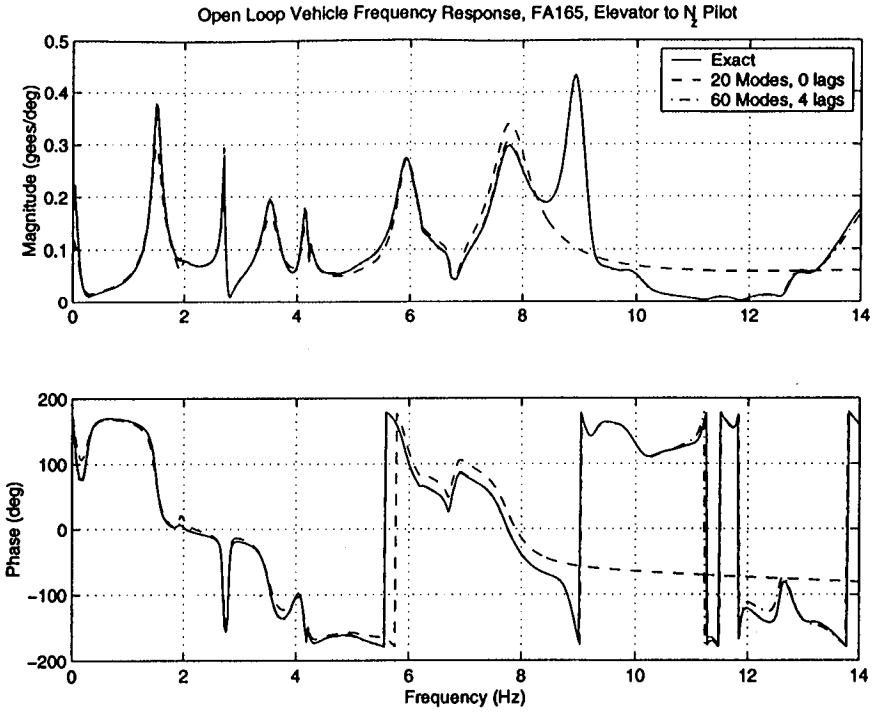

Figure 7.2.1.2: Open Loop Frequency Response, FA165, Elevator to N_z Pilot

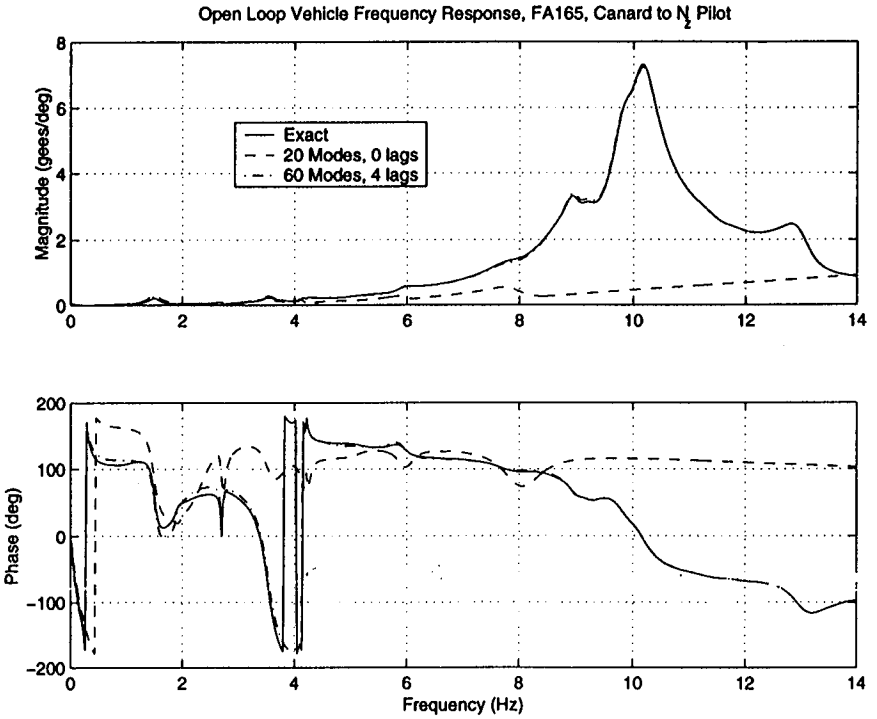

Figure 7.2.1.3: Open Loop Frequency Response, FA165, Canard to N_z Pilot

The agreement for the frequency response from the canard command input shows the greatest differences between the 20 and 60 mode representations. This is a nearly co-located transfer function that exhibits significant content due to inertial effects of the canard itself. These inertial effects, due largely to surface mass imbalance, result in the transfer function having a +2 slope, or +40 dB/dec, at high frequency. It is interesting to note that even for modes still included in the 20 mode model, there is a significant difference when compared with the 60 mode model[3].

Similar frequency response plots for the FA124 and FA824 flight conditions are shown in Appendix section A.1 in Figs. A.1.1–A.1.6.

7.2.2 Compensator Analysis

The LQG compensator defined by the optimal regular and optimal estimator designs[2] is a dynamic compensator. The compensators designed in this report use sensors located at 13 body centerline locations distributed from nose to tail. Specifically, the compensator uses the following sensors:

- 13 body centerline pitch rate sensors (q)
- 13 body centerline normal load factor sensors (N_z)
- 1 nominal center of mass altitude rate sensor ($\dot{h}_{\rm cm}$)
- 1 nominal center of mass altitude sensor ($h_{\rm cm}$)
- 9 control surface sensors (position, rate, and acceleration for the canard, stabilizer, and elevator surfaces).

The surface positions, rates, and accelerations are assumed to be directly measurable, and are not estimated by the estimator. The output of the compensator are surface position commands to the canard, stabilizer, and elevator.

In many of the open loop vehicle frequency response plots shown in Figs.7.2.1.1–7.2.1.3 and A.1.1–A.1.6, magnitude does not roll off with increasing frequency (some, in fact increase with frequency). In order to minimize the adverse affects of unmodeled high frequency dynamics and noise, it is important that the compensator assume an aggressive role in rolling off high frequency signal content.

Figures 7.2.2.1–7.2.2.4 show the compensator frequency response from measured $q_{\rm nose}$, $N_{z_{\rm nose}}$, $\dot{h}_{\rm cm}$, and $h_{\rm cm}$ to commanded canard, stabilizer, and elevator for flight condition FA165. As is evident, the majority of the compensator dynamics are clustered in the relatively broad range of 1–10 Hz. Beyond 10 Hz, the transfer functions roll off at between 20 and 40 dB per decade, depending on the particular actuator and sensor. Figures A.1.7–A.1.14 in Appendix section A.1 show similar compensator frequency response results for the FA165 and FA824 flight conditions.

[3]At 6 Hz, which is below the cutoff point for the 20 mode model, there is roughly a factor of 2 discrepancy in magnitude between the 20 and 60 mode models

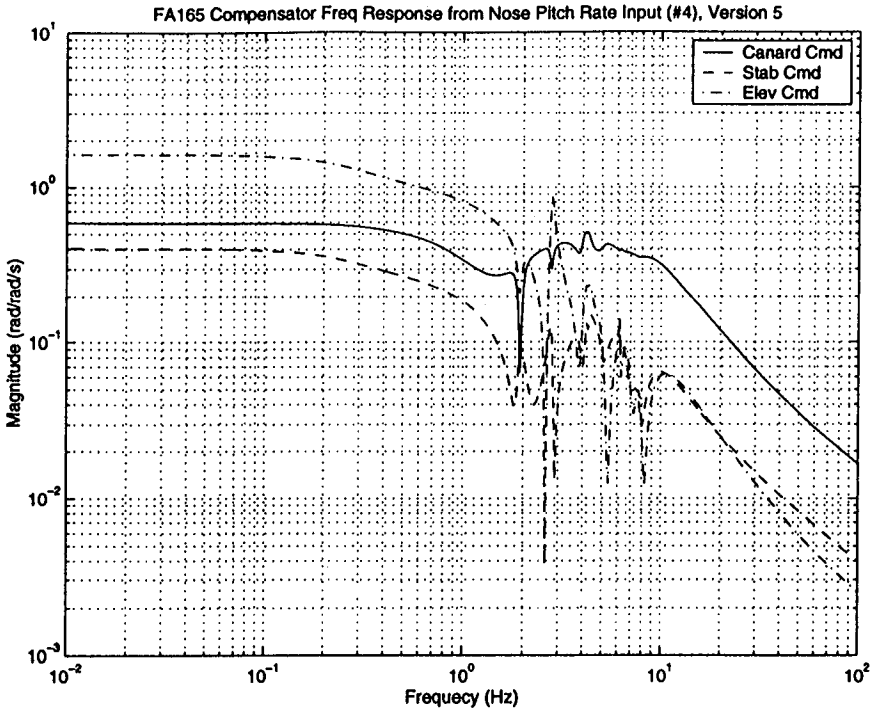

Figure 7.2.2.1: FA165 Compensator Frequency Response: Nose Pitch Rate Input (#4)

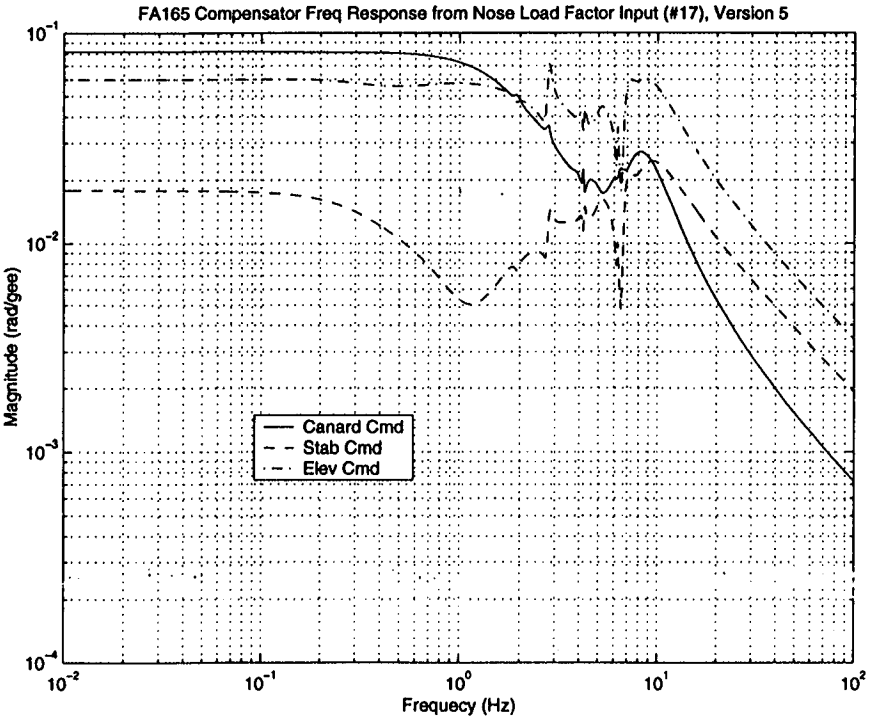

Figure 7.2.2.2: FA165 Compensator Frequency Response: Nose Load Factor Input (#17)

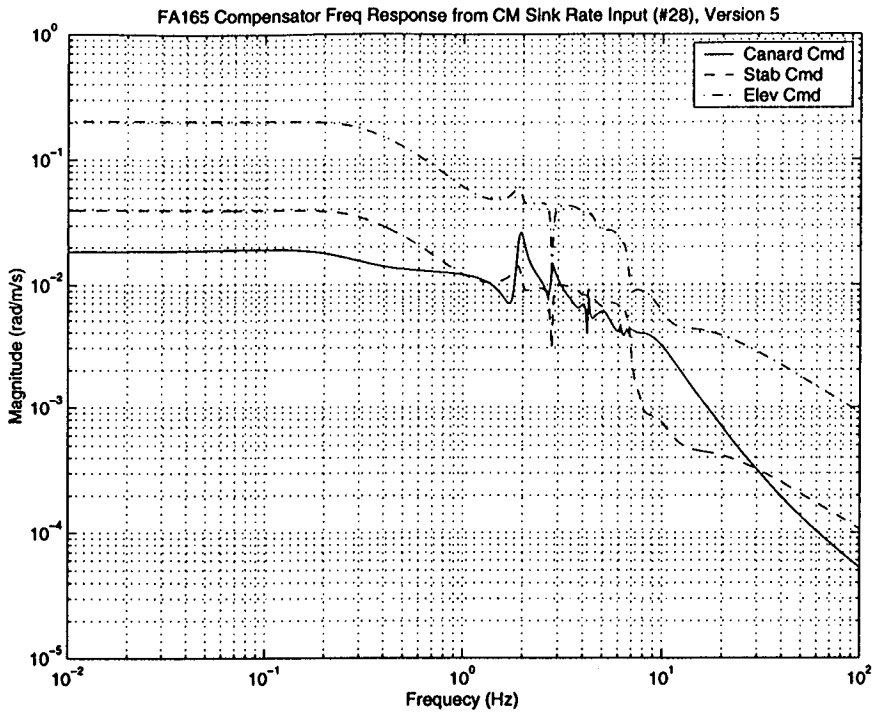

Figure 7.2.2.3: FA165 Compensator Frequency Response: CM Sink Rate Input (#28)

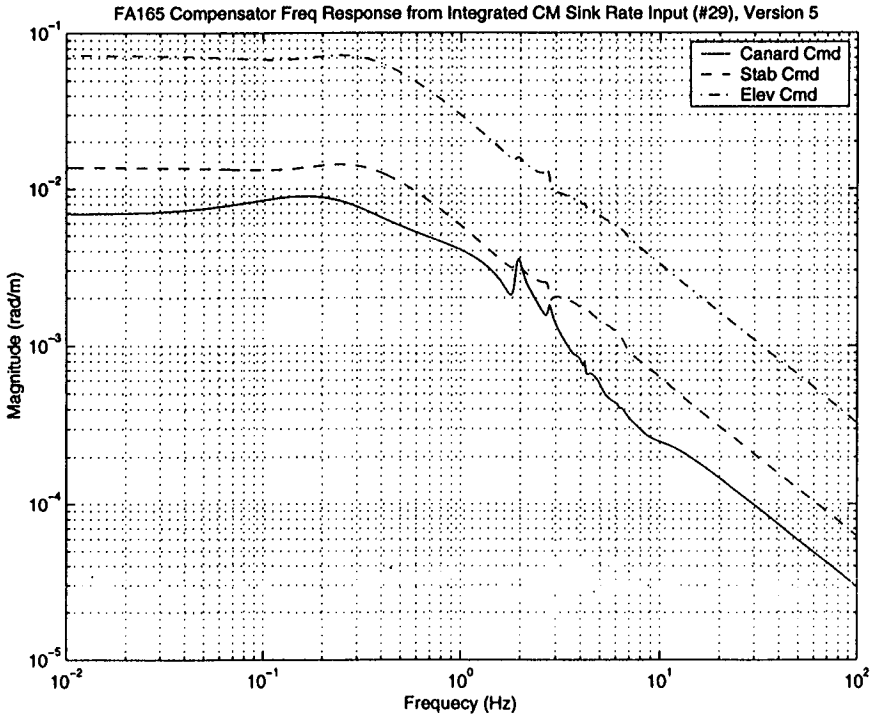

Figure 7.2.2.4: FA165 Compensator Frequency Response: Integrated CM Sink Rate Input (#29)

The results presented here are for version 5 of the control law design. An earlier design (version 3) is also referenced by other sections of this document. Time did not allow for investigating control law robustness to unmodeled dynamics and uncertainties in modeled dynamics, but such studies would most likely indicate that lower bandwidth and more aggressive roll off are desirable. Future control law design iterations will more thoroughly investigate robustness and aim at achieving more aggressive roll off and a lower bandwidth.

7.2.3 Closed Loop Analysis

As mentioned earlier, the 20 mode 0 lag vehicle model was used for control law design purposes in an effort to minimize controller order. By using this control law design to close a loop around the higher fidelity 60 mode 4 lag model, one effectively introduces unmodeled plant dynamics.

Figures 7.2.3.1–7.2.3.3 demonstrate the effectiveness of the control design in suppressing structural mode excitation for the M1, Mach 0.65, 35,000 ft flight condition. For the most part the

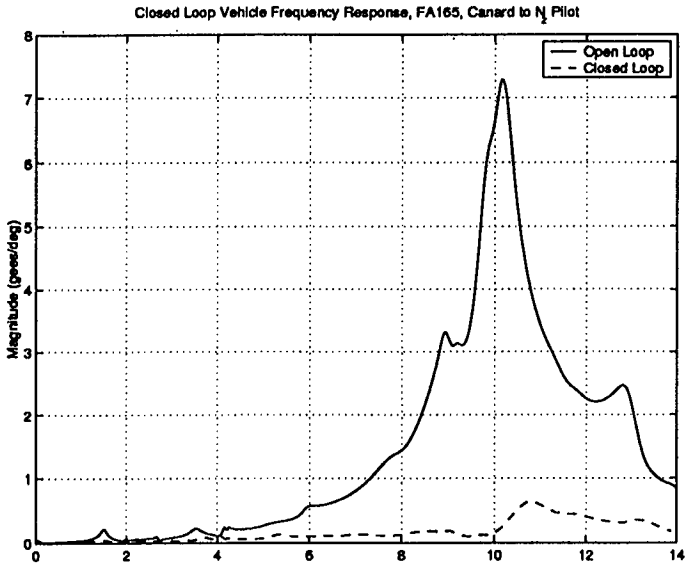

Figure 7.2.3.1: FA165 Closed Loop Frequency Response from Canard to N_z Pilot

control law significantly reduces structural mode excitation across the frequency spectrum. There are, however, some areas exhibiting slight modal accentuation, but this is not felt to be significant.

It is noteworthy that the computational time required to generate the frequency response results for the FA165 flight condition using the 60 mode 4 lag Roger model plus control law was roughly an order of magnitude longer than that required for the p-transform results shown in Section 5.1. The Roger results involved frequency response generation for roughly a 380th order system (360th order vehicle model, 20th order control law), whereas the p-transform results involved roughly a 120th order system (60th order vehicle mode, 60th order control law). Additional closed loop frequency response plots for the FA165 and FA824 flight conditions are shown in Appendix section A.1 in Figs. A.1.15–A.1.20.

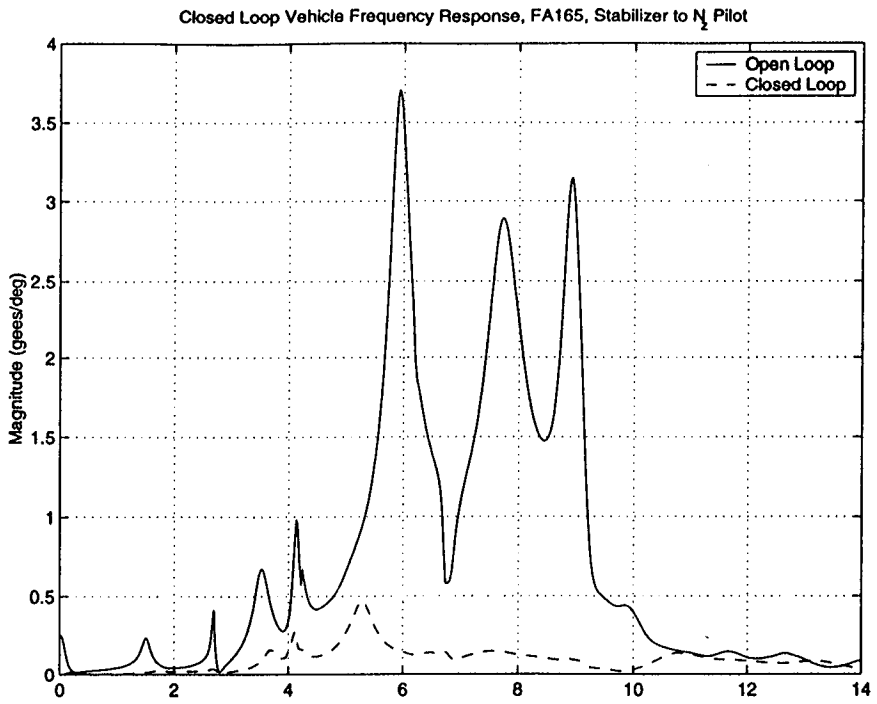

Figure 7.2.3.2: FA165 Closed Loop Frequency Response from Stabilizer to N_z Pilot

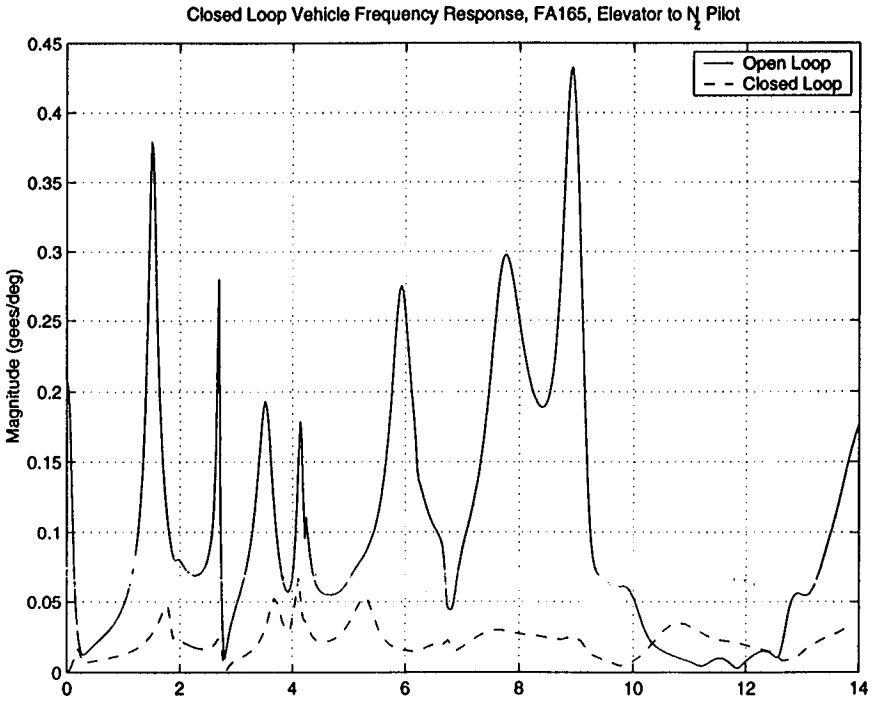

Figure 7.2.3.3: FA165 Closed Loop Frequency Response from Elevator to N_z Pilot

7.3 Flutter Analysis Results

APEX p-k flutter analyses were performed for the Mach/mass conditions considered in Section 4.0. The open loop results are documented in Reference 2 for various Mach/mass conditions and are also included in Appendix C of this document.

The present effort is focused on establishing the process to implement higher order control laws into the p-k flutter analysis. Also, it should be noted that the control laws are point designed for specific flight condition. However, the p-k flutter analysis can be used to identify the flutter sensitivity due to speed and other control law variables such as gain and phase. The control laws implementation into the APEX process was first established by validation with other analysis processes (loads and controls). Several versions of control laws were then made available in an effort to improve the control laws performance and also minimize its impact on structural responses. Therefore, the match point p-k flutter analysis was performed using the control laws of version 3 and 5. The closed loop flutter solution is shown in Figures 7.3.1 to 7.3.4 for version 5 control laws and the flutter results are included in Appendix B for the version 3 control laws. The results show that the elastic modes exhibit flutter stability up to 10 Hz for nominal gain for version 5 control laws of conditions 2,3 and 4. However, 9.8 Hz and 1.9 Hz flutter instabilities were observed for condition 1 (M=0.65, altitude=35k, mass M1). Further evaluation of the control laws including the gain and phase margin determination at various speeds has not been done at this time.

The present analytical results show that the low frequency modes exhibited stability at nominal gain for many of the conditions analyzed as compared to the QSAE design based control laws of Reference 3. The study demonstrates that an adequate number of sensors combined with use of flexible models for control law design would reduce the interaction effects between the flexible structure and the control system.

The system transfer function for control laws implementation into the APEX p-k flutter process was initially based on the real A, B, C and D matrices generated by the MATLAB process. This required inversion of (sI-A) matrix during the iterative flutter process. The computational time required for a typical flutter analysis was significantly high. In order to eliminate the inversion process and hence reduce the computational time, Control law diagonalization was performed for generation of A, B, C and D matrices using the MATLAB process. This reduced the computational time for flutter by 33% (3.53 hours versus 5.26 hours on RS6000 workstation for a typical flutter analysis). However, this process improvement resulted in the use of complex matrices for A, B, C and D instead of real matrices and this has not been a problem. The comparison of results

between the two processes is shown in Figure 7.3.5 and the results are found to be essentially the same.

As part of ASE methodology development and to support the ASM flutter model design activities, flutter analysis was performed to study the effect of mounting springs on flutter for the TCA scaled airplane analytical model (based on NASTRAN FEM), in Langley TDT wind-tunnel conditions. The effects of model mount spring rate and Mach number on ASM flutter are summarized in Figure 7.3.6 for g=0.0 and 0.03 damping levels. The parameter sensitivities of the mounting springs (front and aft) revealed the following:

1) Two flutter mechanisms are identified for a nominal spring rate of 68 LB / in for front and aft mounts. They are 4.5 to 6.5 Hz spring mount flutter mode and 16 to 18 Hz basic flutter mode of primary interest.

2) The spring mount flutter mechanism is sensitive to the spring rates of the front and aft mounts.

3) The two flutter mechanisms are basically uncoupled and the basic flutter mechanism (18 Hz) is insensitive to the spring rates.

4) Unequal spring rates of the front and aft mount would alleviate the mount flutter instability.

5) The spring rates of 132 to 264 LB / in would shift the first wing elastic mode frequency by about 20% (from 12.3 Hz to 14.8 Hz) and the second elastic mode frequency by about 5% (from 14.6 Hz to 15.3 Hz). The effect of this on the ASE requirements need to be examined.

6) The spring mount mode appears to be more "q (dynamic pressure)" dependent based on this linear analysis at lower spring rates.

7) The basic flutter mode is highly sensitive to Mach number as expected and follows the trend of airplane analytical results.

Following the trends based on this analysis, the nominal mounting spring rate has been changed to 100 LB / in at this time.

7.4 Loads Analysis Results

7.4.1 ELFINI Loads Basis

This study has emphasized the process establishment for gust loads and not the real design. Only four conditions are analyzed to demonstrate the process and for future refinement. The results of Elfini loads basis method (open loop results) for the four selected conditions have been reported in Reference 2.

Also, the results for condition 1 (M=0.65, MT1) were used to correlate with the modal based common process, and good agreements are observed.

All the gust loads analysis results, relevant to the open loop analysis, are reported in Reference 2. The results include the frequency response functions of vertical shear, vertical bending moment and torsion, and the root-mean-square values, at the roots of main wing and horizontal stabilizer. Also, the span load distributions along the wing and horizontal stabilizer quarter chord and loads along the fuselage stations are reported in Reference 2. In general, MT1 mass configuration gives slightly higher load levels. Also, for the supersonic conditions significantly lower load levels are observed because of the lower gust level at higher altitude.

7.4.2 Closed Loop Effects on PSD Gust Loads

The control laws effects are identified by comparing the open and closed loop responses for the PSD gust loads using the second order models. Comparison of open loop versus closed loop transfer functions, power spectra and cumulative RMS values for the four flight conditions considered are included in Appendix C. Different control law versions (version 3 and 5) were used in an effort to minimize the adverse structures / control systems interaction effects and improve flutter stability characteristics. Version 5 control law was considered to give better control characteristics and possibly minimize the impact on structural responses. It should be noted that the results that have been generated for the four conditions have not been thoroughly understood at this time. Figures 7.4.2.1 through 7.4.2.12 show the maximum incremental loads, for the open and closed loop conditions of four mach / mass cases considered, integrated along the wing and stabilizer span and fuselage loads integrated along the stream wise axis. It is to be noted that the fuselage loads actually include the wing and stabilizer loads. The results show that wing loads were generally reduced for three of the four conditions and is attributed to the flight controls loop closure and resulting in higher damping and increased frequency of the short period pitch mode. However, fuselage loads and stabilizer loads in general are higher in the closed loop solution because of the active control action of the canard, stabilizer and elevator.

7.4.3 Discrete Gust Loads Analysis

Discrete gust loads have been calculated for two typical flight loads cases. The first is for Mach 0.65 at 35,000 ft altitude and the second is for Mach 2.40 at 66,000 ft for mass case MT1. Also, the effect of gust gradient length was evaluated and the envelopes for the integrated loads along the wing and stabilizer span and loads integrated along the fuselage in the stream wise direction have been calculated. These results along with detailed discussions have been presented in Reference 2. The comparison of the open versus

closed loop results reveal that closed loop wing loads are slightly lower than the open loop loads, but closed loop fuselage and stabilizer loads exceed the open loop results due to active control action.

8.0 Conclusions

This aeroservoelastic investigation has demonstrated the following:

1) The common FEM model and common modal EOM for control law design, flutter and dynamic gust loads analyses have been used in an integrated fashion.

2) The control law design process using Multiple-Input Multiple-Output (MIMO) design strategy has been established.

3) The PSD gust loads using the modal approach correlated well with the ELFINI loads basis approach for the open loop system.

4) Reduction in responses at the pilot station is observed due to the active control system for the selected conditions.

5) The PSD gust loads analysis for three of the four selected conditions showed that the control laws reduced the gust loads on the wing. However, the loads increased on the fore body, aft body and on the horizontal tail due to increased activity of the active controls. The impact of the control laws on the overall loads (combined static and dynamic) on the design loads was not examined at this time.

6) The p-k based flutter analysis, frequency domain based PSD gust loads analysis and state-space based time domain loads analysis methods should be used concurrently for design verification and validation of control laws.

7) The P-transform method appears to be an attractive method for generating low order vehicle models required for ASE control law design but should be used in addition to higher fidelity models.

9.0 Recommendations

1) Incorporate more stringent and realistic requirements in to the control design process such as frequency, damping, gain and phase margin requirements.

2) Evaluate the gust loads impact on the airplane design by quantifying the results and comparing gust loads results to the 2.5g maneuver design loads.

3) Apply the processes developed to the lateral/directional control system.

HSCT MODEL PTSD, SYMMETRIC FLUTTER ANALYSIS, M=0.65, MASS:M1
CLOSED LOOP SOLUTION, 44 STATES CONTROL LAW WITH 38 INPUT SENSORS, VER 5

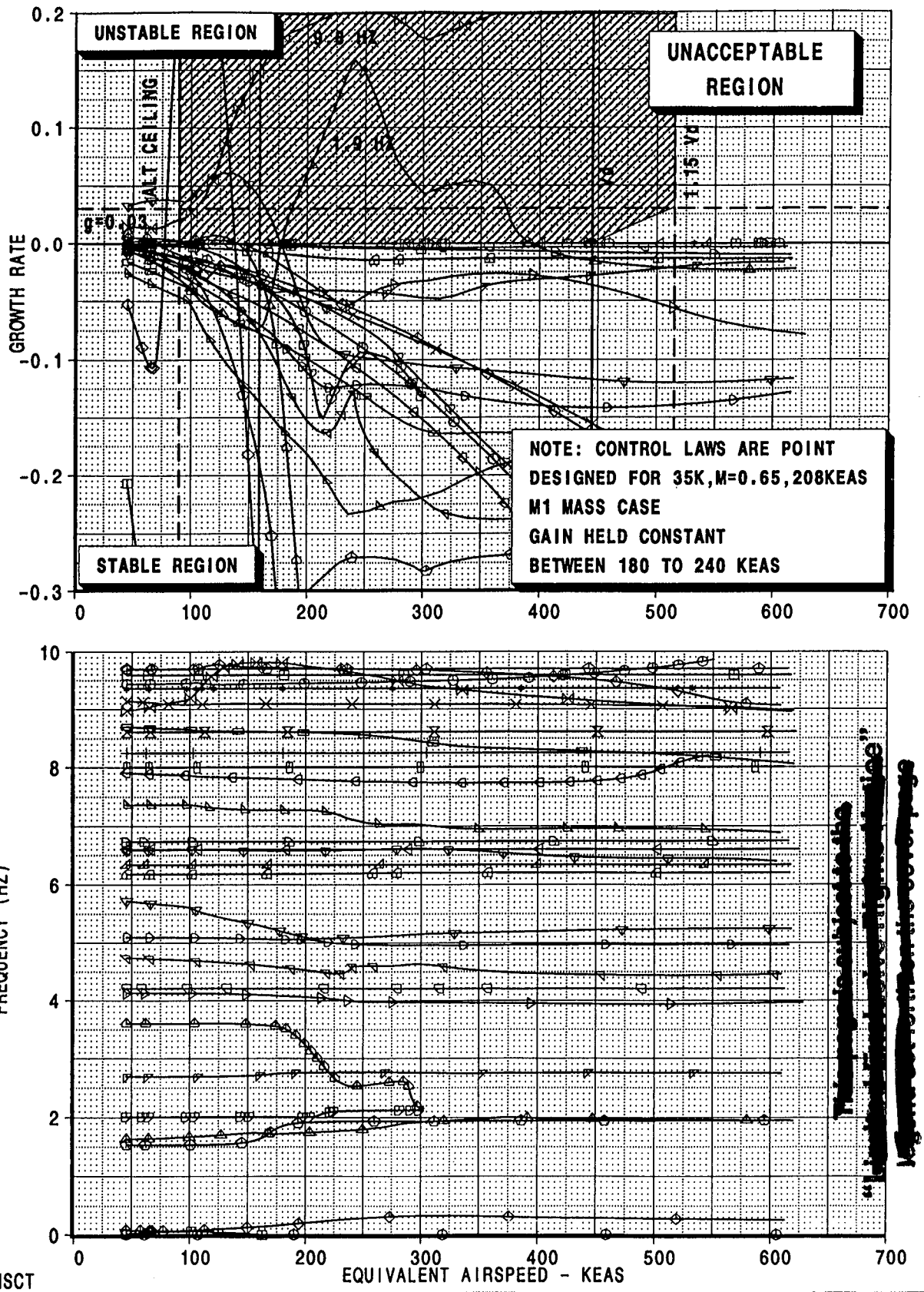

HSCT

CALC	K.S.NAGARAJA	24Jun99	REVISED	DATE	CLOSED LOOP SOLUTION STRENGTH SIZED AIRPLANE DITS MODEL PTSD	HSCT FIG 7.3.1
CHECK						
APPD.						
APPD.					BOEING	PAGE 24
PLOT						

[A]: /acct/ksn8042/ASE/PLOTS/VGPLOTS/mach65.esb
[B]: /acct/ksn8042/ASE/PTC/M65/M1/FLUTLP/COM/DOC1/CL5/IMPR/b865t5a6g5eC3x4_1_i1C1.esb
[C]: /acct/ksn8042/ASE/PTC/M65/M1/FLUTLP/COM/DOC1/CL5/IMPR/b865t5a6g5eC3x4_1_i1_10hzC1.esb

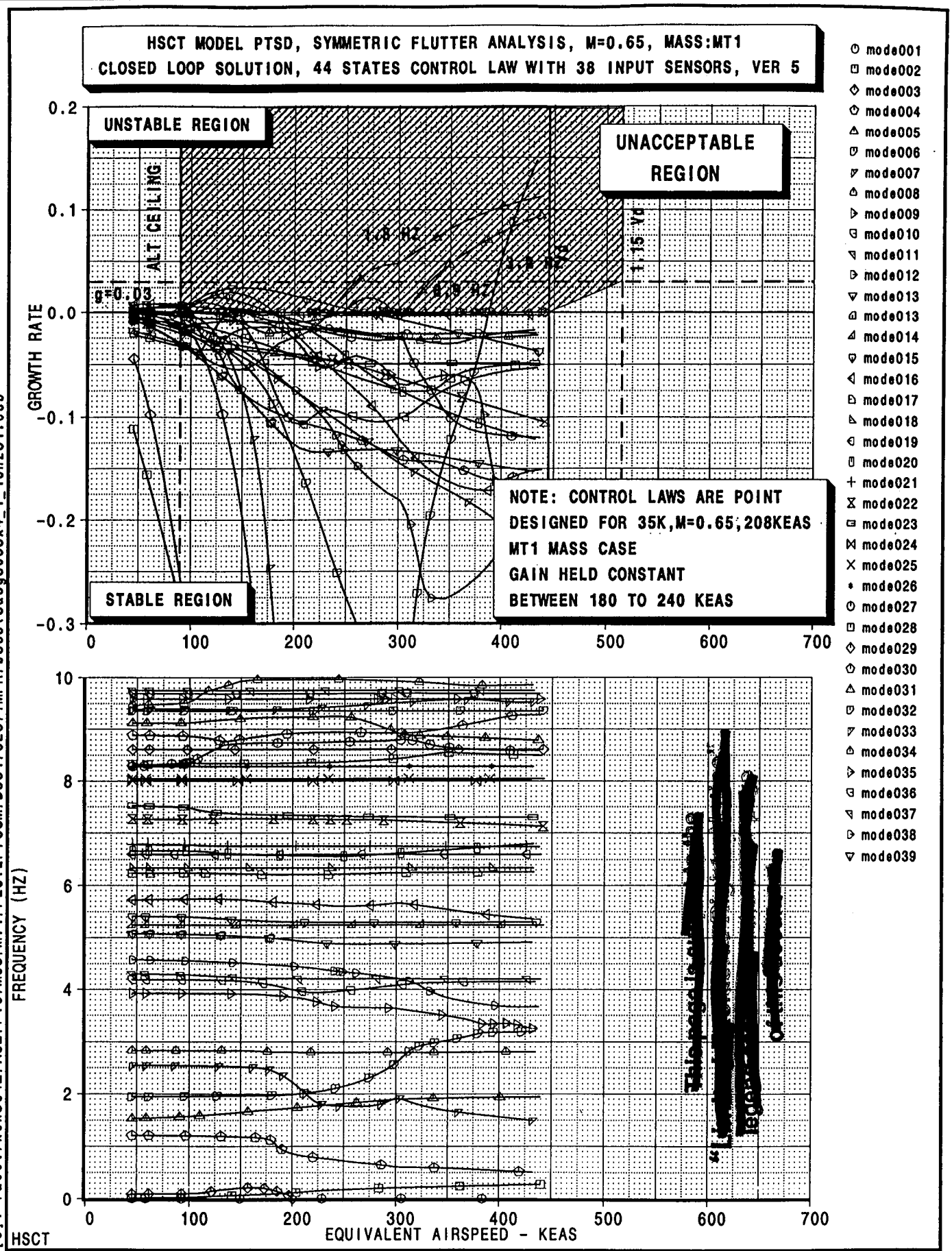

HSCT

[A]: /acct/ksn8042/ASE/PLOTS/VGPLOTS/mach65.esb
[B]: /acct/ksn8042/ASE/PTC/M65/MT1/FLUTLP/COM/DOC1/CL5/IMPR/b865t5a6g5eC3x4_1_i1C1.esb
[C]: /acct/ksn8042/ASE/PTC/M65/MT1/FLUTLP/COM/DOC1/CL5/IMPR/b865t5a6g5eC3x4_1_10hzC1.esb

CALC	K.S.NAGARAJA	24Jun99	REVISED	DATE	CLOSED LOOP SOLUTION STRENGTH SIZED AIRPLANE DITS MODEL PTSD	HSCT FIG 7.3.2
CHECK						
APPD.						
APPD.					BOEING	PAGE 25
PLOT						

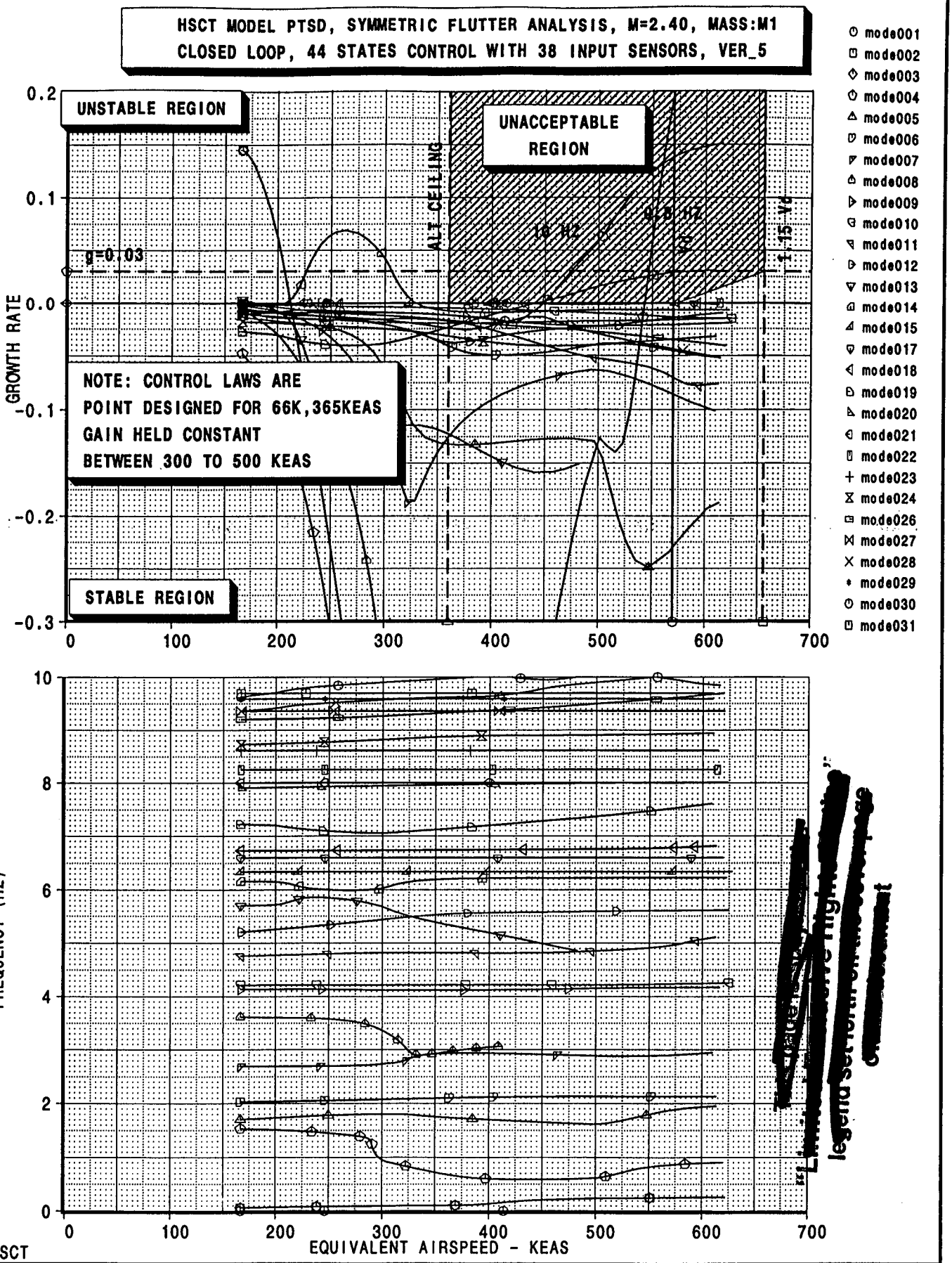

CALC	K.S.NAGARAJA	29Jun99	REVISED	DATE	CLOSED LOOP SOLUTION STRENGTH SIZED AIRPLANE DITS MODEL PTSD	HSCT FIG 7.3.3
CHECK						
APPD.						
APPD.					BOEING	PAGE 26
PLOT						

A]: /acct/k/ksn8042/ASE/PLOTS/VGPLOTS/mach26.esb
[B]: /acct/k/ksn8042/ASE/PTC/M24/M1/FLUTLP/COM/DOC1/CL5/IMPR/b86515a6g5eC3x4_1_i1C1.esb
[C]: /acct/k/ksn8042/ASE/PTC/M24/M1/FLUTLP/COM/DOC1/CL5/IMPR/b86515a6g5eC3z4_1_i1_10hzC1.esb

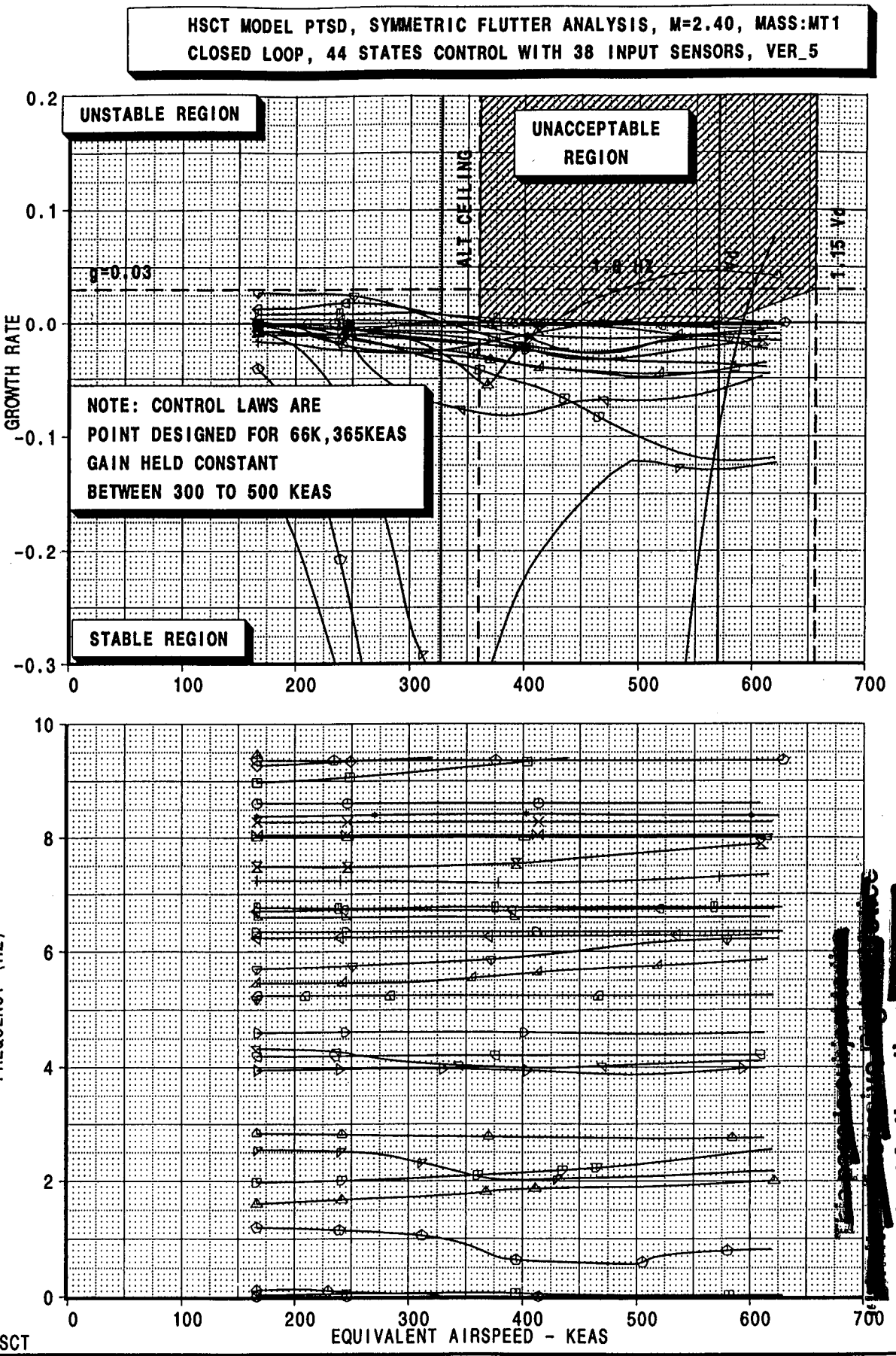

HSCT

CALC	K.S.NAGARAJA	29Jun99	REVISED	DATE	CLOSED LOOP SOLUTION STRENGTH SIZED AIRPLANE DITS MODEL PTSD	HSCT FIG 7.3.4
CHECK						
APPD.						
APPD.					BOEING	PAGE 27
PLOT						

A]: /acct/k/ksn8042/ASE/PLOTS/VGPLOTS/mach26.esb
[B]: /acct/k/ksn8042/ASE/PTC/M24/MT1/FLUTLP/COM/DOC1/CL5/IMPR/b865t5a6g5eC3x4_1_i1C1.esb
[C]: /acct/k/ksn8042/ASE/PTC/M24/MT1/FLUTLP/COM/DOC1/CL5/IMPR/b865t5a6g5eC3x4_1_i1_10hzC1.esb

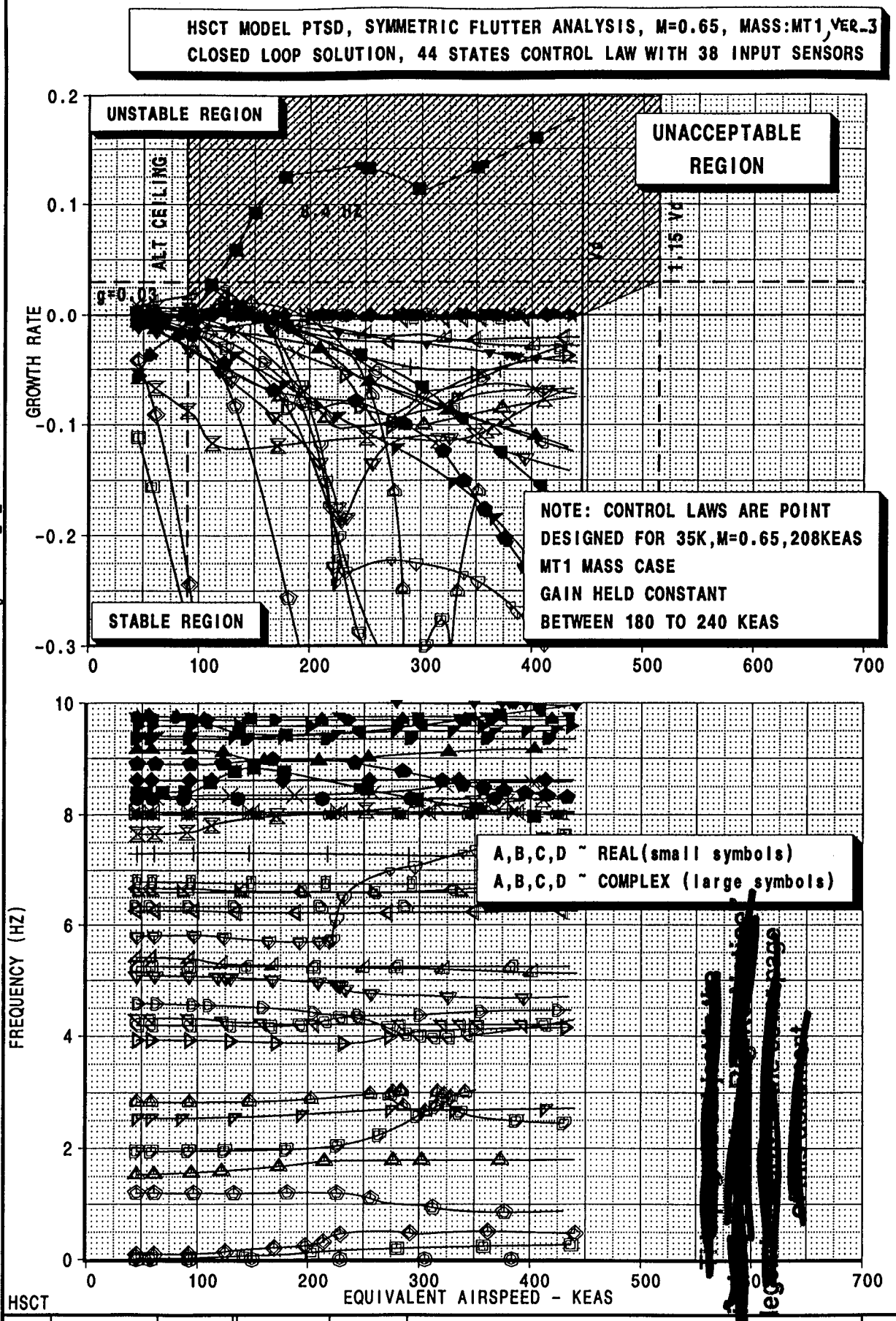

'C]: /acct/ksn8042/ASE/PTC/M65/MT1/FLUTLP/COM/DOC1/CL3/[illegible]R/b865t5a6g5eC3x4_1_i1C1.esb
.D]: /acct/ksn8042/ASE/PTC/M65/MT1/FLUTLP/COM/DOC1/CL3/[illegible]5a6g5eC3x4_2C1.esb
[E]: /acct/ksn8042/ASE/PTC/M65/MT1/FLUTLP/COM/DOC1/CL3/b865t5a6g5eC3x4_3C1.esb
[F]: /acct/ksn8042/ASE/PTC/M65/MT1/FLUTLP/COM/DOC1/CL3/IMPR/b865t5a6g5eC3x4_1_10hzC1.esb

CALC	K.S.NAGARAJA	10Jun99	REVISED	DATE	CLOSED LOOP SOLUTION STRENGTH SIZED AIRPLANE DITS MODEL PTSD	HSCT
CHECK						FIG 7.3.5
APPD.						
APPD.					BOEING	PAGE 28
PLOT						

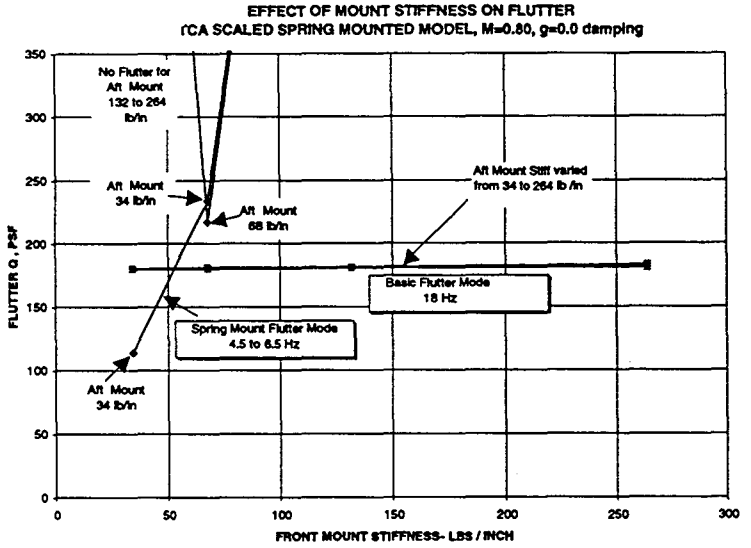

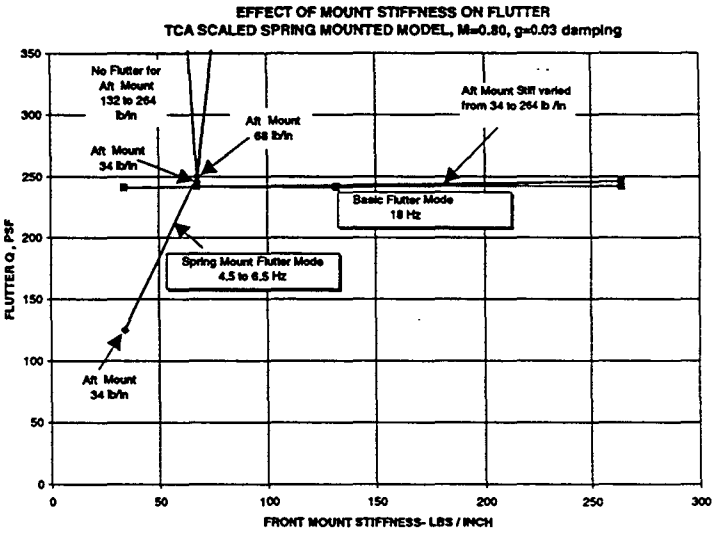

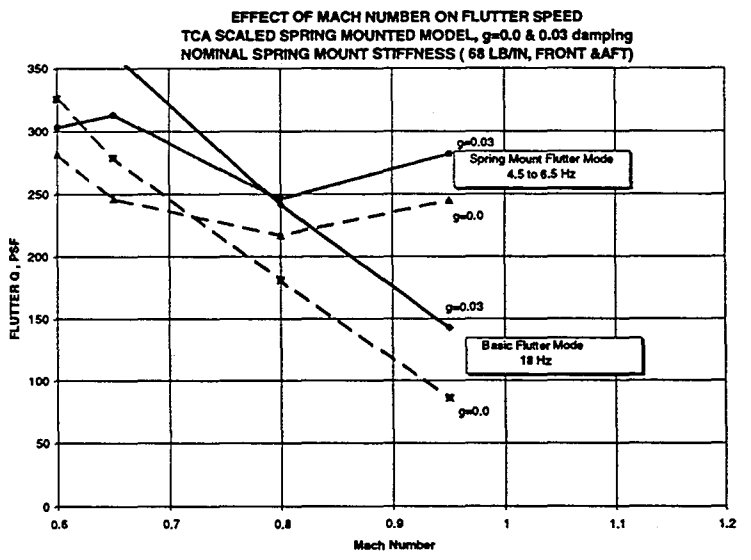

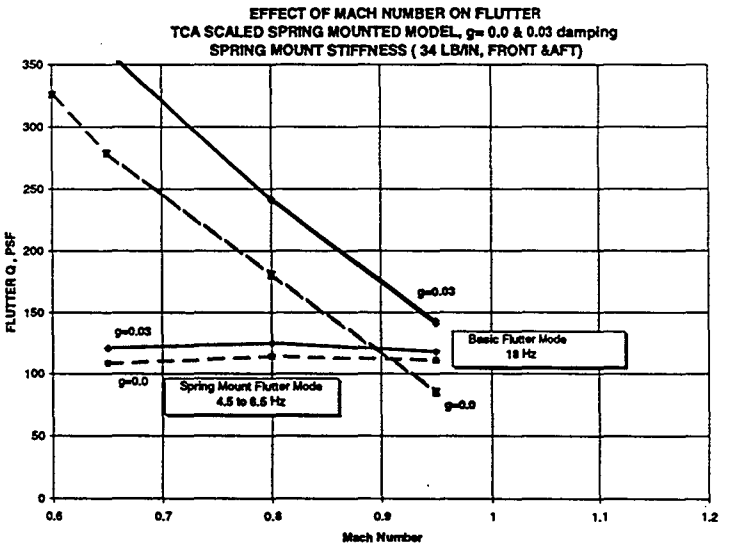

FIG 7.3.6 EFFECT OF MACH NUMBER AND MOUNT STIFFNESS ON FLUTTER
(TCA AIRPLANE SCALED SPRING MOUNTED MODEL)

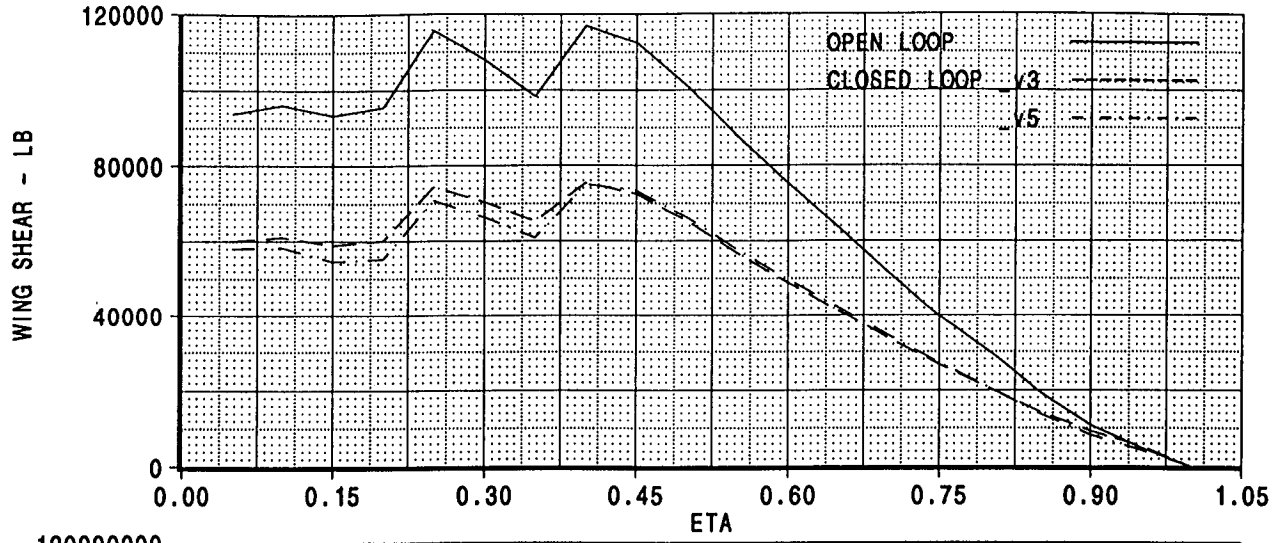

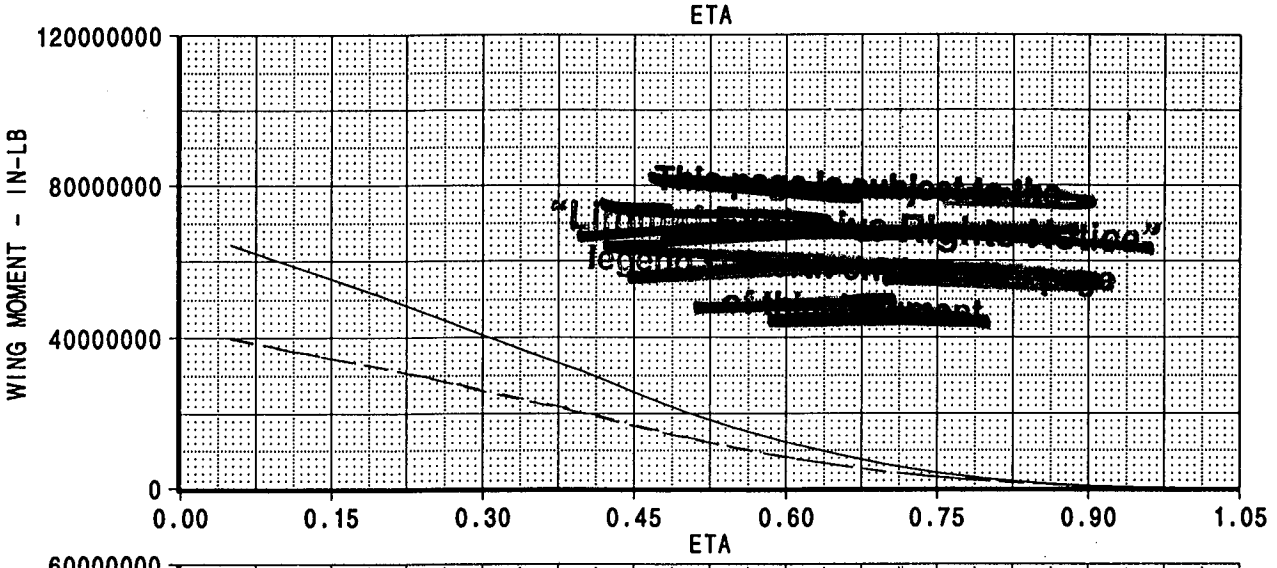

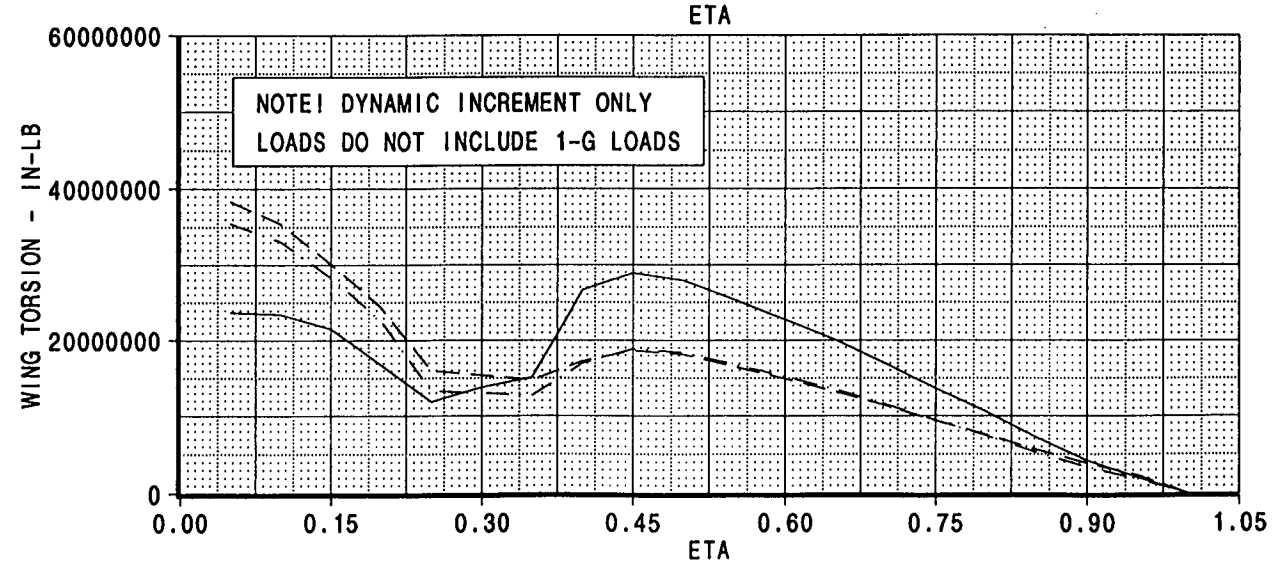

[A]: /acct/ksn8042/SOLVER/psd_gust_M1m0p65.esb
[B]: /acct/ksn8042/SOLVER/psd_gust_M1m0p65_fb.esb
[C]: /acct/ksn8042/SOLVER/psd_gust_M1m0p65_fb_v5.esb

CALC	K.S.NAGARAJA	23Jun99	REVISED	DATE	SYMMETRICAL VERTICAL PSD GUST CASE MODEL=PTSD MASS=M1 MACH=0.65 ALT=35K COMPARISON OPEN VERSUS CLOSED LOOP	HSCT
CHECK						FIG 7.4.2.1
APPD.						
APPD.					BOEING	PAGE 30

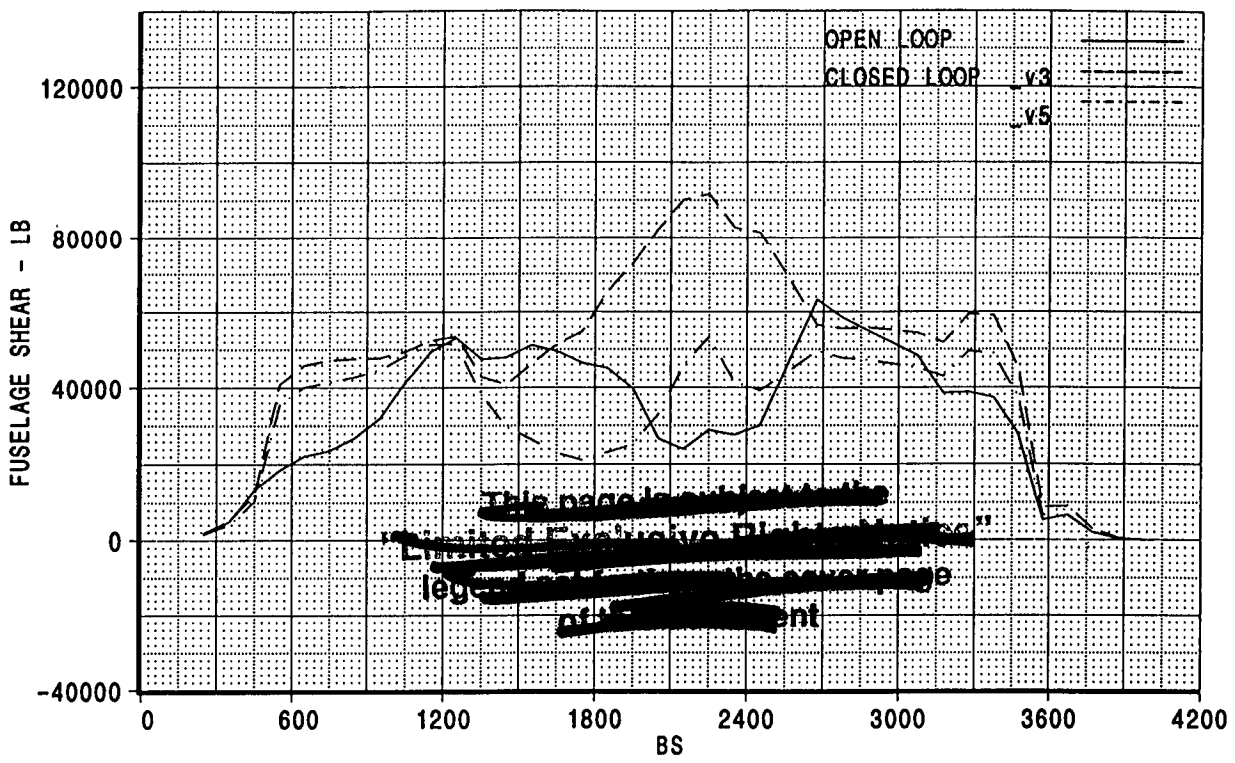

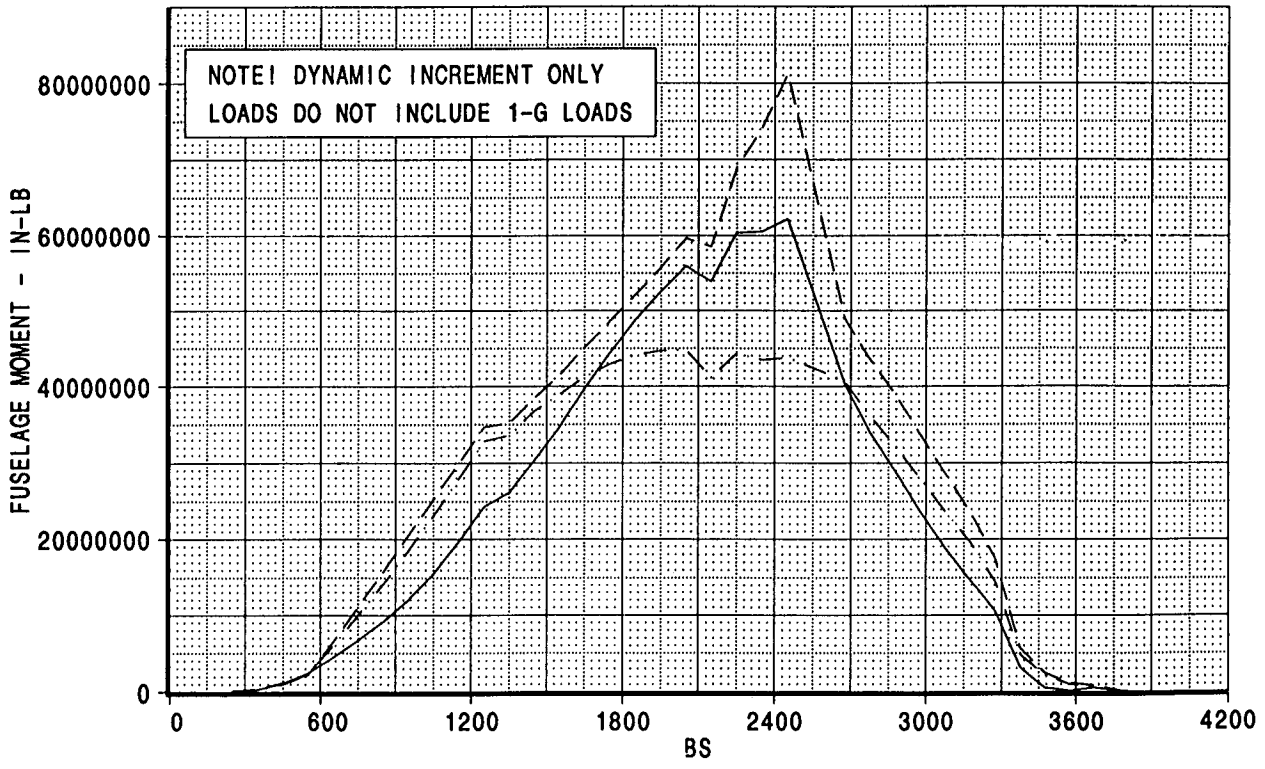

[A]: /acct/ksn8042/SOLVER/psd_gust_M1m0p65.esb
[B]: /acct/ksn8042/SOLVER/psd_gust_M1m0p65_fb.esb
[C]: /acct/ksn8042/SOLVER/psd_gust_M1m0p65_fb_v5.esb

CALC	K.S.NAGARAJA	23Jun99	REVISED	DATE	SYMMETRIC VERTICAL PSD GUST CASE MODEL=PTSD MASS=M1 MACH 0.65 ALT=35K COMPARISON OPEN VERSUS CLOSED LOOP	HSCT
CHECK						FIG 7.4.2.2
APPD.						
APPD.					BOEING	PAGE 31

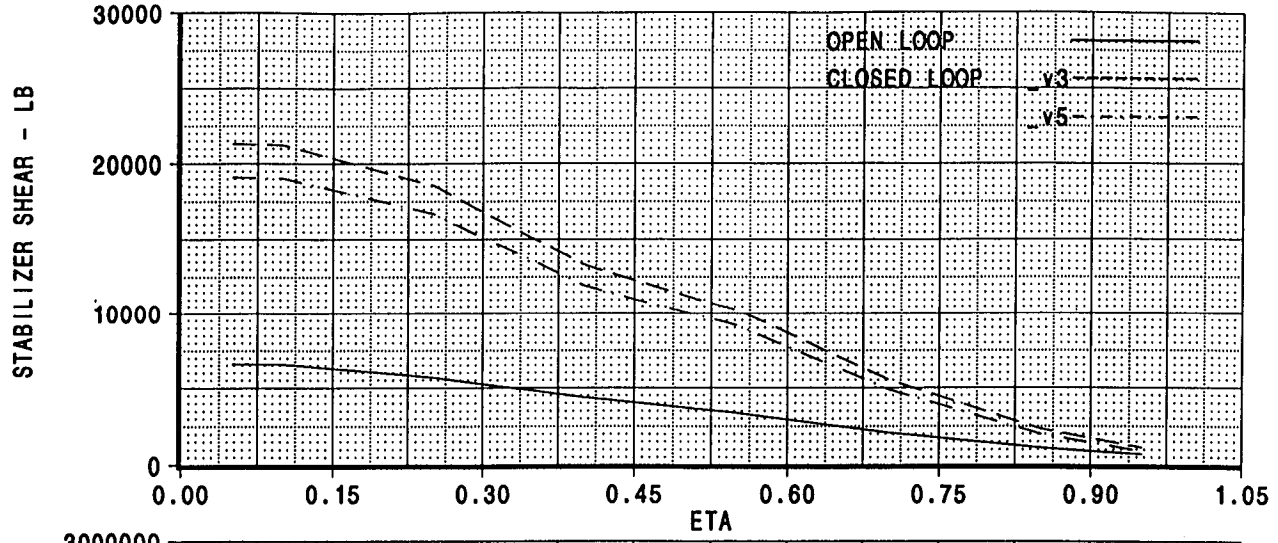

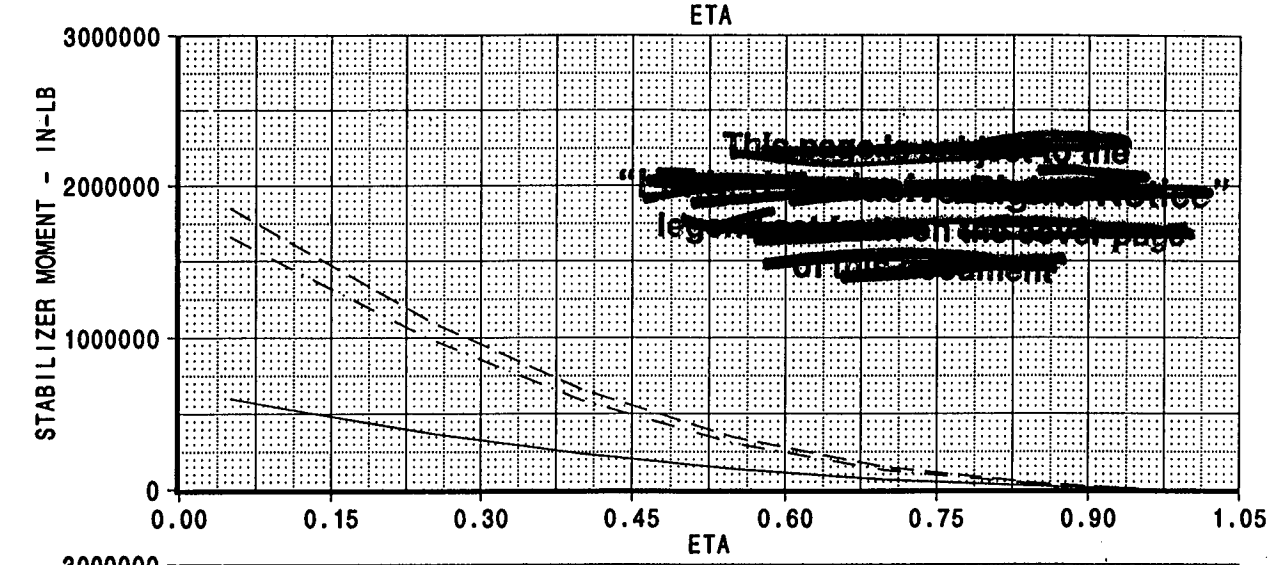

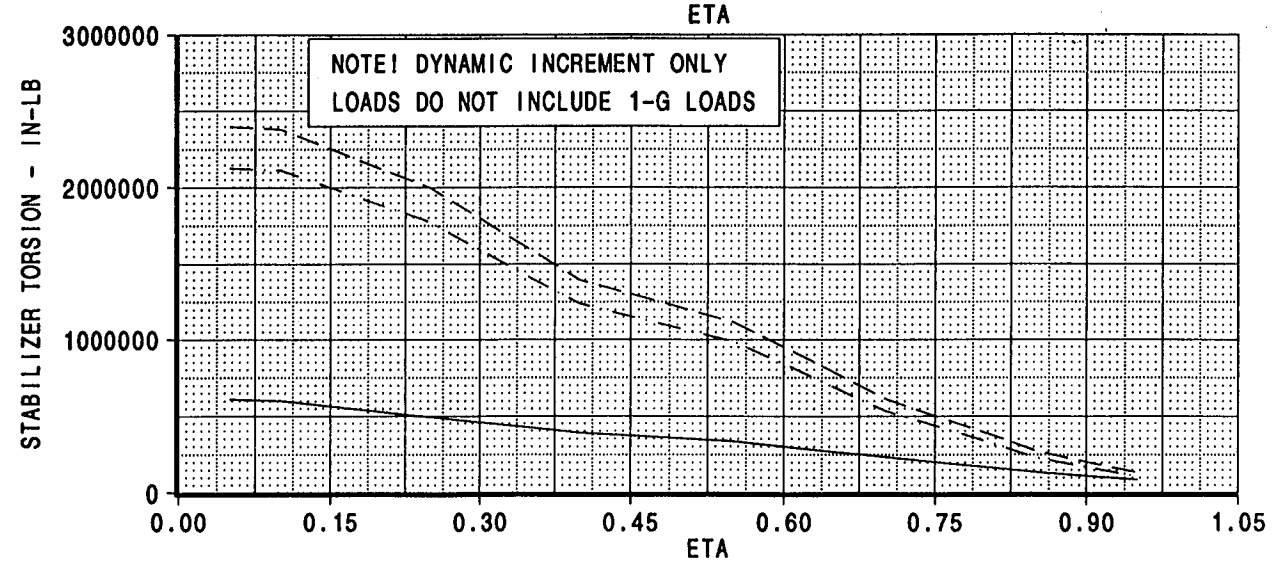

[A]: /acct/ksn8042/SOLVER/psd_gust_M1m0p65.esb
[B]: /acct/ksn8042/SOLVER/psd_gust_M1m0p65_fb.esb
[C]: /acct/ksn8042/SOLVER/psd_gust_M1m0p65_fb_v5.esb

CALC	K.S.NAGARAJA	23Jun99	REVISED	DATE	SYMMETRICAL VERTICAL PSD GUST CASE MODEL=PTSD MASS=M1 MACH=0.65 ALT=35K COMPARISON OPEN VERSUS CLOSED LOOP	HSCT
CHECK						FIG 7.4.2.3
APPD.						
APPD.					BOEING	PAGE 32

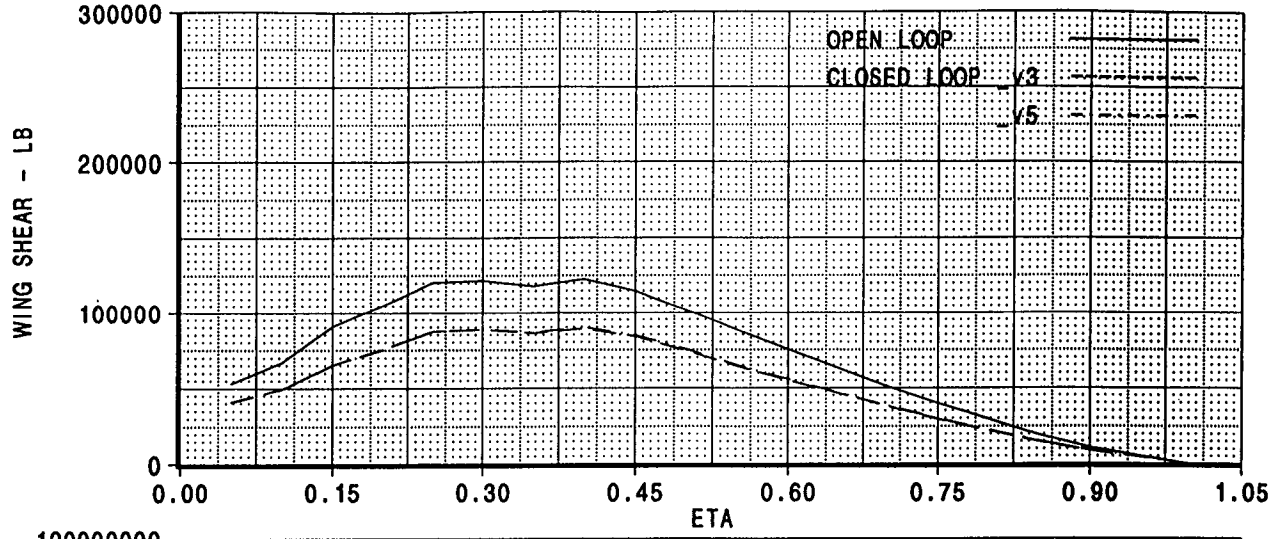

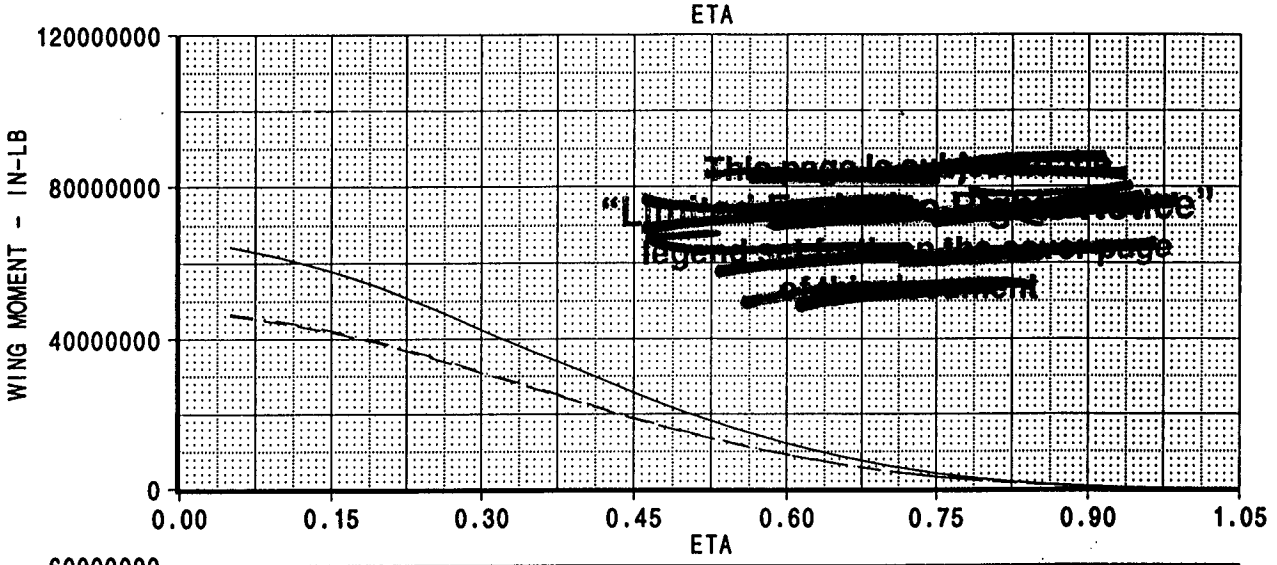

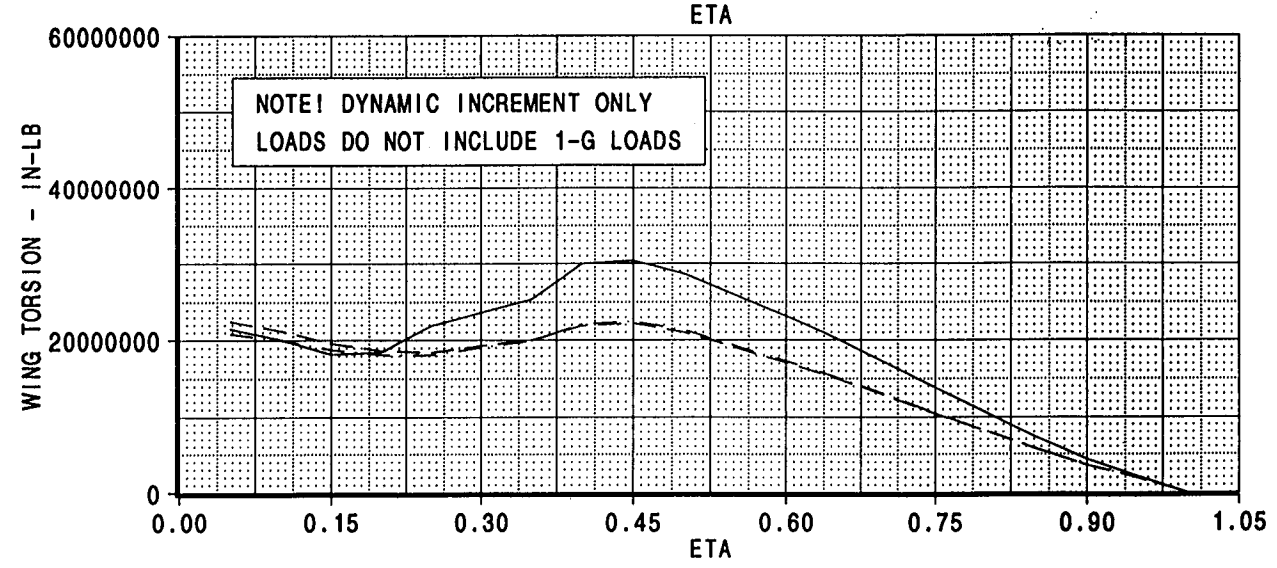

[A]: /acct/ksn8042/SOLVER/psd_gust_MT1m0p65.esb
[B]: /acct/ksn8042/SOLVER/psd_gust_MT1m0p65_fb.esb
[C]: /acct/ksn8042/SOLVER/psd_gust_MT1m0p65_fb_v5.esb

CALC	K.S.NAGARAJA	23Jun99	REVISED	DATE	SYMMETRICAL VERTICAL PSD GUST CASE MODEL=PTSD MASS=MT1 MACH=0.65 ALT=35K COMPARISON OPEN VERSUS CLOSED LOOP	HSCT FIG 7.4.2.4
CHECK						
APPD.						
APPD.					BOEING	PAGE 33

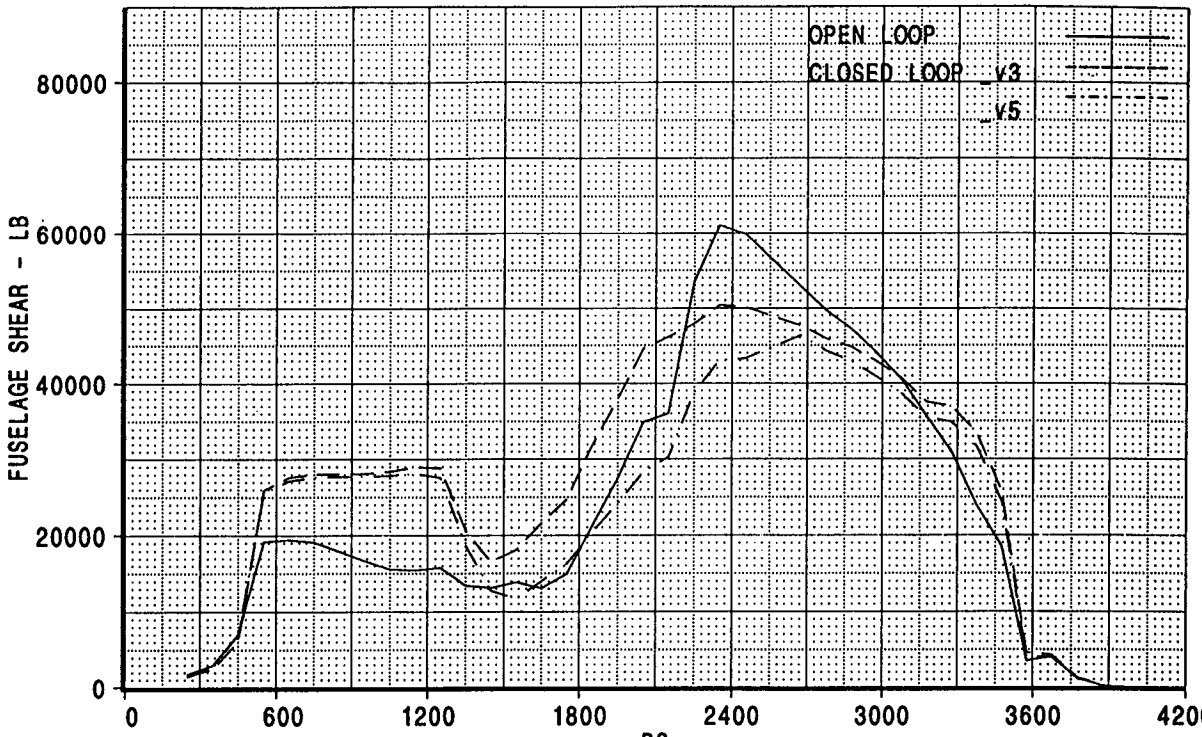

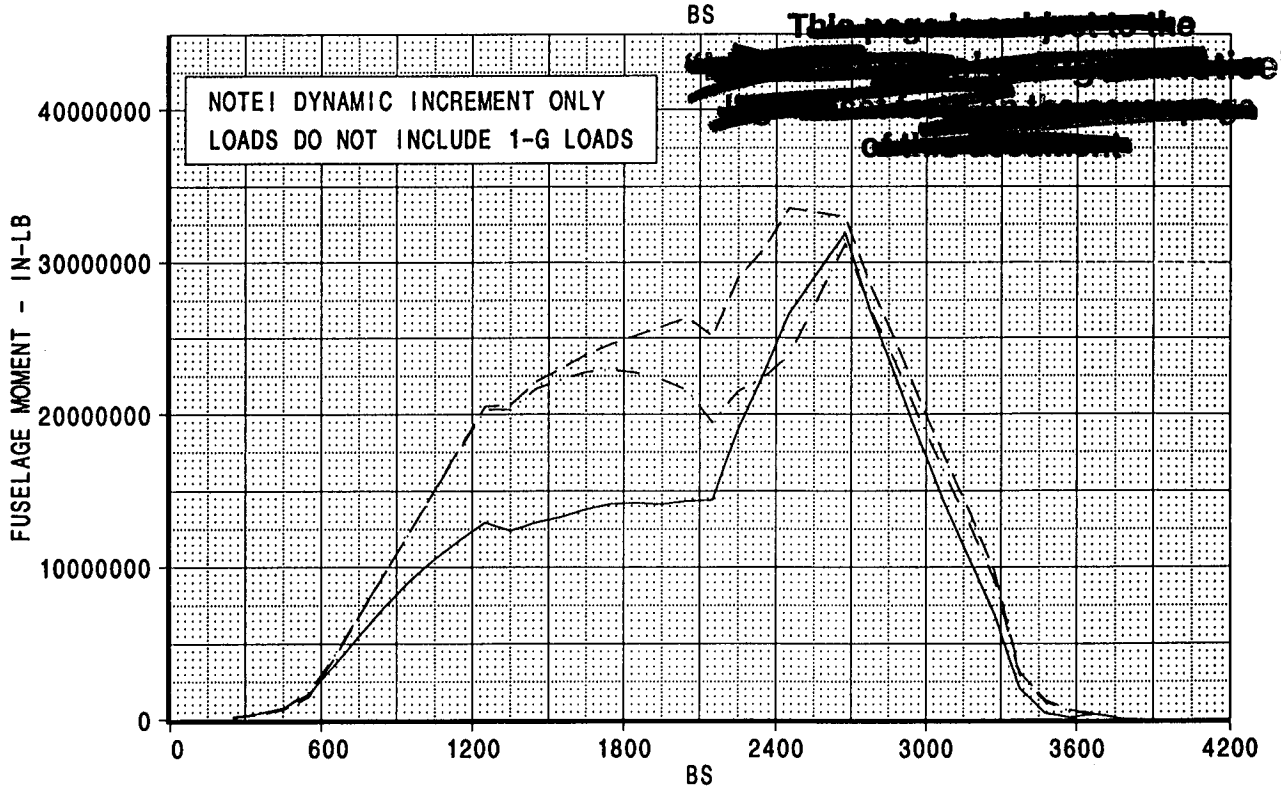

[A]: /acct/ksn8042/SOLVER/psd_gust_MT1m0p65.esb
[B]: /acct/ksn8042/SOLVER/psd_gust_MT1m0p65_fb.esb
[C]: /acct/ksn8042/SOLVER/psd_gust_MT1m0p65_fb_v5.esb

CALC	K.S.NAGARAJA	23Jun99	REVISED	DATE	SYMMETRIC VERTICAL PSD GUST CASE MODEL=PTSD MASS=MT1 MACH 0.65 ALT=35K COMPARISON OPEN VERSUS CLOSED LOOP	HSCT
CHECK						FIG 7.4.2.5
APPD.						
APPD.					BOEING	PAGE 34

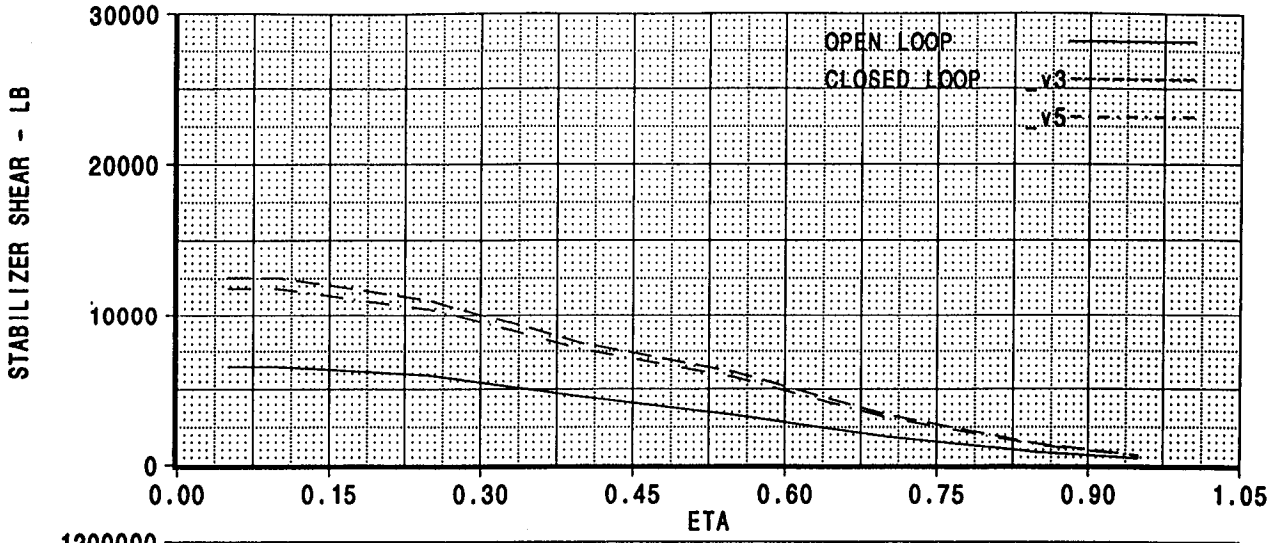

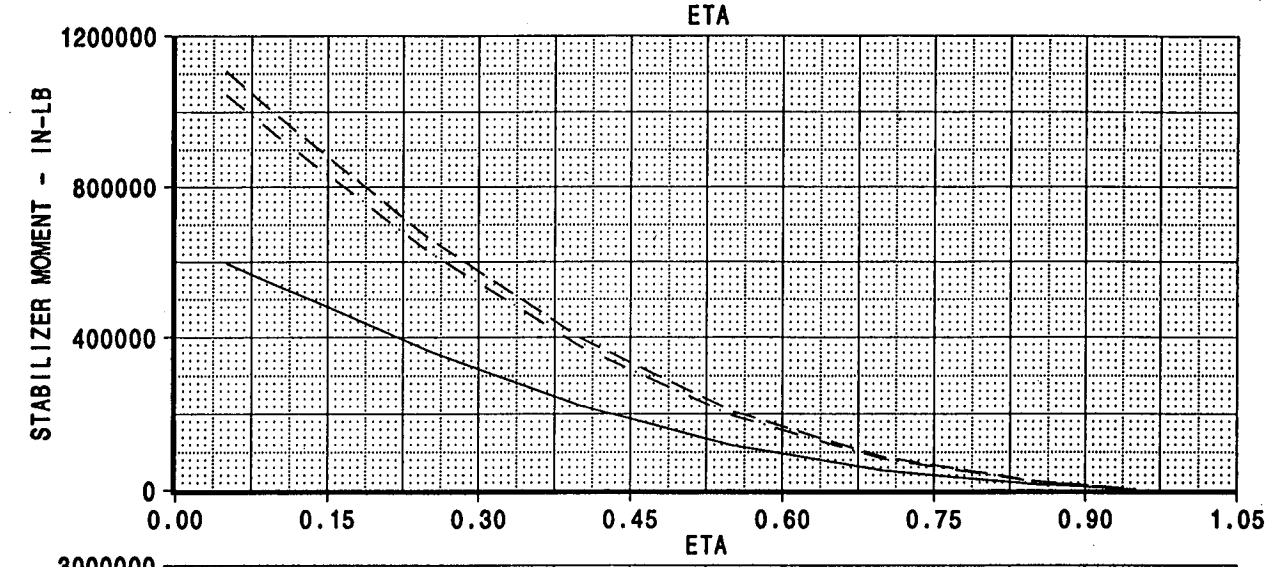

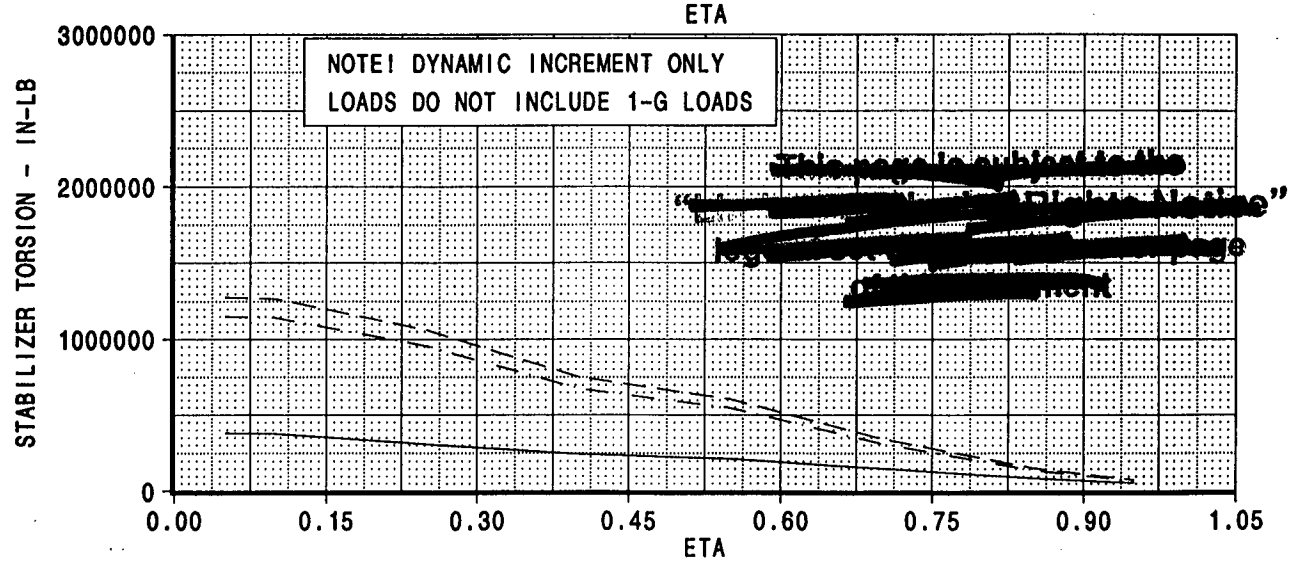

[A]: /acct/ksn8042/SOLVER/psd_gust_MT1m0p65.esb
[B]: /acct/ksn8042/SOLVER/psd_gust_MT1m0p65_fb.esb
[C]: /acct/ksn8042/SOLVER/psd_gust_MT1m0p65_fb_v5.esb

CALC	K.S.NAGARAJA	23Jun99	REVISED	DATE	SYMMETRICAL VERTICAL PSD GUST CASE MODEL=PTSD MASS=MT1 MACH=0.65 ALT=35K COMPARISON OPEN VERSUS CLOSED LOOP	HSCT FIG 7.4.2.6
CHECK						
APPD.						
APPD.					BOEING	PAGE 35

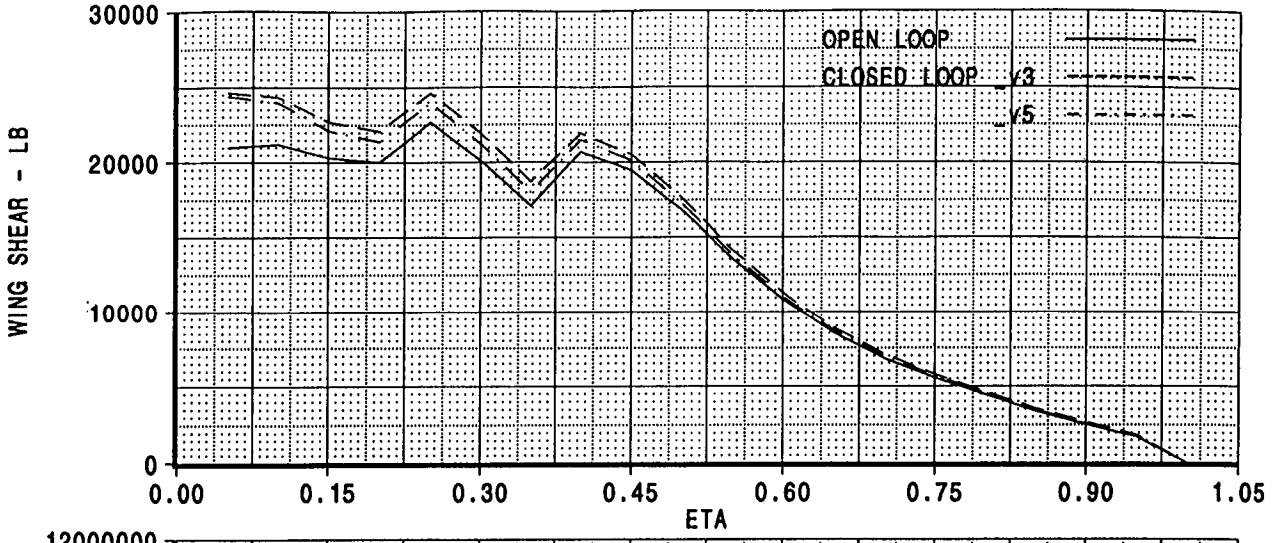

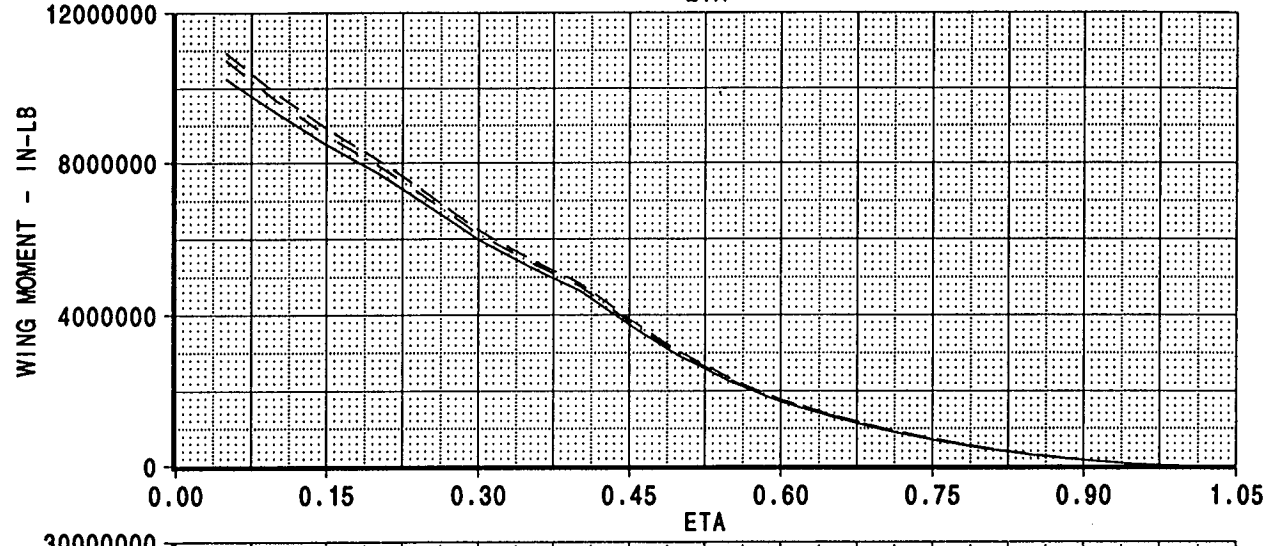

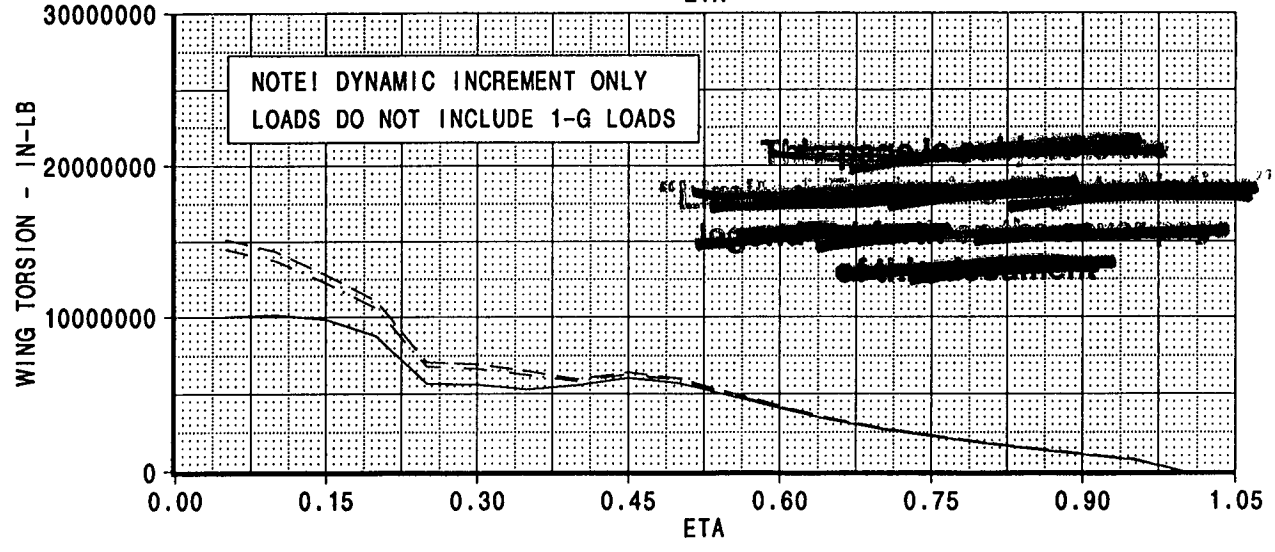

[A]: /acct/ksn8042/SOLVER/psd_gust_M1m2p40.esb
[B]: /acct/ksn8042/SOLVER/psd_gust_M1m2p40_fb.esb
[C]: /acct/ksn8042/SOLVER/psd_gust_M1m2p40_fb_v5.esb

CALC	K.S.NAGARAJA	23Jun99	REVISED	DATE	SYMMETRICAL VERTICAL PSD GUST CASE MODEL=PTSD MASS=M1 MACH=2.40 ALT=66K COMPARISON OPEN VERSUS CLOSED LOOP	HSCT FIG 7.4.2.7
CHECK						
APPD.						
APPD.					BOEING	PAGE 36

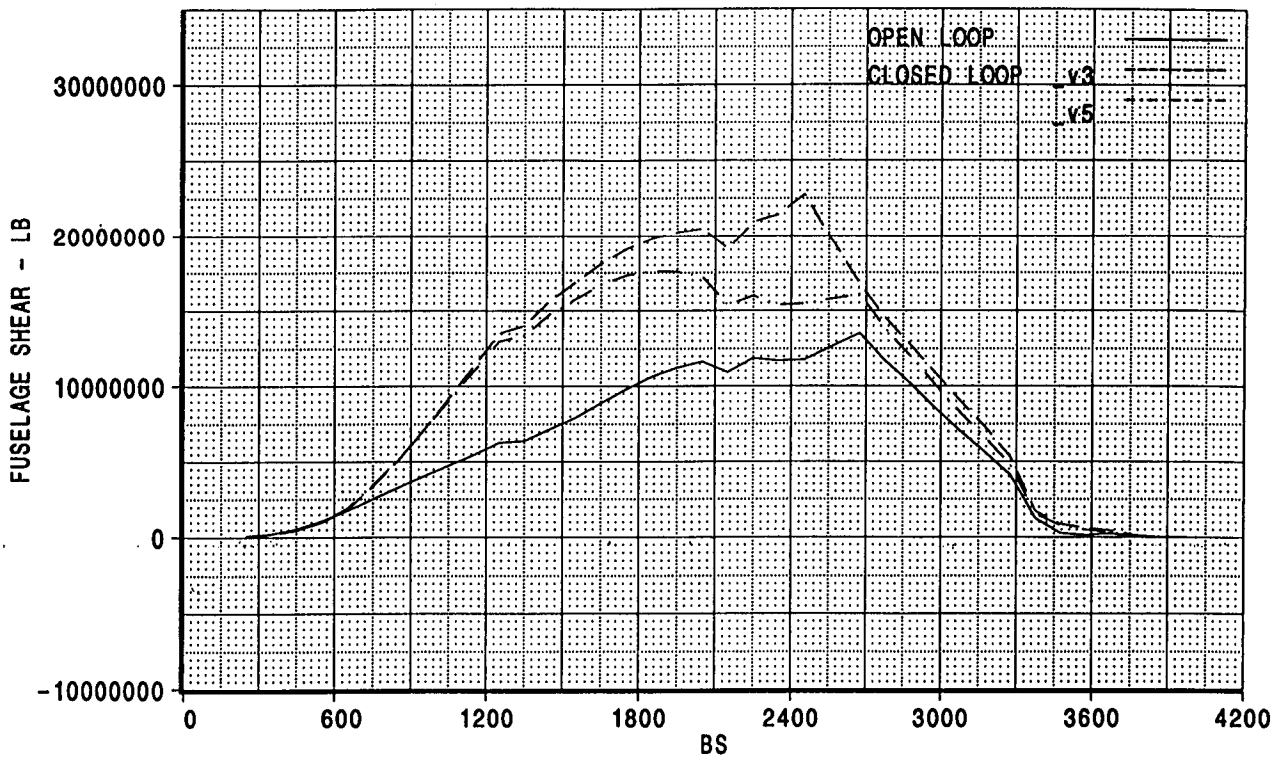

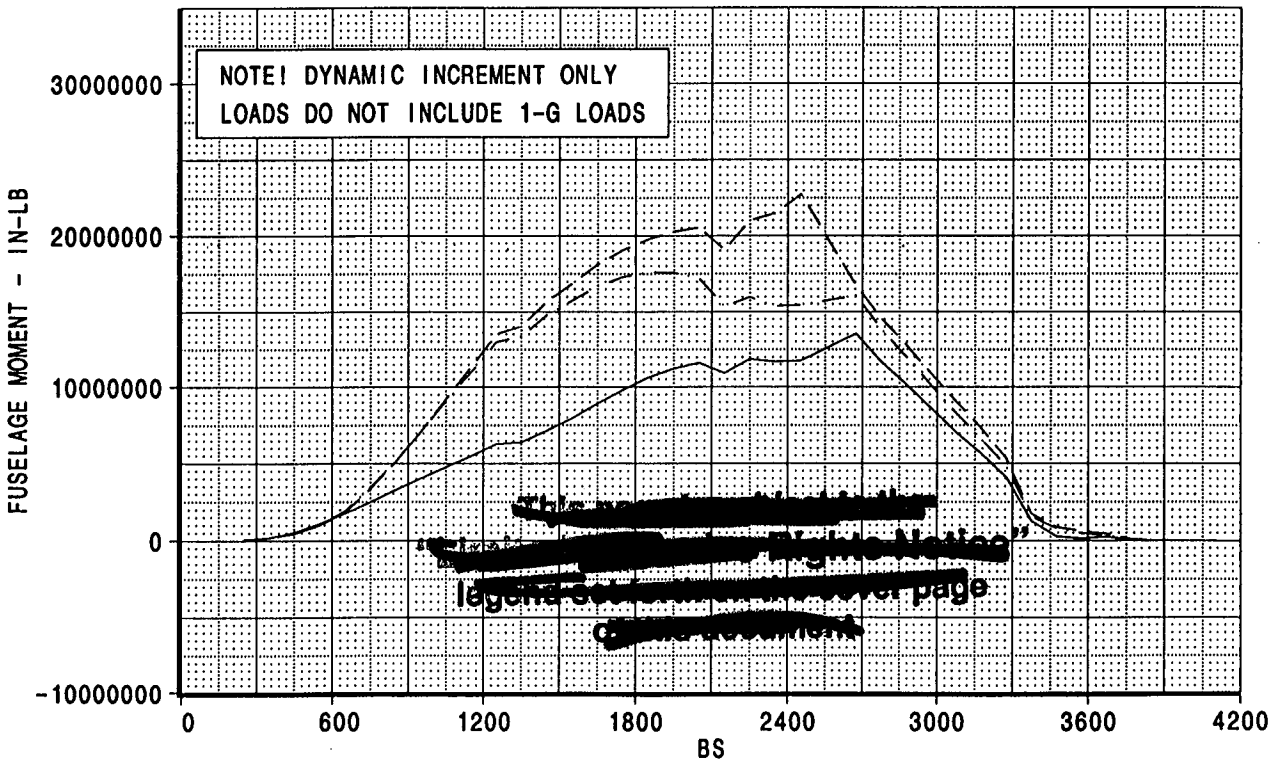

[A]: /acct/ksn8042/SOLVER/psd_gust_M1m2p40.esb
[B]: /acct/ksn8042/SOLVER/psd_gust_M1m2p40_fb.esb
[C]: /acct/ksn8042/SOLVER/psd_gust_M1m2p40_fb_v5.esb

CALC	K.S.NAGARAJA	23Jun99	REVISED	DATE	SYMMETRIC VERTICAL PSD GUST CASE MODEL=PTSD MASS=M1 MACH 2.40 ALT=66K COMPARISON OPEN VERSUS CLOSED LOOP	HSCT
CHECK						FIG 7.4.2.8
APPD.						
APPD.					BOEING	PAGE 37

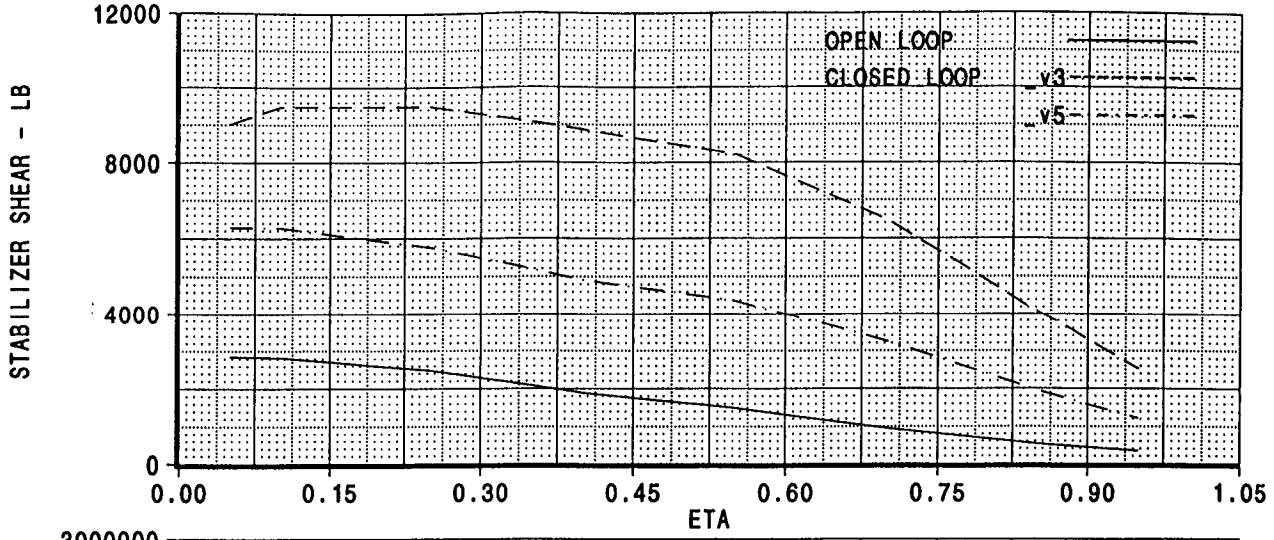

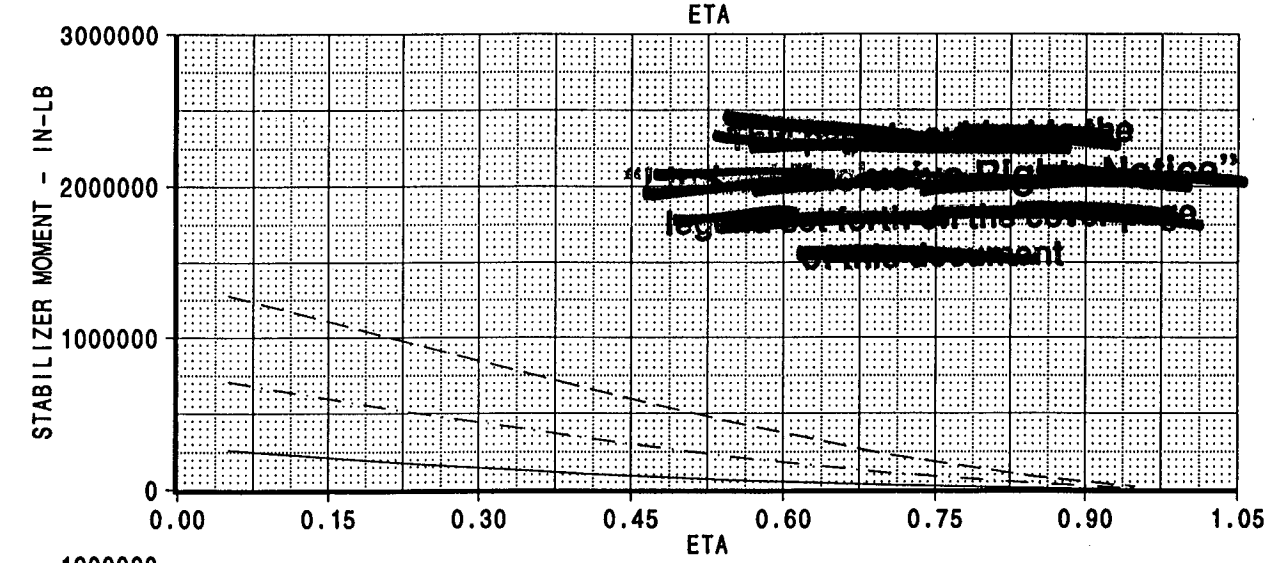

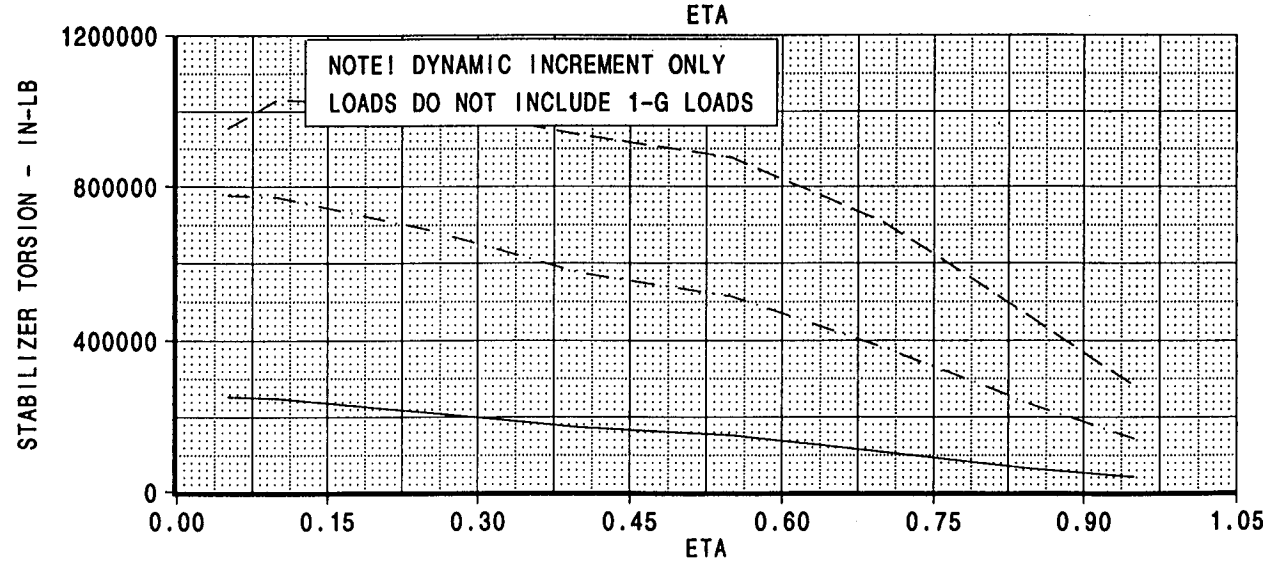

[A]: /acct/ksn8042/SOLVER/psd_gust_M1m2p40.esb
[B]: /acct/ksn8042/SOLVER/psd_gust_M1m2p40_fb.esb
[C]: /acct/ksn8042/SOLVER/psd_gust_M1m2p40_fb_v5.esb

CALC	K.S.NAGARAJA	23Jun99	REVISED	DATE	SYMMETRICAL VERTICAL PSD GUST CASE	HSCT
CHECK					MODEL=PTSD MASS=M1 MACH=2.40 ALT=66K	FIG 7.4.2.9
APPD.					COMPARISON OPEN VERSUS CLOSED LOOP	
APPD.					BOEING	PAGE 38

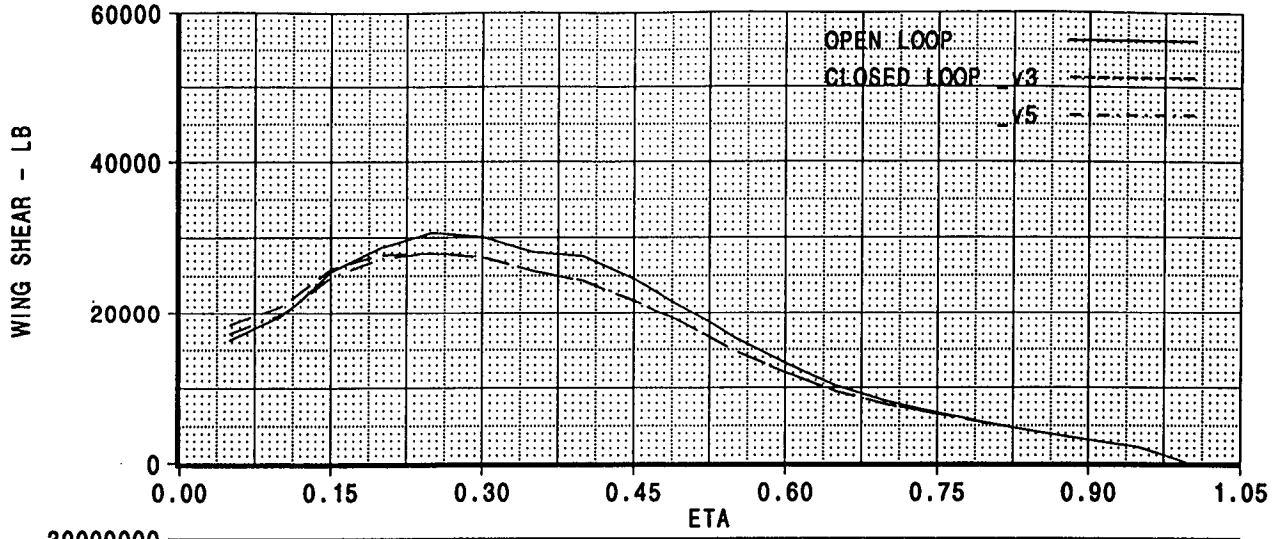

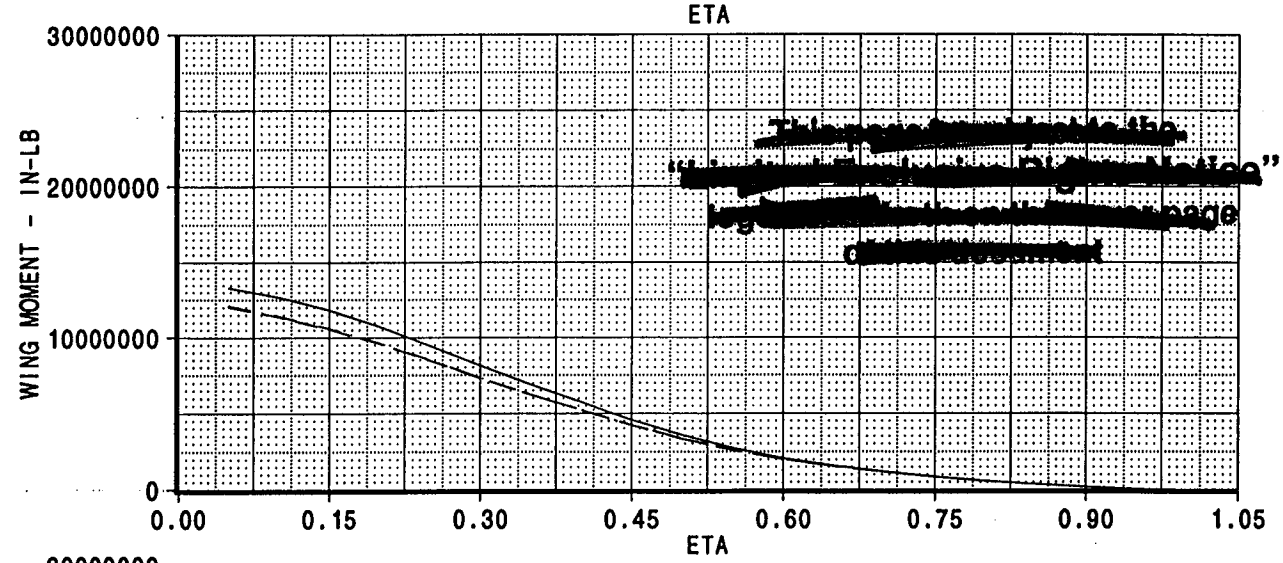

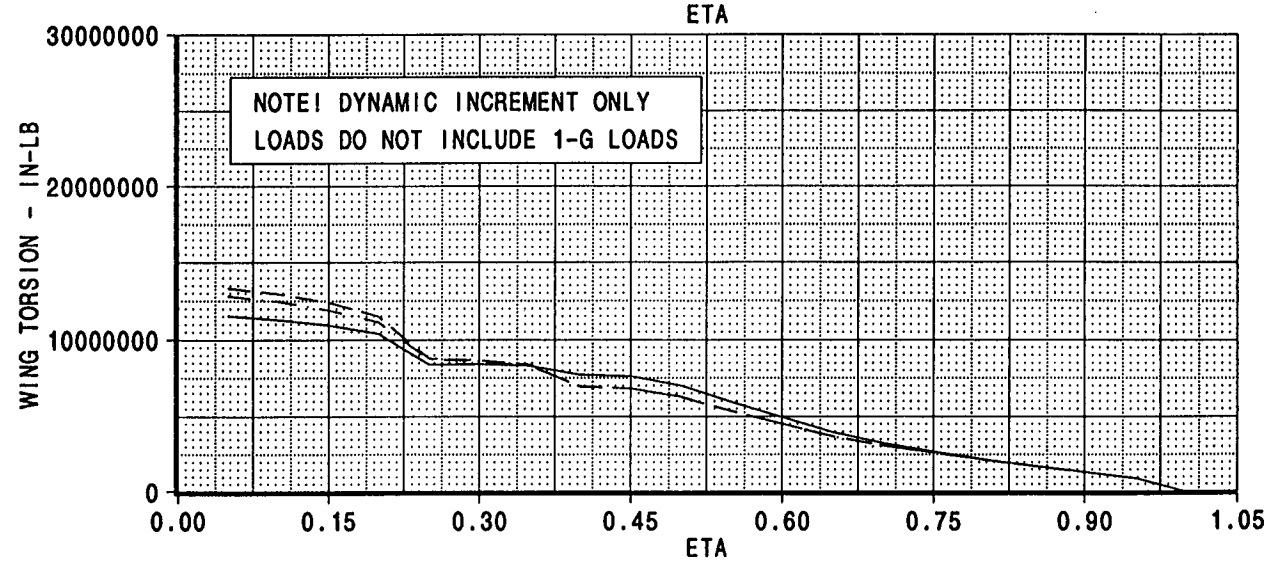

[A]: /acct/ksn8042/SOLVER/psd_gust_MT1m2p40.esb
[B]: /acct/ksn8042/SOLVER/psd_gust_MT1m2p40_fb.esb
[C]: /acct/ksn8042/SOLVER/psd_gust_MT1m2p40_fb_v5.esb

CALC	K.S.NAGARAJA	23Jun99	REVISED	DATE	SYMMETRICAL VERTICAL PSD GUST CASE MODEL=PTSD MASS=MT1 MACH=2.40 ALT=66K COMPARISON OPEN VERSUS CLOSED LOOP	HSCT
CHECK						FIG 7.4.2.10
APPD.						
APPD.					BOEING	PAGE 39

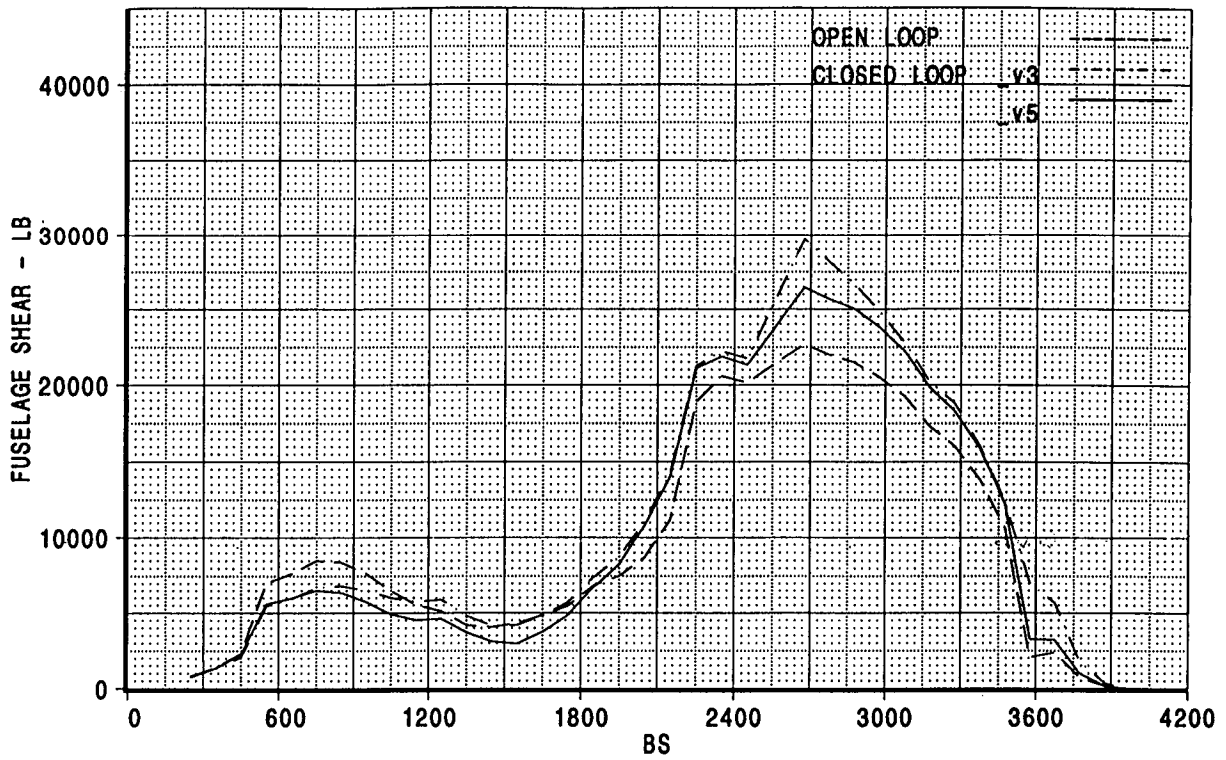

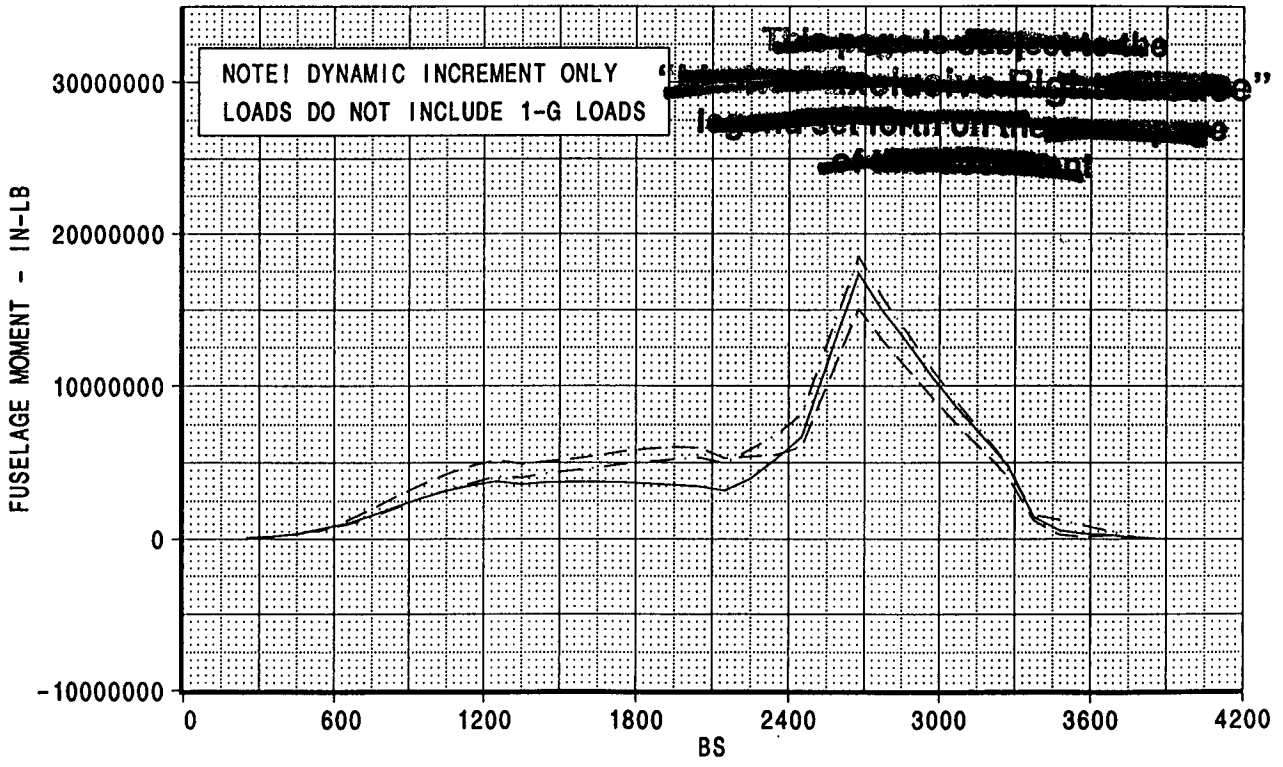

[A]: /acct/ksn8042/SOLVER/psd_gust_MT1m2p40.esb
[B]: /acct/ksn8042/SOLVER/psd_gust_MT1m2p40_fb.esb
[C]: /acct/ksn8042/SOLVER/psd_gust_MT1m2p40_fb_v5.esb

CALC	K.S.NAGARAJA	23Jun99	REVISED	DATE	SYMMETRIC VERTICAL PSD GUST CASE MODEL=PTSD MASS=MT1 MACH 2.40 ALT=66K COMPARISON OPEN VERSUS CLOSED LOOP	HSCT FIG 7.4.2.11
CHECK						
APPD.						
APPD.					BOEING	PAGE 40

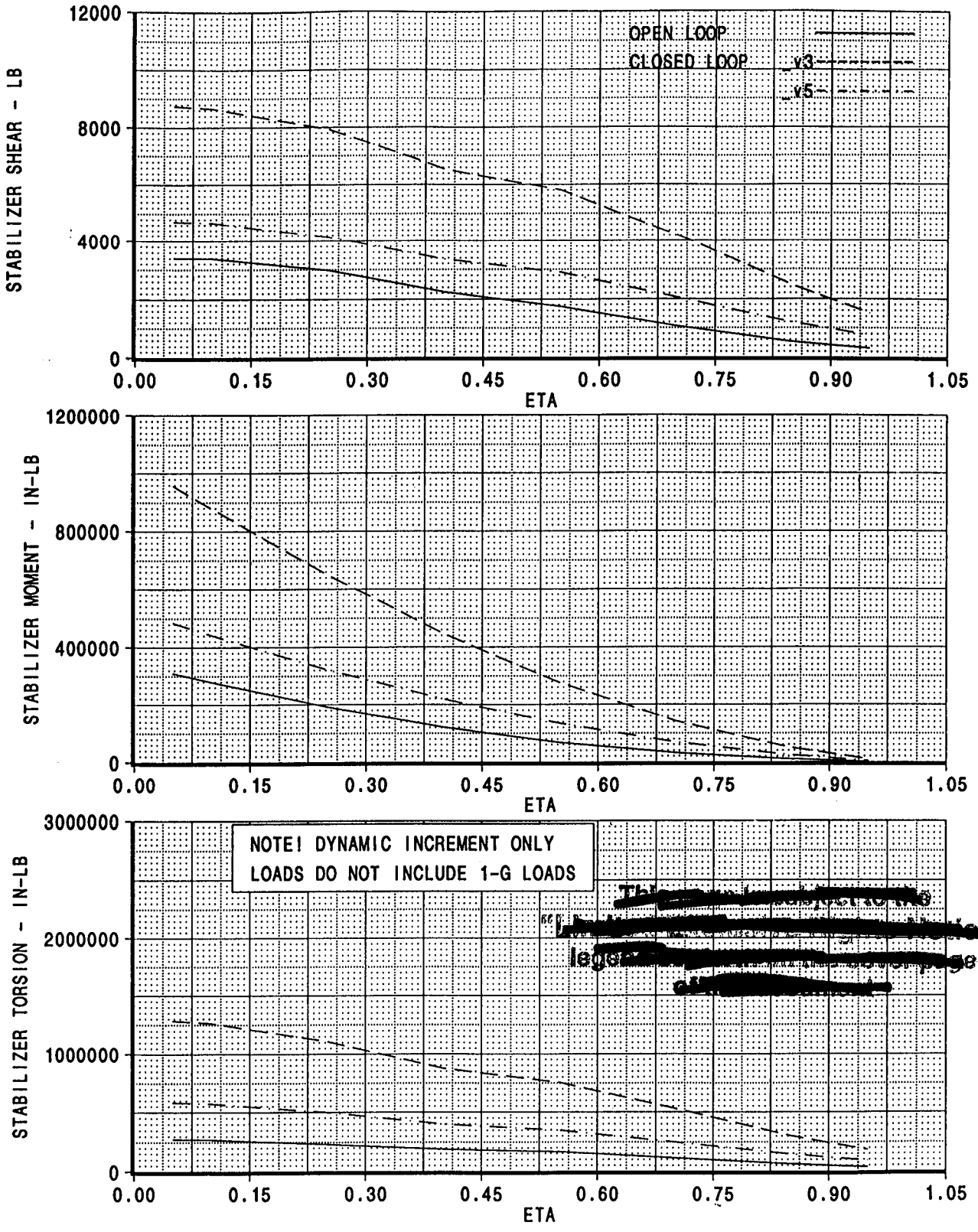

[A]: /acct/ksn8042/SOLVER/psd_gust_MT1m2p40.esb
[B]: /acct/ksn8042/SOLVER/psd_gust_MT1m2p40_fb.esb
[C]: /acct/ksn8042/SOLVER/psd_gust_MT1m2p40_fb_v5.esb

CALC	K.S.NAGARAJA	23Jun99	REVISED	DATE	SYMMETRICAL VERTICAL PSD GUST CASE	HSCT
CHECK					MODEL=PTSD MASS=MT1 MACH=2.40 ALT=66K	FIG 7.4.2.12
APPD.					COMPARISON OPEN VERSUS CLOSED LOOP	
APPD.					BOEING	PAGE 41

APPENDIX A

State Space Modeling and Control Laws

A State Space Modeling and Control Laws

A.1 Control Law Performance Analysis

Open Loop Model Analysis

This section provides additional information on the state-space vehicle models for flight conditions FA124 and FA824. Figures A.1.1–A.1.3 present comparisons of open loop frequency response characteristics for FA124, and Figs. A.1.4 –A.1.6 provide similar information for FA824.

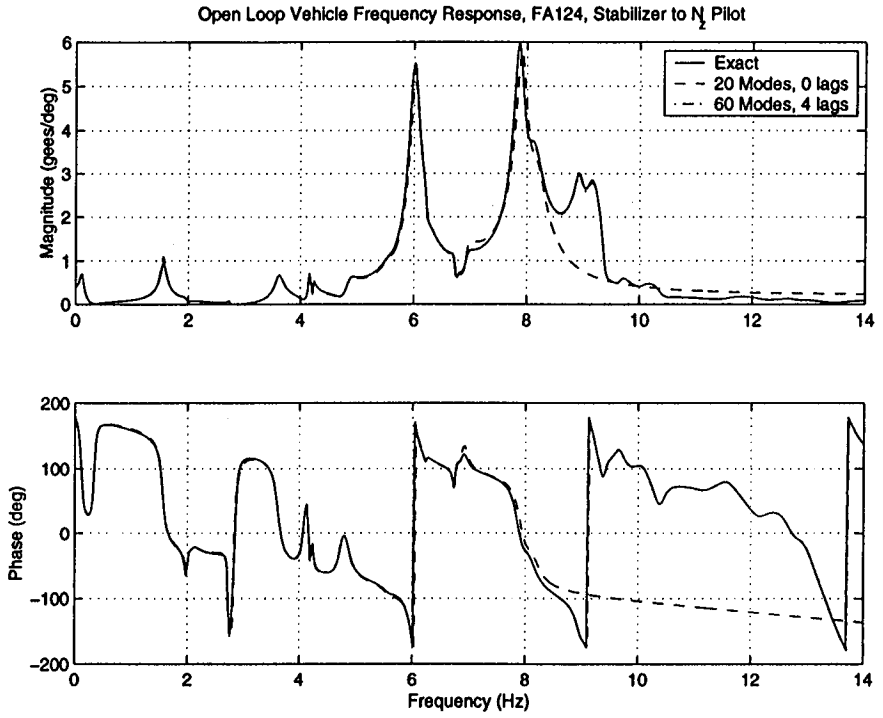

Figure A.1.1: Open Loop Frequency Response, FA124, Stabilizer to N_z Pilot

Compensator Analysis

This section provides additional information on the control law designs evaluated in this report. This information is in the form of compensator frequency response plots for select input/output pairs for flight conditions FA165 and FA824. Figures A.1.7–A.1.10 depict the frequency responses for the M1, Mach 2.4, 66,000 feet flight condition, and Figs. A.1.11–A.1.14 depict the frequency responses for the MT1, Mach 2.4, 66,000 feet flight condition.

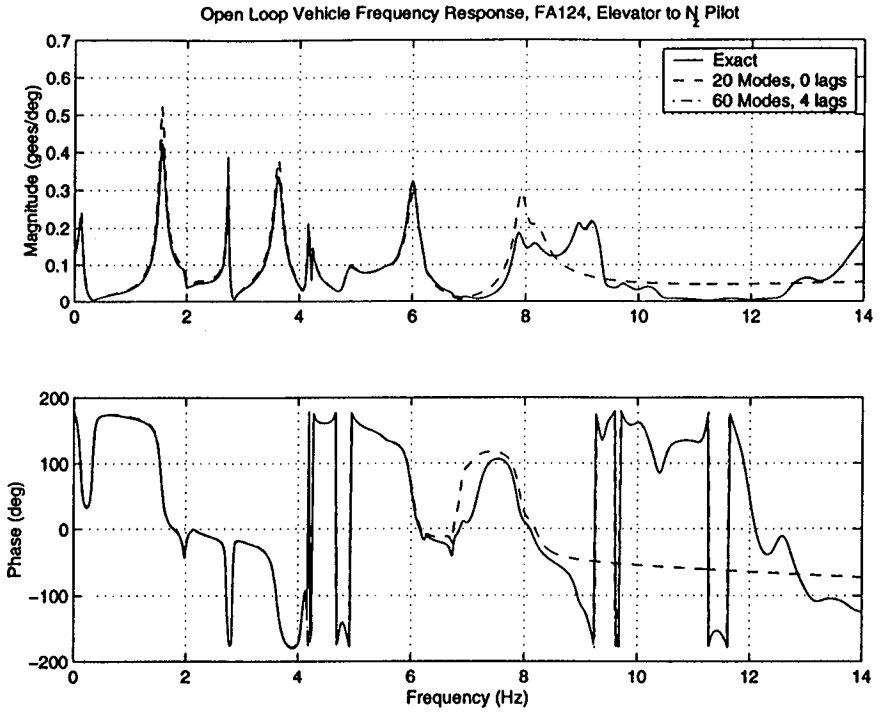

Figure A.1.2: Open Loop Frequency Response, FA124, Elevator to N_z Pilot

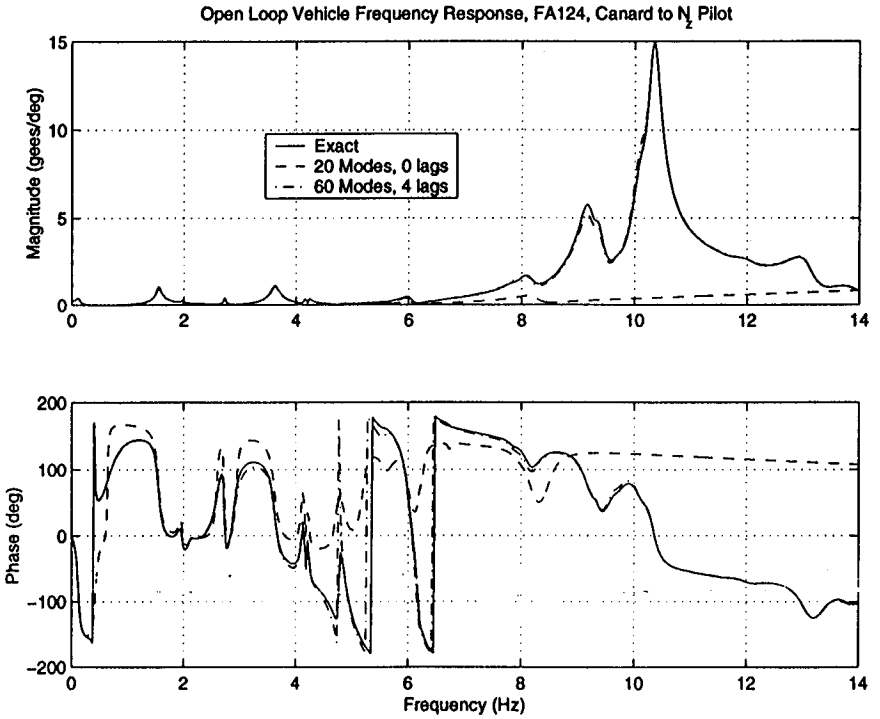

Figure A.1.3: Open Loop Frequency Response, FA124, Canard to N_z Pilot

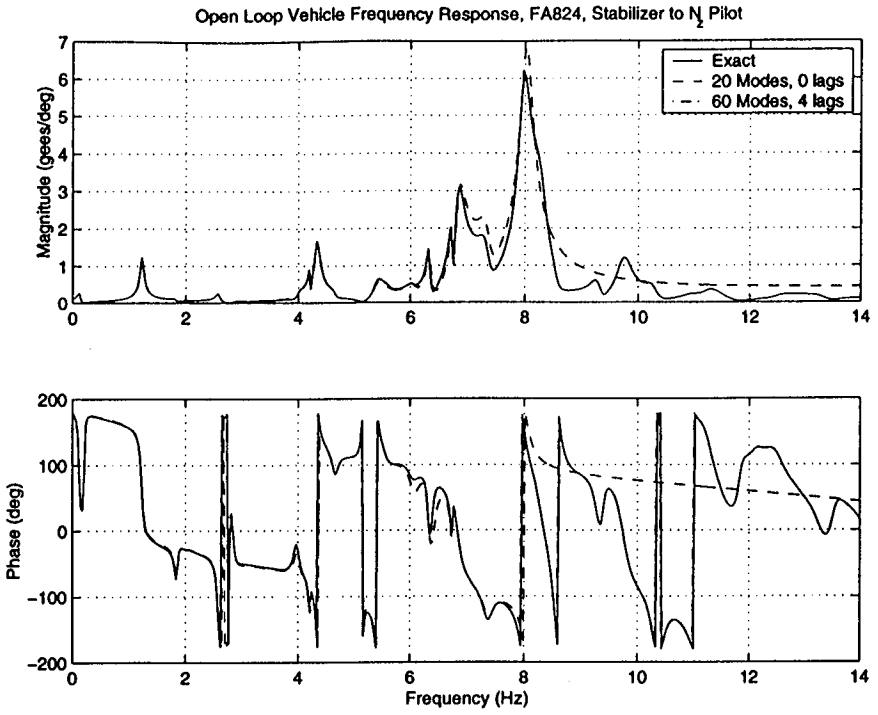

Figure A.1.4: Open Loop Frequency Response, FA824, Stabilizer to N_z Pilot

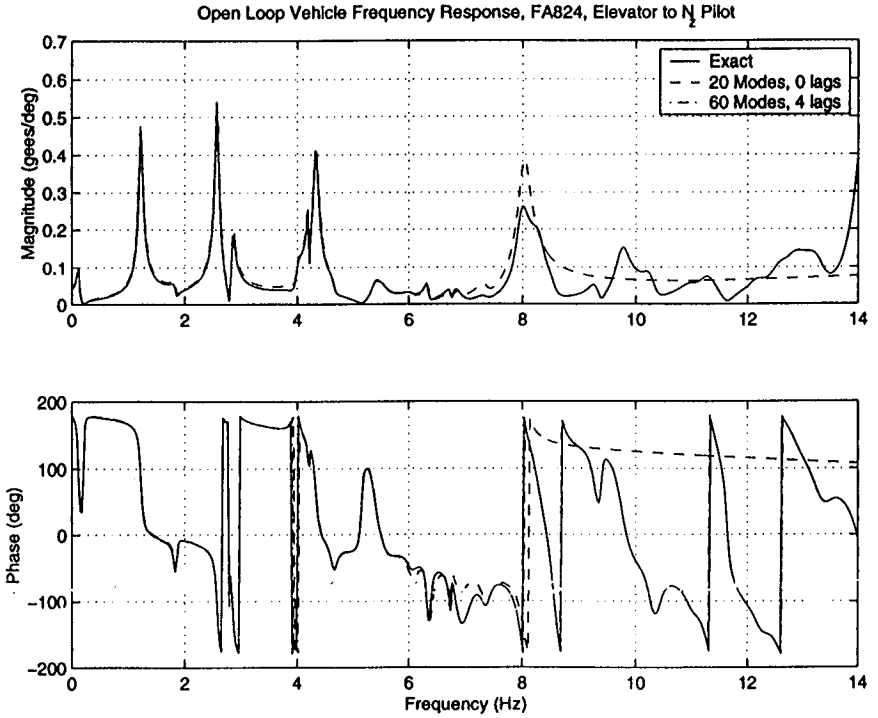

Figure A.1.5: Open Loop Frequency Response, FA824, Elevator to N_z Pilot

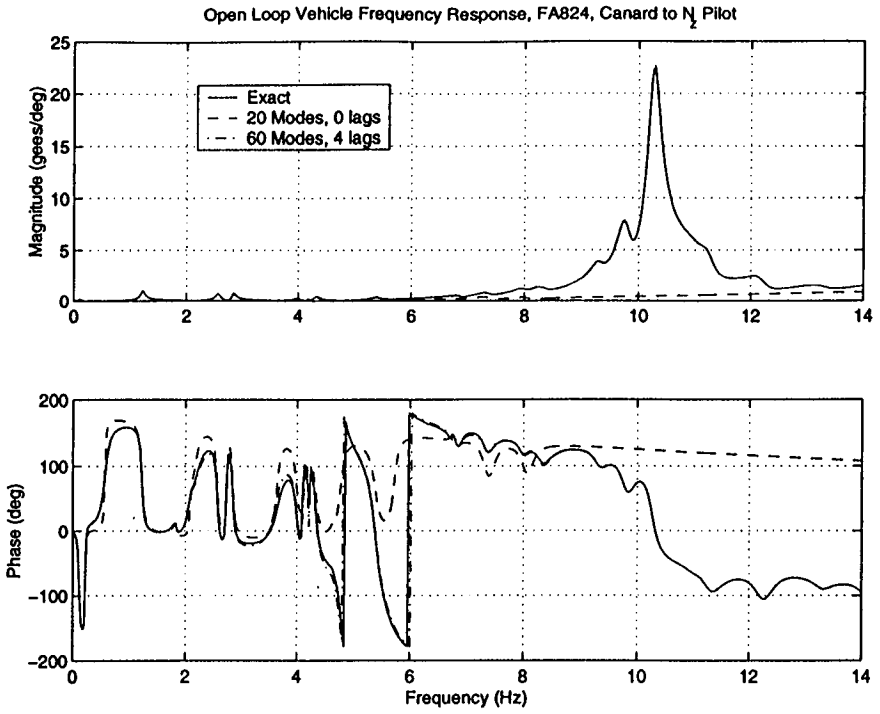

Figure A.1.6: Open Loop Frequency Response, FA824, Canard to N_z Pilot

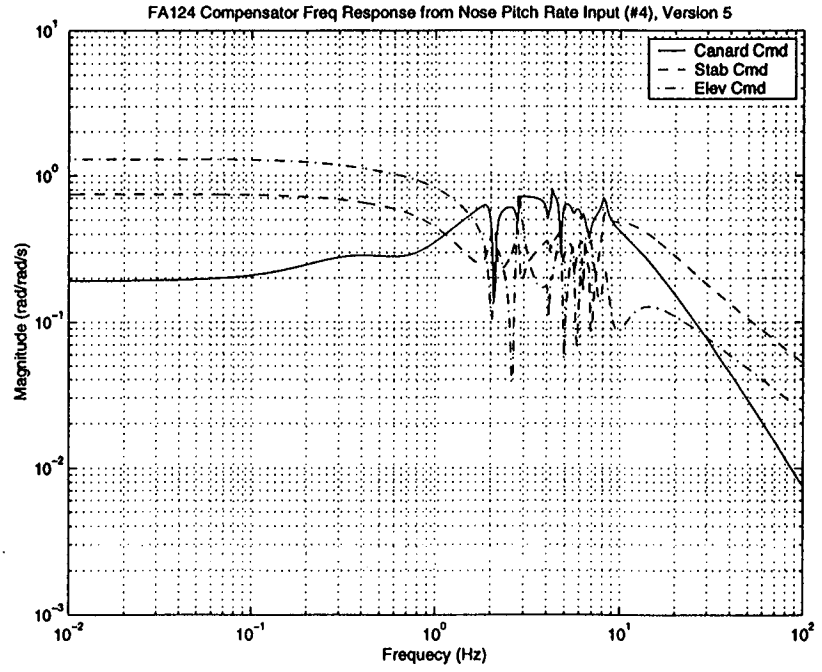

Figure A.1.7: FA124 Compensator Frequency Response: Nose Pitch Rate Input (#4)

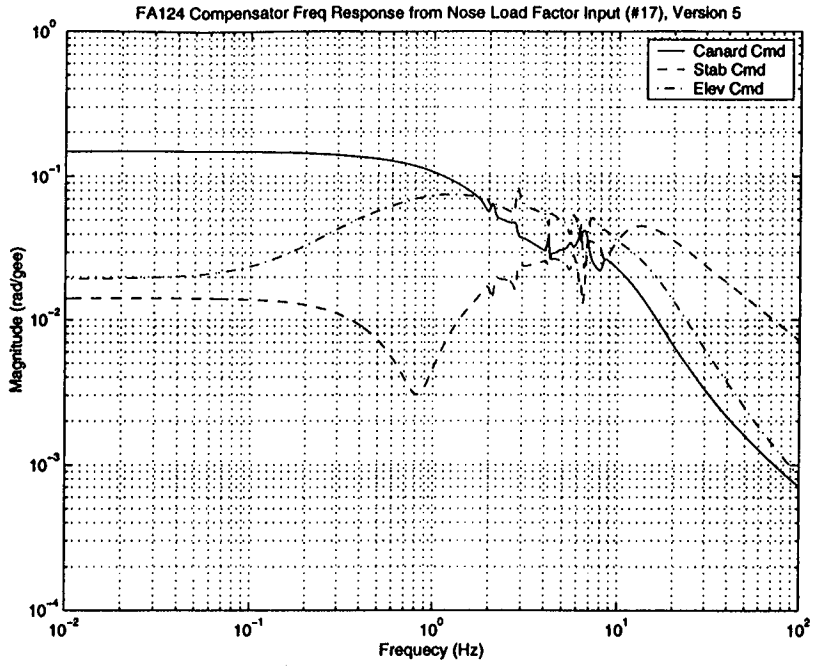

Figure A.1.8: FA124 Compensator Frequency Response: Nose Load Factor Input (#17)

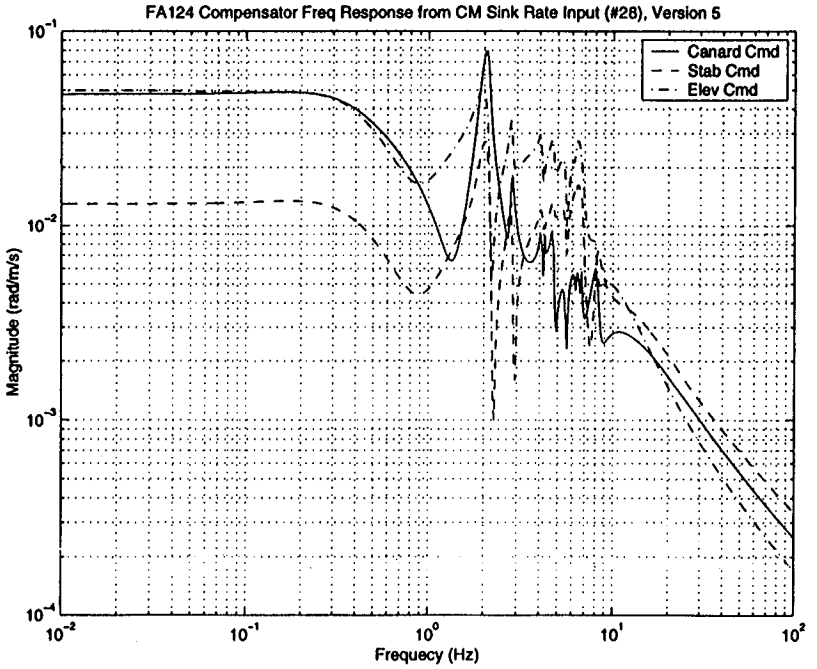

Figure A.1.9: FA124 Compensator Frequency Response: CM Sink Rate Input (#28)

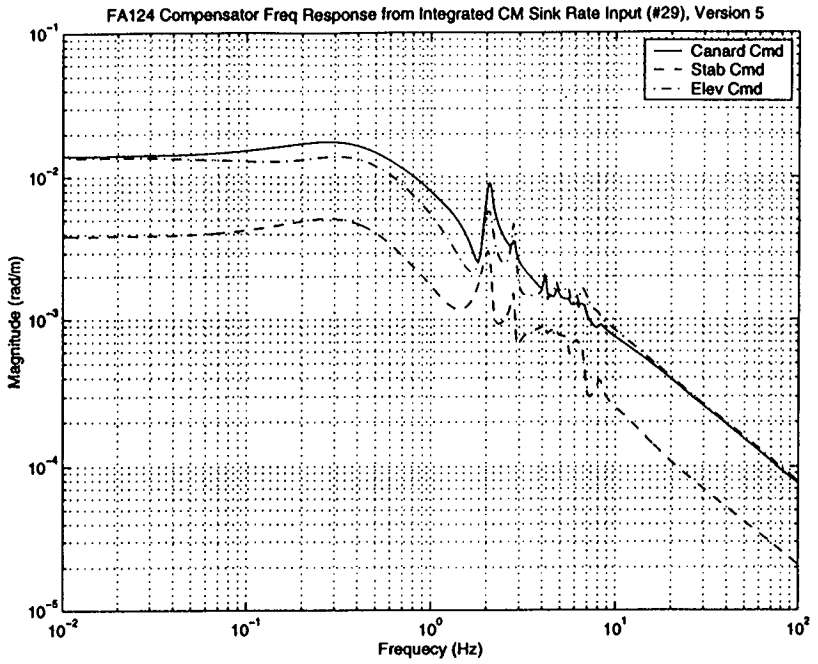

Figure A.1.10: FA124 Compensator Frequency Response: Integrated CM Sink Rate Input (#29)

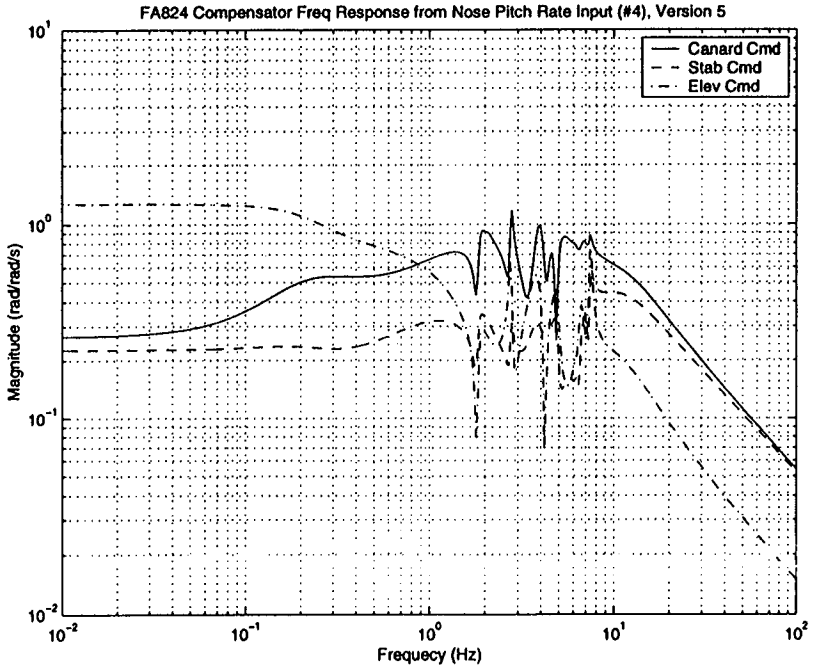

Figure A.1.11: FA824 Compensator Frequency Response: Nose Pitch Rate Input (#4)

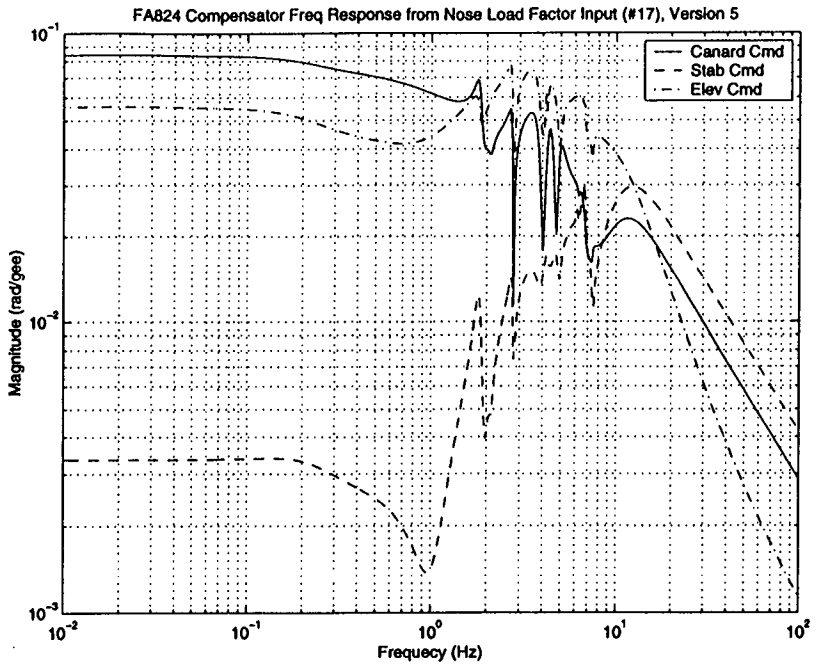

Figure A.1.12: FA824 Compensator Frequency Response: Nose Load Factor Input (#17)

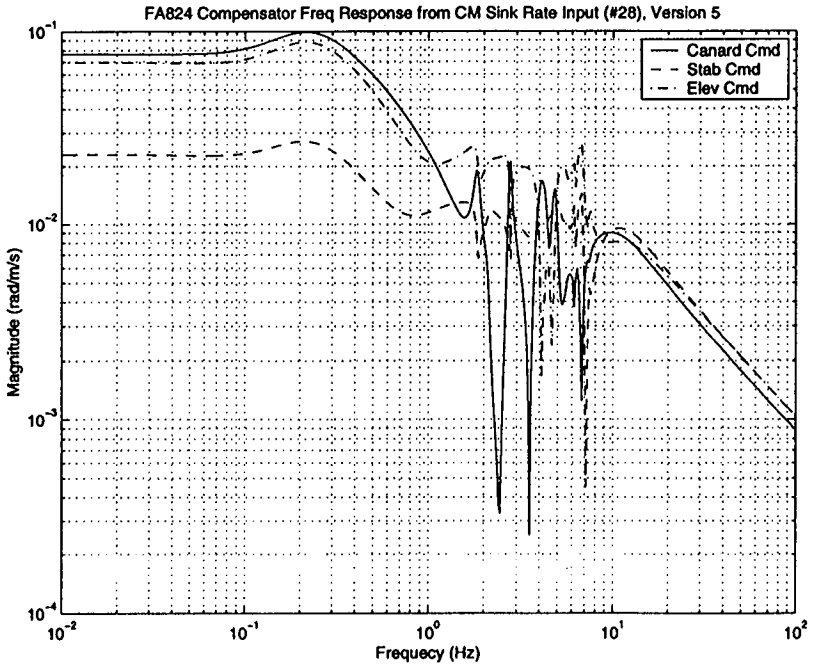

Figure A.1.13: FA824 Compensator Frequency Response: CM Sink Rate Input (#28)

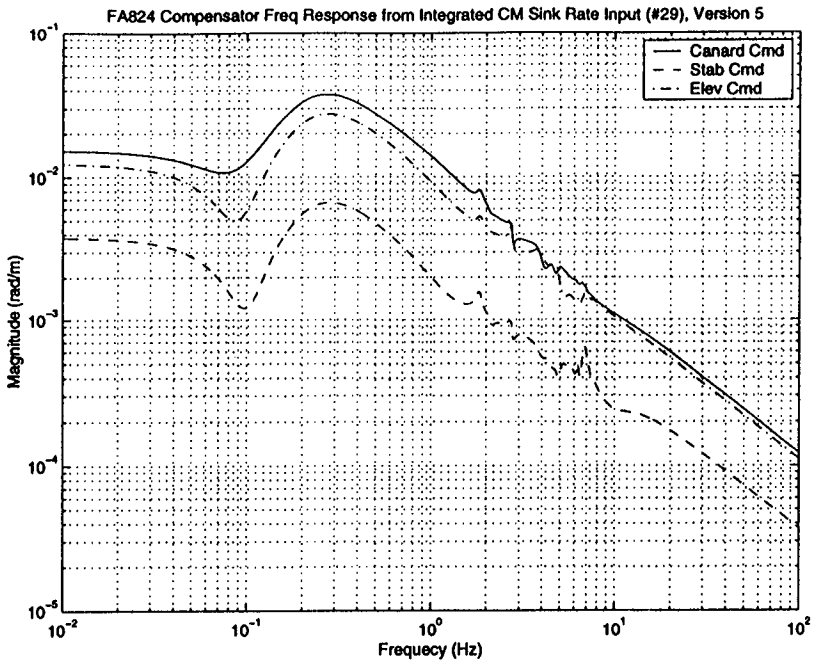

Figure A.1.14: FA824 Compensator Frequency Response: Integrated CM Sink Rate Input (#29)

Closed Loop Analysis

Figures A.1.15–A.1.20 demonstrate the effectiveness of the control design in suppressing structural mode excitation for the FA124 and FA824 flight conditions.

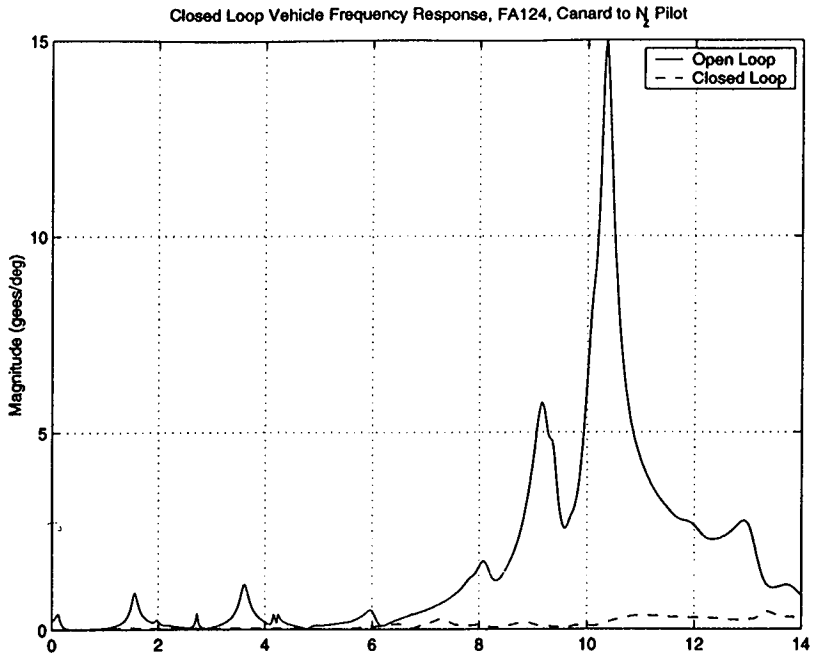

Figure A.1.15: FA124 Closed Loop Frequency Response from Canard to N_z Pilot

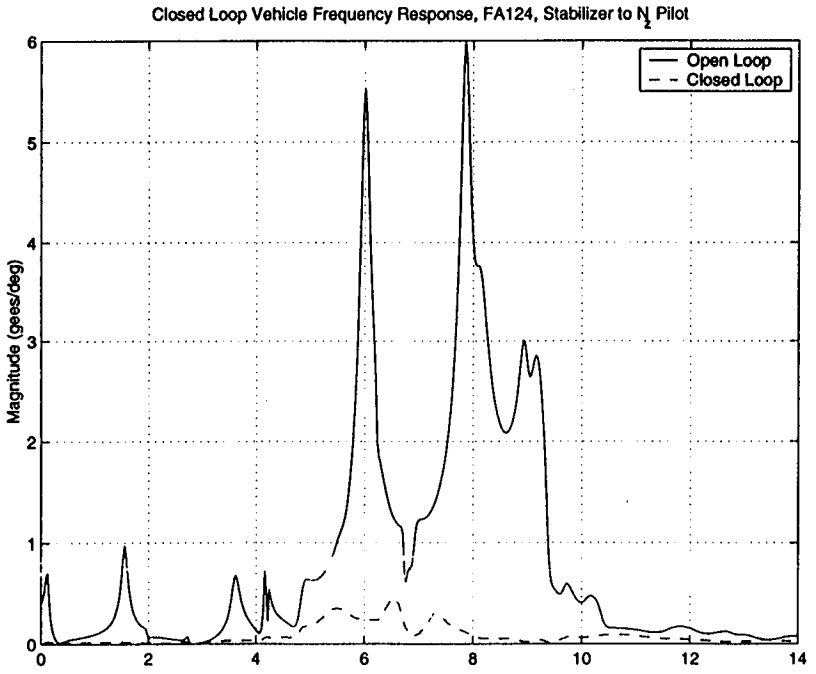

Figure A.1.16: FA124 Closed Loop Frequency Response from Stabilizer to N_z Pilot

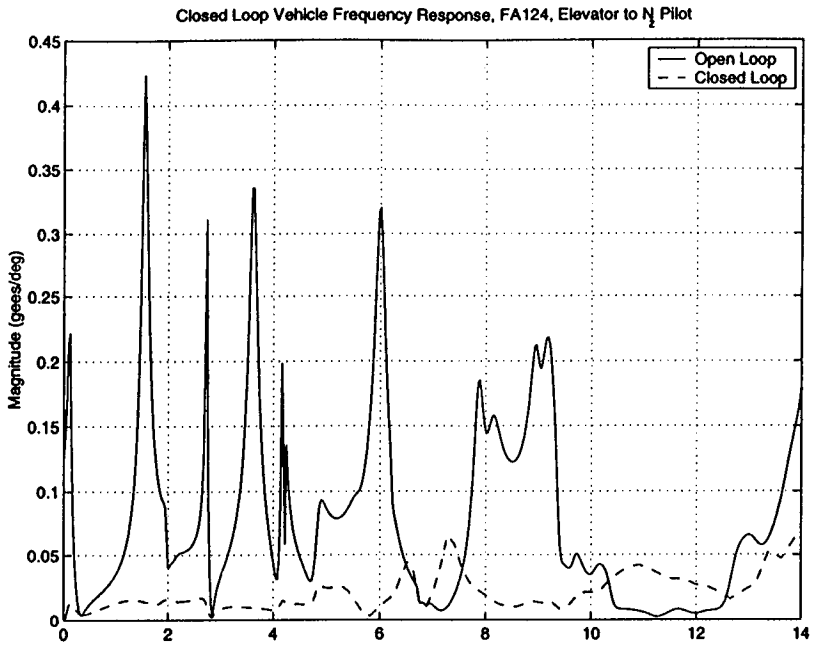

Figure A.1.17: FA124 Closed Loop Frequency Response from Elevator to N_z Pilot

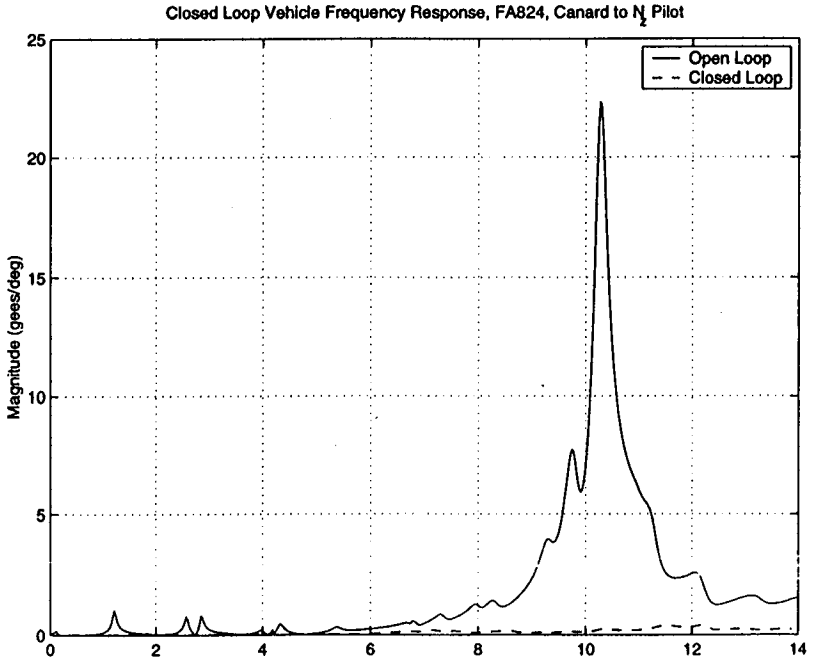

Figure A.1.18: FA824 Closed Loop Frequency Response from Canard to N_z Pilot

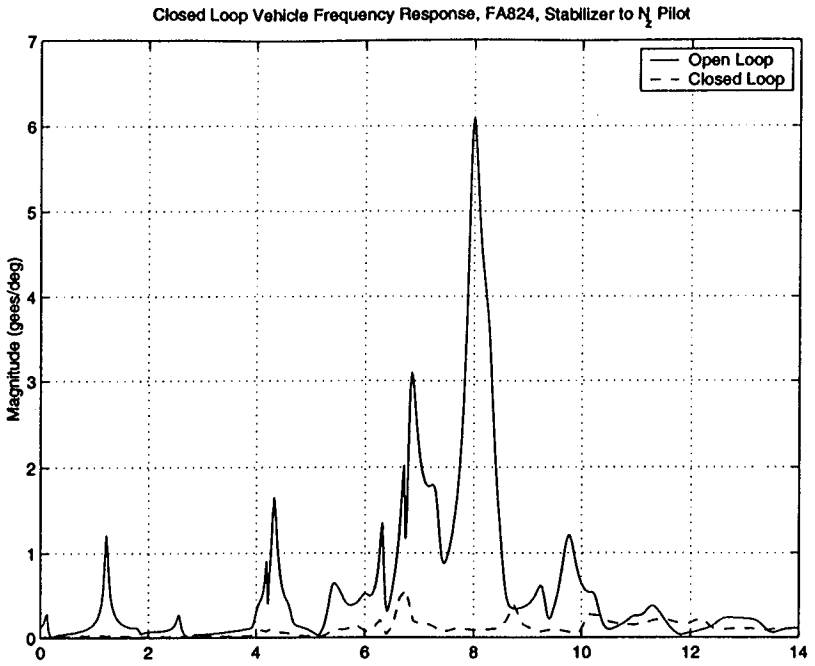

Figure A.1.19: FA824 Closed Loop Frequency Response from Stabilizer to N_z Pilot

A.2 State Space Modeling: The P-transform Method

- Iterative procedure for extracting flutter roots.
- Unsteady aerodynamics approximated by aerodynamics evaluated at the current root being converged upon.
- Traditional method uses eigenvalue extraction.
- Process:
  1. Gather input data: M, K, Q, Φ, k.
  2. Calculate desired viscous damping matrix C.
  3. Governing equation

$$\left(Ms^2 + Cs + K - q_d Q(\hat{s})\right) q(s) = 0 \tag{A.1}$$

  4. Partition M, C, K, and Q into 2×2 blocks corresponding to structural modes and surface deflections. Example:

$$M = \begin{bmatrix} M_{ss} & M_{s\delta_c} \\ M_{\delta_c s} & M_{\delta_c \delta_c} \end{bmatrix} \tag{A.2}$$

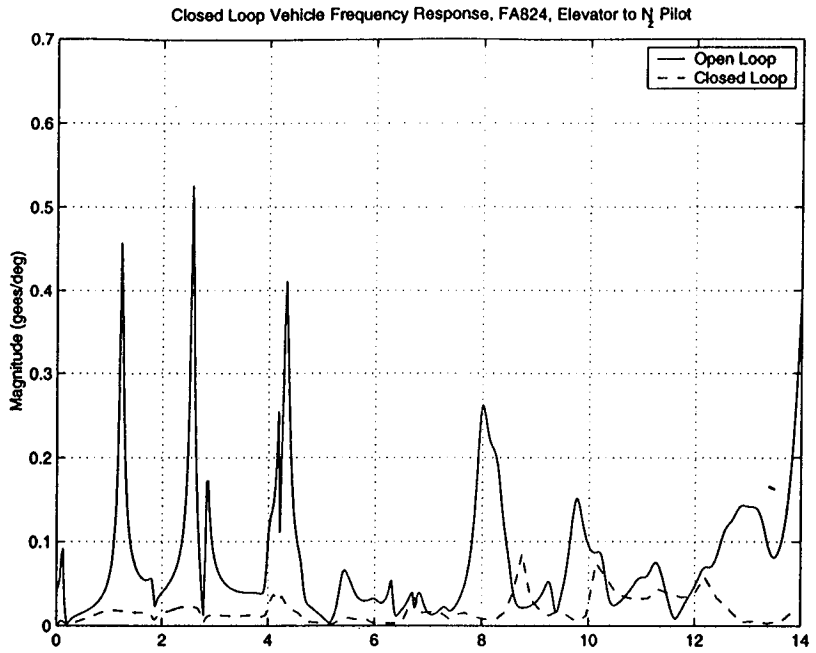

Figure A.1.20: FA824 Closed Loop Frequency Response from Elevator to N_z Pilot

5. Discard lower set of equations involving $(\cdot)_{\delta_c s}$ and $(\cdot)_{\delta_c \delta_c}$ quantities. Yields

$$\left\{M_{ss}s^2 + C_{ss}s + K_{ss} - q_d Q_{ss}(\hat{s})\right\} q_s(s) = -\left\{M_{s\delta_c}s^2 + C_{s\delta_c}s + K_{s\delta_c} - q_d Q_{s\delta_c}(\hat{s})\right\} q_{\delta_c}(s) \quad \text{(A.3)}$$

6. Assume zero damping on all roots

$$q_d Q(\hat{s}) q(s) = q_d Q^R(\hat{s}) q(s) + i q_d Q^I(\hat{s}) q(s) \quad \text{(A.4)}$$

$$q_d Q(\hat{s}) q(t) = q_d Q^R(\hat{s}) q(t) + \frac{i}{s} q_d Q^I(\hat{s}) \dot{q}(t) \quad \text{(A.5)}$$

$$\approx q_d Q^R q(t) + \frac{b}{kV} q_d Q^I(\hat{s}) \dot{q}(t) \quad \text{(A.6)}$$

7. Substitute Eq.(A.6) into Eq.(A.3). Yields new governing equation used throughout PK process

$$\begin{aligned} \ddot{q}_s(t) = {} & M_{ss}^{-1}\left(q_d \frac{b}{kV} Q_{ss}^I - C_{ss}\right) \dot{q}_s(t) \\ & + M_{ss}^{-1}\left(q_d Q_{ss}^R - K_{ss}\right) q_s(t) \\ & - M_{ss}^{-1} M_{s\delta_c} \ddot{q}_{\delta_c}(t) \\ & + M_{ss}^{-1}\left(q_d \frac{b}{kV} Q_{s\delta_c}^I - C_{s\delta_c}\right) \dot{q}_{\delta_c}(t) \\ & + M_{ss}^{-1}\left(q_d Q_{s\delta_c}^R - K_{s\delta_c}\right) q_{\delta_c}(t) \end{aligned} \quad \text{(A.7)}$$

8. Convert Eq.(A.7) to first order state-space form

$$\dot{x} = Ax + Bu \tag{A.8}$$

where

$$A = \begin{bmatrix} M_{ss}^{-1}\left(q_d \frac{b}{kV} Q_{ss}^I - C_{ss}\right) & M_{ss}^{-1}\left(q_d Q_{ss}^R - K_{ss}\right) \\ I & 0 \end{bmatrix} \tag{A.9}$$

$$B = \begin{bmatrix} -M_{ss}^{-1} M_{s\delta_c} & 0 \\ M_{ss}^{-1}\left(q_d \frac{b}{kV} Q_{s\delta_c}^I - C_{s\delta_c}\right) & 0 \\ M_{ss}^{-1}\left(q_d Q_{s\delta_c}^R - K_{s\delta_c}\right) & 0 \end{bmatrix}^T \tag{A.10}$$

$$x = \begin{bmatrix} q_s \\ q_{\delta_c} \end{bmatrix} \quad u = \begin{bmatrix} \ddot{\delta}_c \\ \dot{\delta}_c \\ \delta_c \end{bmatrix} \tag{A.11}$$

9. Now perform PK iteration using A matrix, Eq.(A.9).
   (a) Interpolate Q to current value of i^{th} eigenvalue.
   (b) Form A matrix for interpolated Q.
   (c) Extract eigenvalues (λ) and eigenvectors (ν) of A.
   (d) Compare i_{th} eigenvalue with previous iteration. If difference is large, go to step 9a
   (e) Store converged eigenvalue and eigenvector in Λ and T, respectively.
   (f) Generate in-vacuuo mode $B_{iv} = B$ matrix, Eq.(A.10).
   (g) Transform B_{iv} into in-air mode equivalent $B_{ia} = T^{-1} B_{iv}$. Save row of B_{ia} corresponding to converged root only.
   (h) If not done, goto step 9a and converge on next root.
10. Form in-air A matrix $A_{ia} = \Lambda$
11. Convert final in-air matrices back to in-vacuuo coordinates

$$A_{\text{ptrans}} = A_{iv} = T A_{ia} T^{-1} \tag{A.12}$$

$$B_{\text{ptrans}} = B_{iv} = T B_{ia} \tag{A.13}$$

Equations (A.12) and (A.13) represent the finished p-transform A and B state-space matrices.

12. Form output matrices C and D for output equation

$$y = Cx + Du \tag{A.14}$$

For position and velocity outputs, C is composed of rows of the eigenvector matrix Φ. Acceleration outputs involve differentiating Eq.(A.14).

APPENDIX B

Flutter Analysis Results

Open and Closed Loop for Version_3 Control Laws

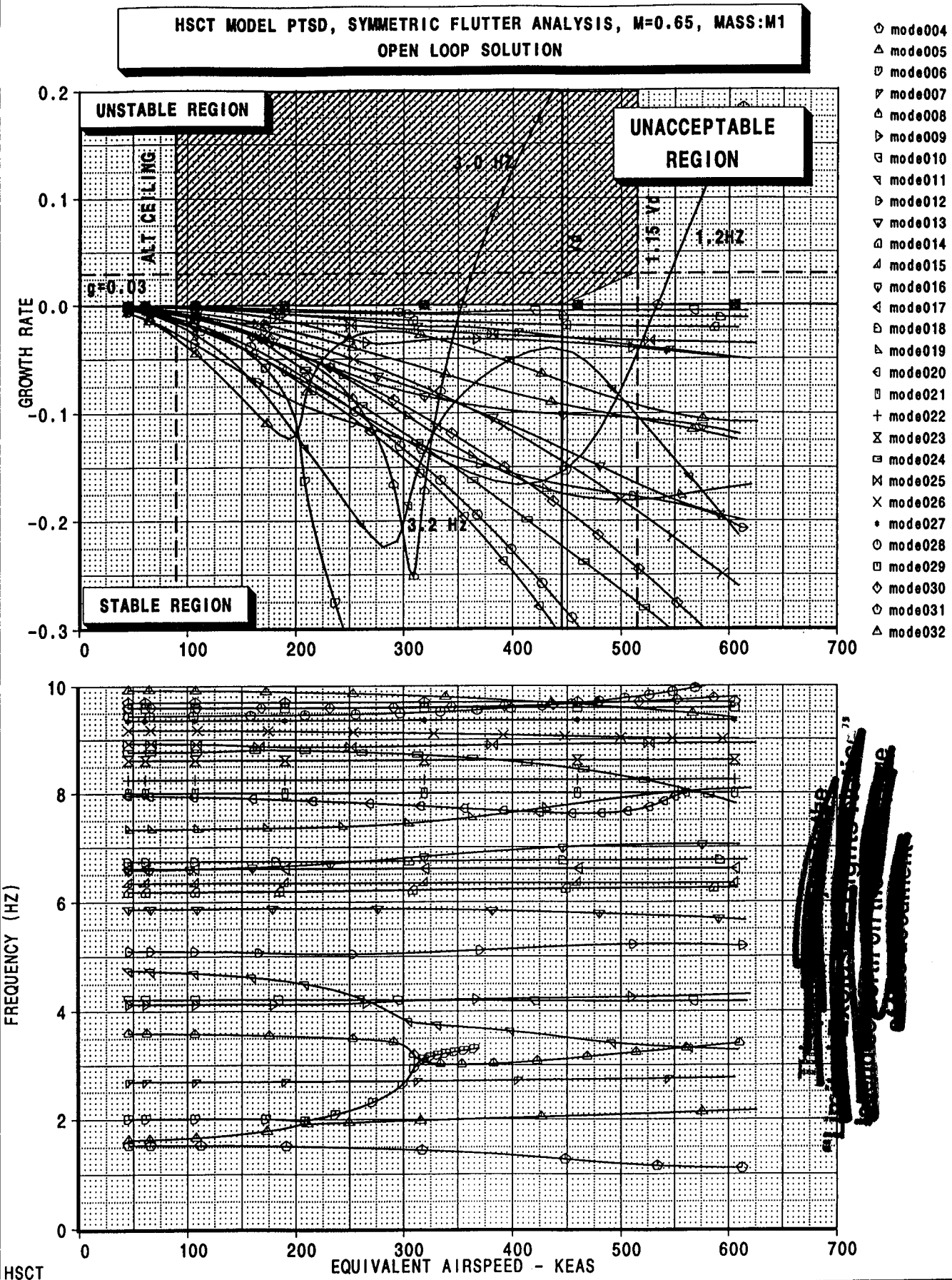

[A]: /acct/ksn8042/ASE/PLOTS/VGPLOTS/mach65.esb
[B]: /acct/ksn8042/ASE/PTC/M65/M1/FLUTLP/COM/DOC1/b86515a6g5eC3xCO.esb

HSCT

CALC	K.S.NAGARAJA	8Jun99	REVISED	DATE	OPEN LOOP SOLUTION STRENGTH SIZED AIRPLANE DITS MODEL PTSD	HSCT FIG B.1
CHECK						
APPD.						
APPD.					BOEING	PAGE 57
PLOT						

HSCT MODEL PTSD, SYMMETRIC FLUTTER ANALYSIS, M=0.65, MASS:MT1
OPEN LOOP SOLUTION

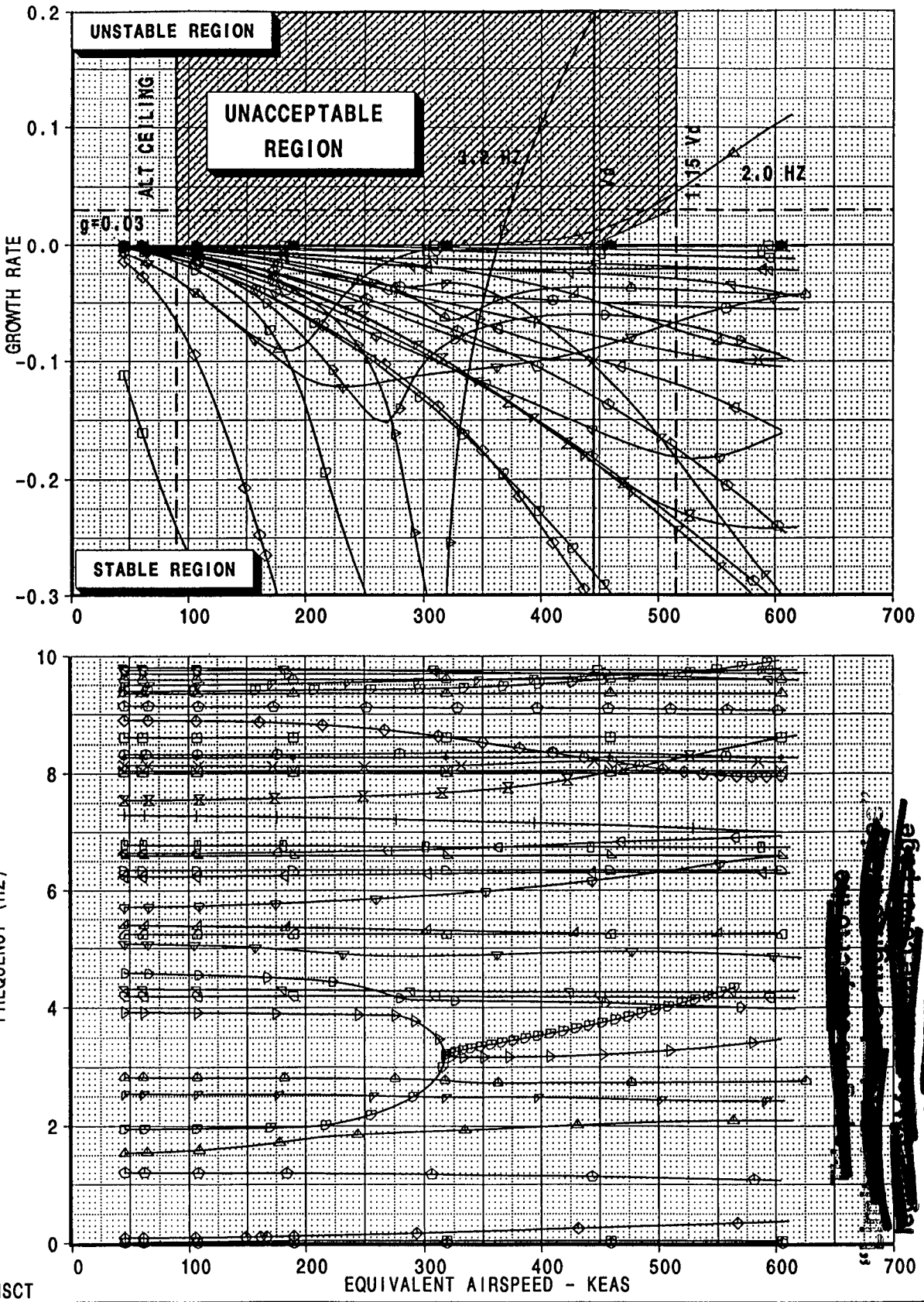

HSCT

[A]: /acct/ksn8042/ASE/PLOTS/VGPLOTS/mach65.esb
[B]: /acct/ksn8042/ASE/PTC/M65/MT1/FLUTLP/COM/DOC1/b865t5a6g5eC3x4_0C0.esb

CALC	K.S.NAGARAJA	12Dec98	REVISED	DATE	OPEN LOOP SOLUTION STRENGTH SIZED AIRPLANE DITS MODEL PTSD	HSCT FIG. B.2
CHECK						
APPD.						
APPD.					BOEING	PAGE 58
PLOT						

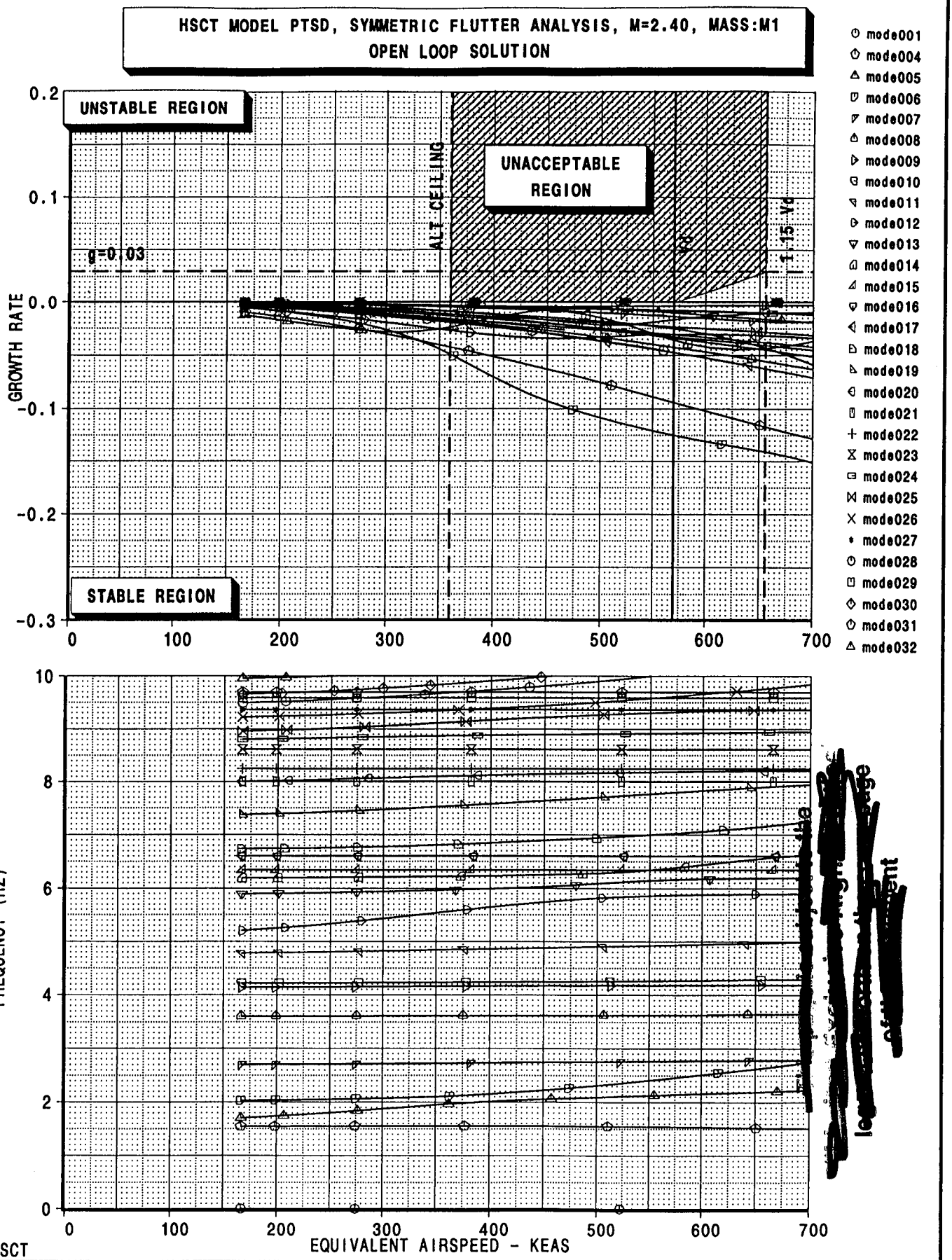

[A]: /acct/ksn8042/ASE/PLOTS/VGPLOTS/mach26.esb
[B]: /acct/ksn8042/ASE/PTC/M24/M1/FLUTLP/COM/DOC1/b865t5a6g5eC3xC0.esb

HSCT

CALC	K.S.NAGARAJA	8Jun99	REVISED	DATE	OPEN LOOP SOLUTION STRENGTH SIZED AIRPLANE DITS MODEL PTSD	HSCT FIG B.3
CHECK						
APPD.						
APPD.					BOEING	PAGE 59
PLOT						

HSCT MODEL PTSD, SYMMETRIC FLUTTER ANALYSIS, M=2.40, MASS:MT1
OPEN LOOP SOLUTION

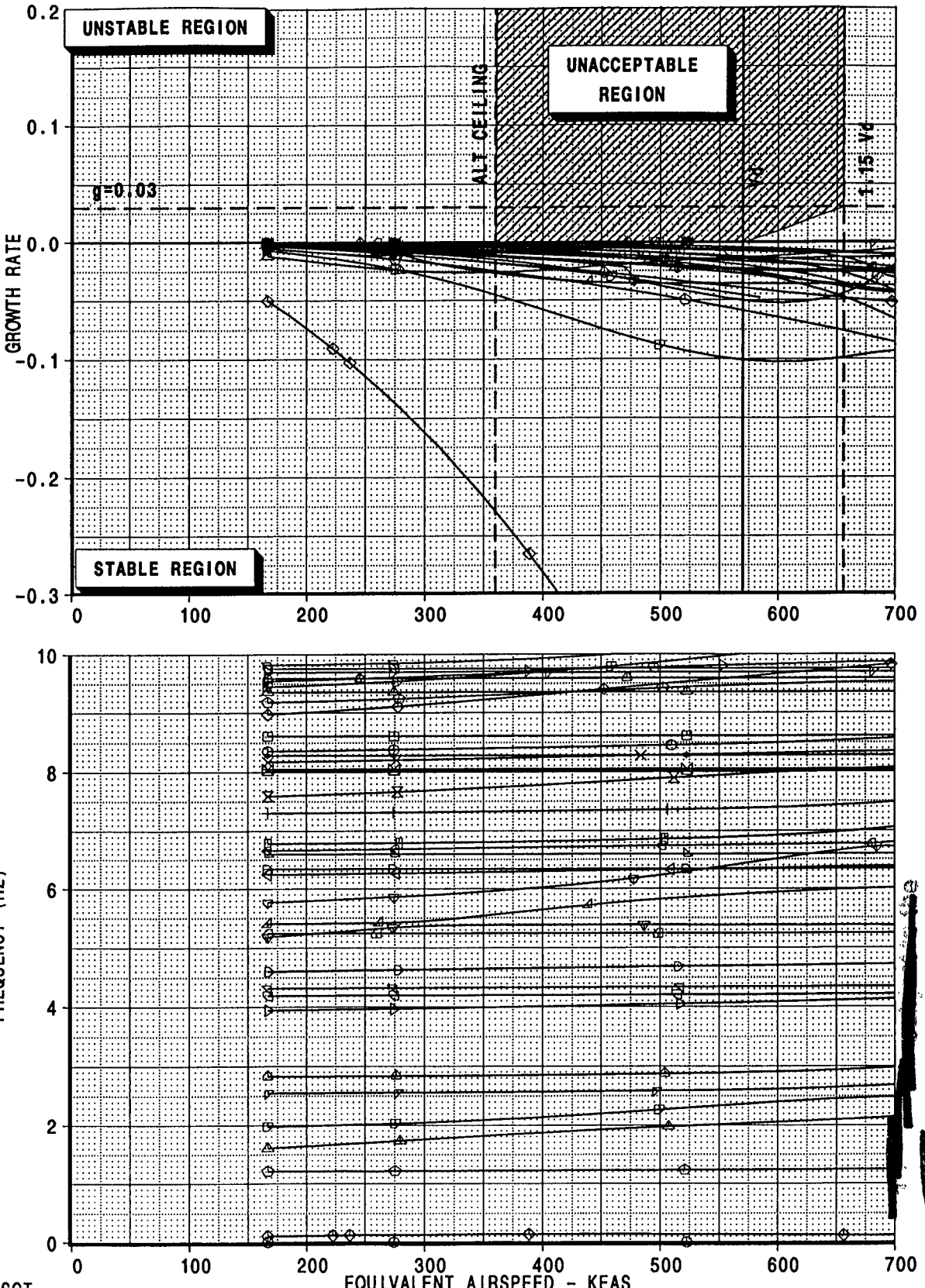

HSCT

[A]: /acct/ksn8042/ASE/PLOTS/VGPLOTS/mach26.esb
[B]: /acct/ksn8042/ASE/PTC/M24/MT1/FLUTLP/COM/DOC1/b86515a6g5eC3x4_OCO.esb

CALC	K.S.NAGARAJA	8Jun99	REVISED	DATE	OPEN LOOP SOLUTION STRENGTH SIZED AIRPLANE DITS MODEL PTSD	HSCT
CHECK						FIG B.4
APPD.						
APPD.					BOEING	PAGE 60
PLOT						

Version 3

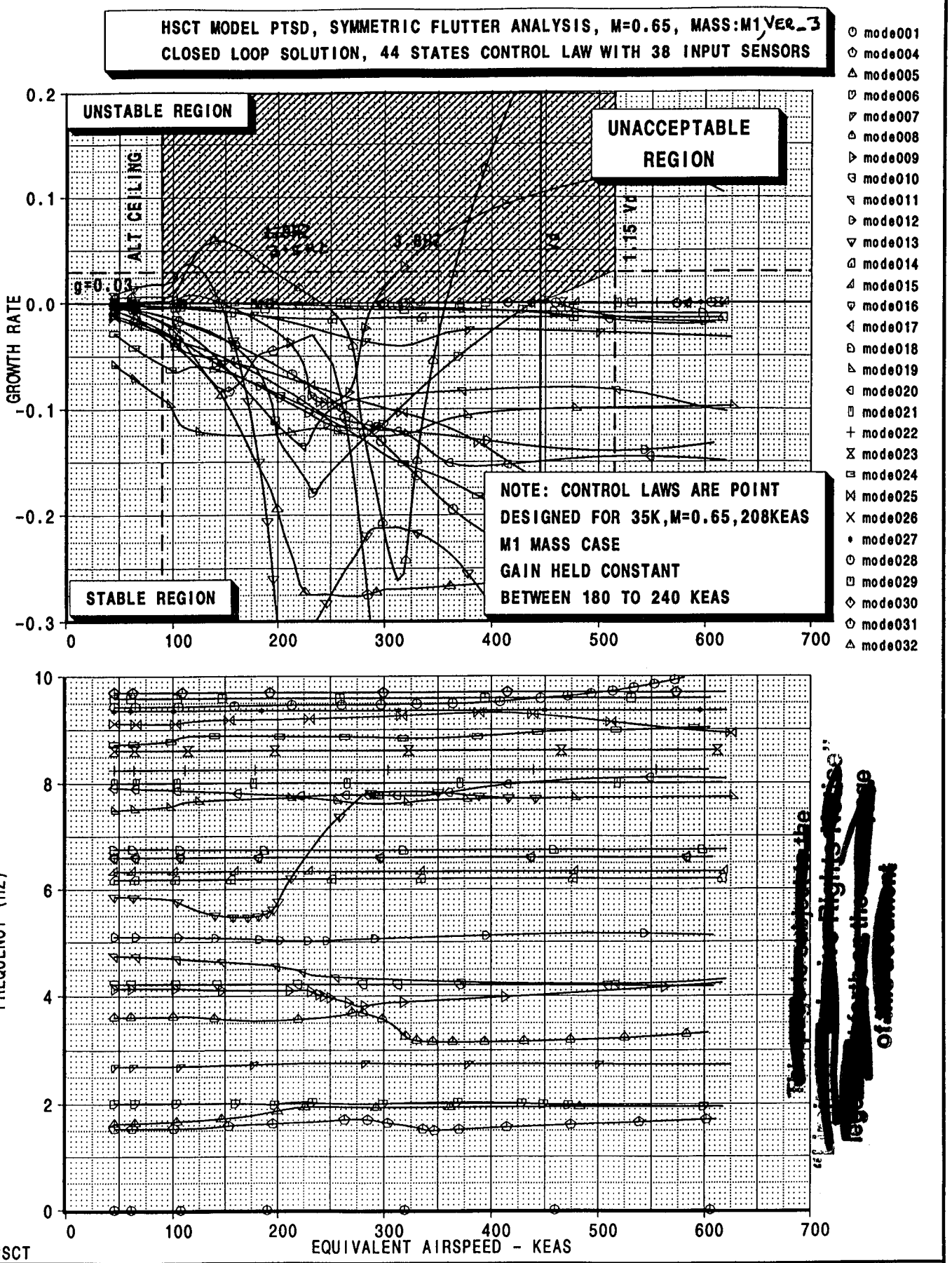

[A]: /acct/ksn8042/ASE/PLOTS/VGPLOTS/mach65.esb
[B]: /acct/ksn8042/ASE/PTC/M65/M1/FLUTLP/COM/DOC1/CL3/IMPR/b86515a6g5eC3x4_1_i1C1.esb

HSCT

CALC	K.S.NAGARAJA	8Jun99	REVISED	DATE	CLOSED LOOP SOLUTION STRENGTH SIZED AIRPLANE DITS MODEL PTSD	HSCT FIG B.5
CHECK						
APPD.						
APPD.					BOEING	PAGE 61
PLOT						

HSCT MODEL PTSD, SYMMETRIC FLUTTER ANALYSIS, M=0.65, MASS:MT1
CLOSED LOOP SOLUTION, 44 STATES CONTROL LAW WITH 38 INPUT SENSORS

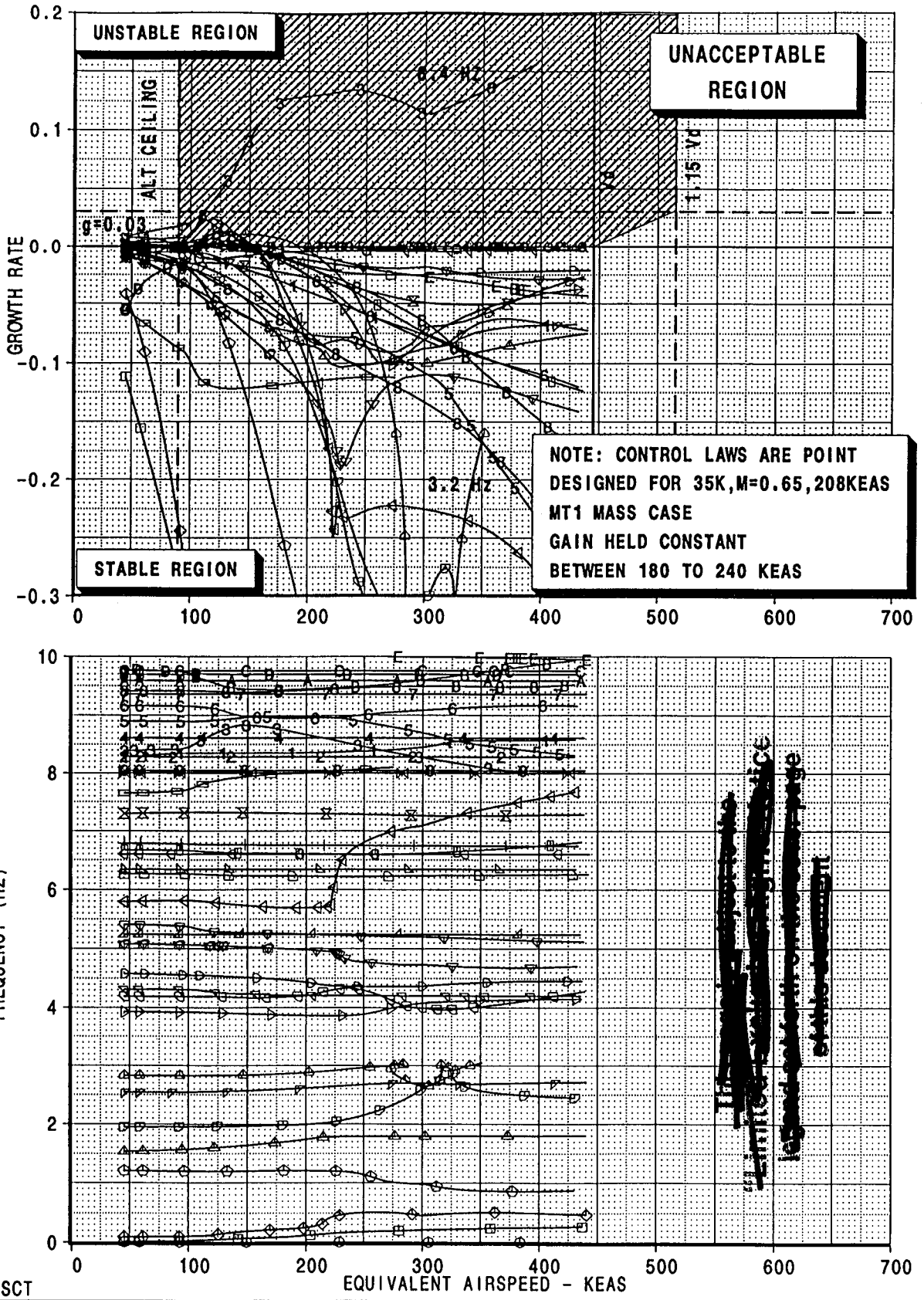

mode001
mode002
mode003
mode004
mode005
mode006
mode007
mode008
mode009
mode010
mode011
mode012
mode013
mode013
mode014
mode015
mode016
mode017
mode018
mode019
mode020
mode021
mode022
mode023
mode024
mode025
mode024
mode025
mode026
mode027
mode028
mode029
mode030
mode031
mode032
mode033
mode034
mode035
mode036
mode037
mode038
mode039
mode040
mode041

HSCT

CALC	K.S.NAGARAJA	12Dec98	REVISED	DATE	CLOSED LOOP SOLUTION STRENGTH SIZED AIRPLANE DITS MODEL PTSD	HSCT FIG 15.6
CHECK						
APPD.						
APPD.						PAGE 62
PLOT					BOEING	

[A]: /acct/ksn8042/ASE/PTC/M65/MT1/FLUTLP/COM/DOC1/CL3 515a6g5eC3x4_1C1.esb
[B]: /acct/ksn8042/ASE/PTC/M65/MT1/FLUTLP/COM/DOC1/CL3/vu65t5a6g5eC3x4_2C1.esb
[C]: /acct/ksn8042/ASE/PTC/M65/MT1/FLUTLP/COM/DOC1/CL3/b865t5a6g5eC3x4_3C1.esb
[D]: /acct/ksn8042/ASE/PTC/M65/MT1/FLUTLP/COM/DOC1/CL3/macnbb.esb

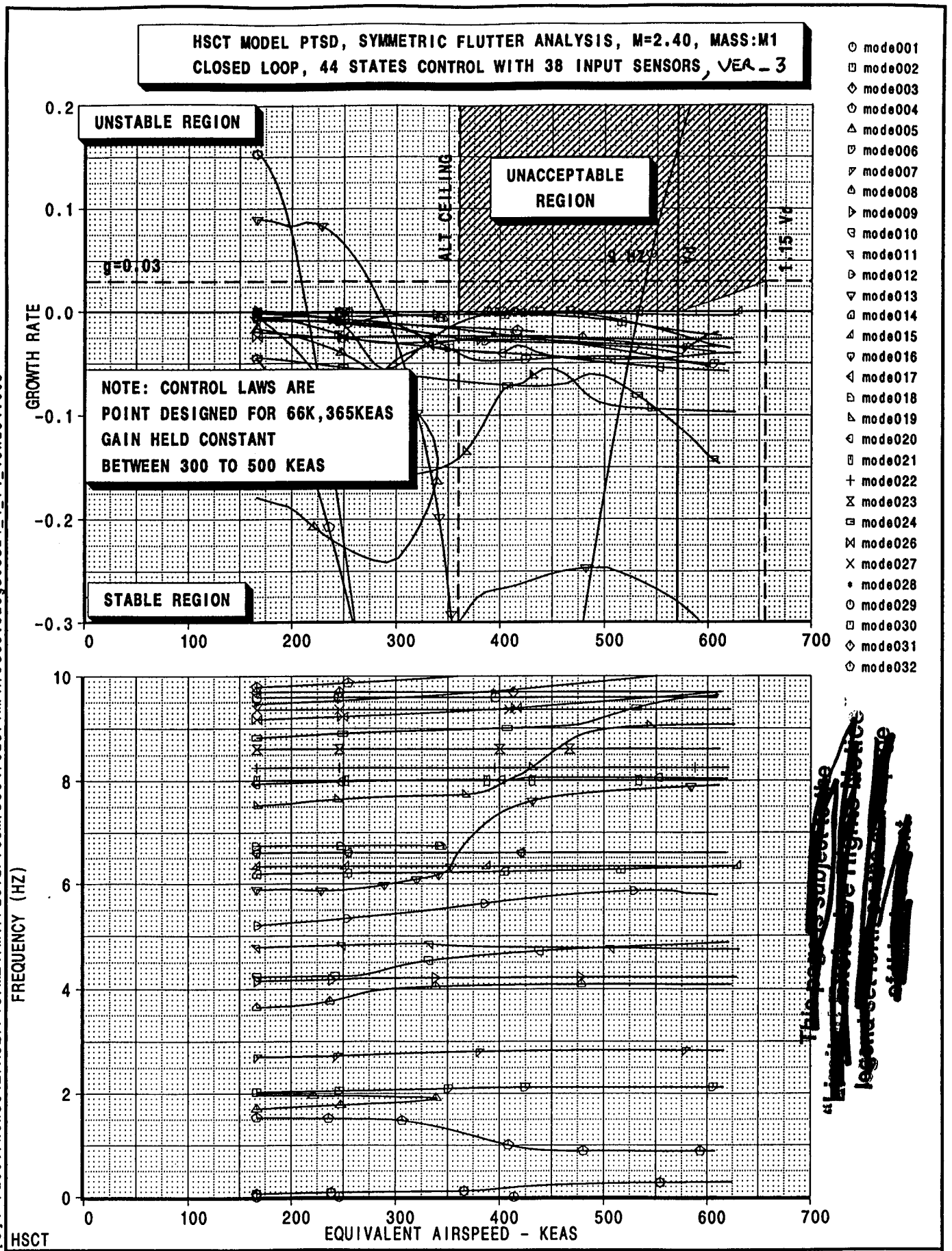

.A]: /acct/ksn8042/ASE/PLOTS/VGPLOTS/mach26.esb
[B]: /acct/ksn8042/ASE/PTC/M24/M1/FLUTLP/COM/DOC1/CL3/IMPR/b86515a6g5eC3x4_1_i1C1.esb
[C]: /acct/ksn8042/ASE/PTC/M24/M1/FLUTLP/COM/DOC1/CL3/IMPR/b86515a6g5eC3z4_1_i1_10hzC1.esb

HSCT

CALC	K.S.NAGARAJA	8Jun99	REVISED	DATE	CLOSED LOOP SOLUTION STRENGTH SIZED AIRPLANE DITS MODEL PTSD	HSCT FIG B.7
CHECK						
APPD.						
APPD.					BOEING	PAGE 63
PLOT						

HSCT MODEL PTSD, SYMMETRIC FLUTTER ANALYSIS, M=2.40, MASS:MT1
CLOSED LOOP, 44 STATES CONTROL WITH 38 INPUT SENSORS, VER_3

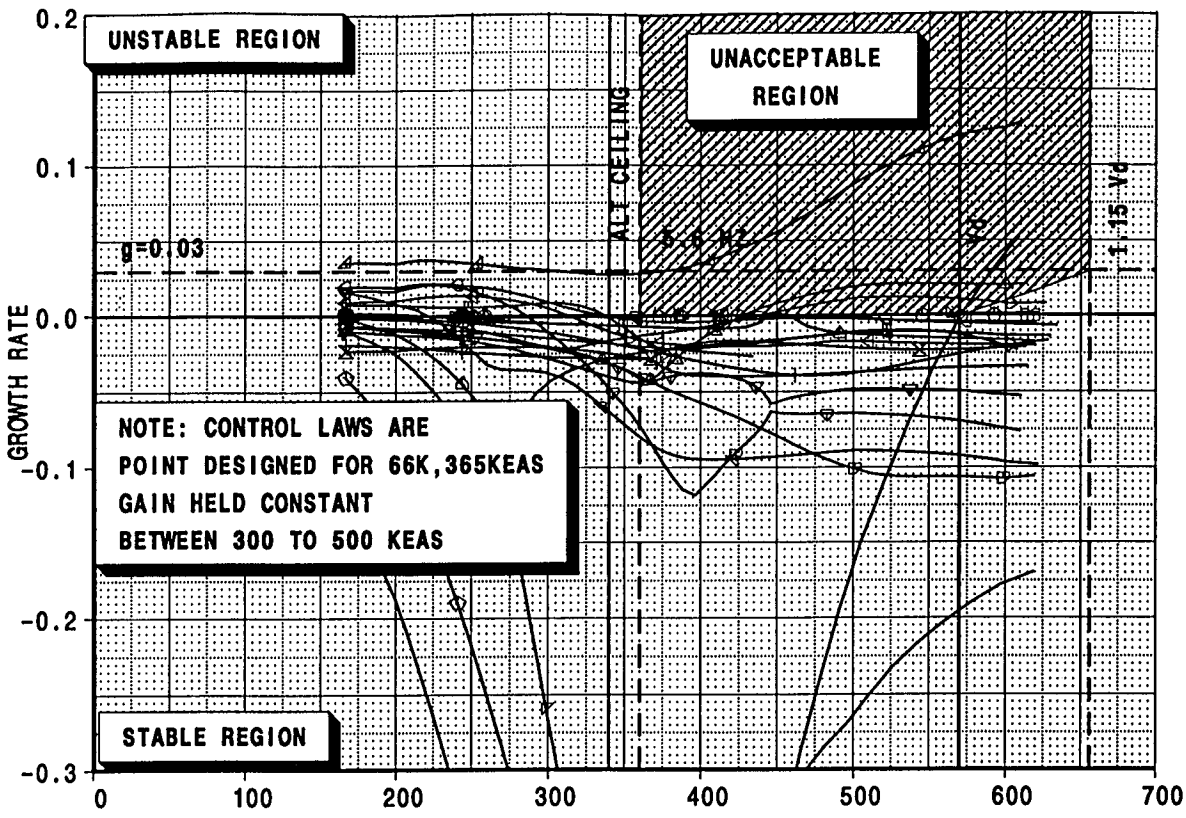

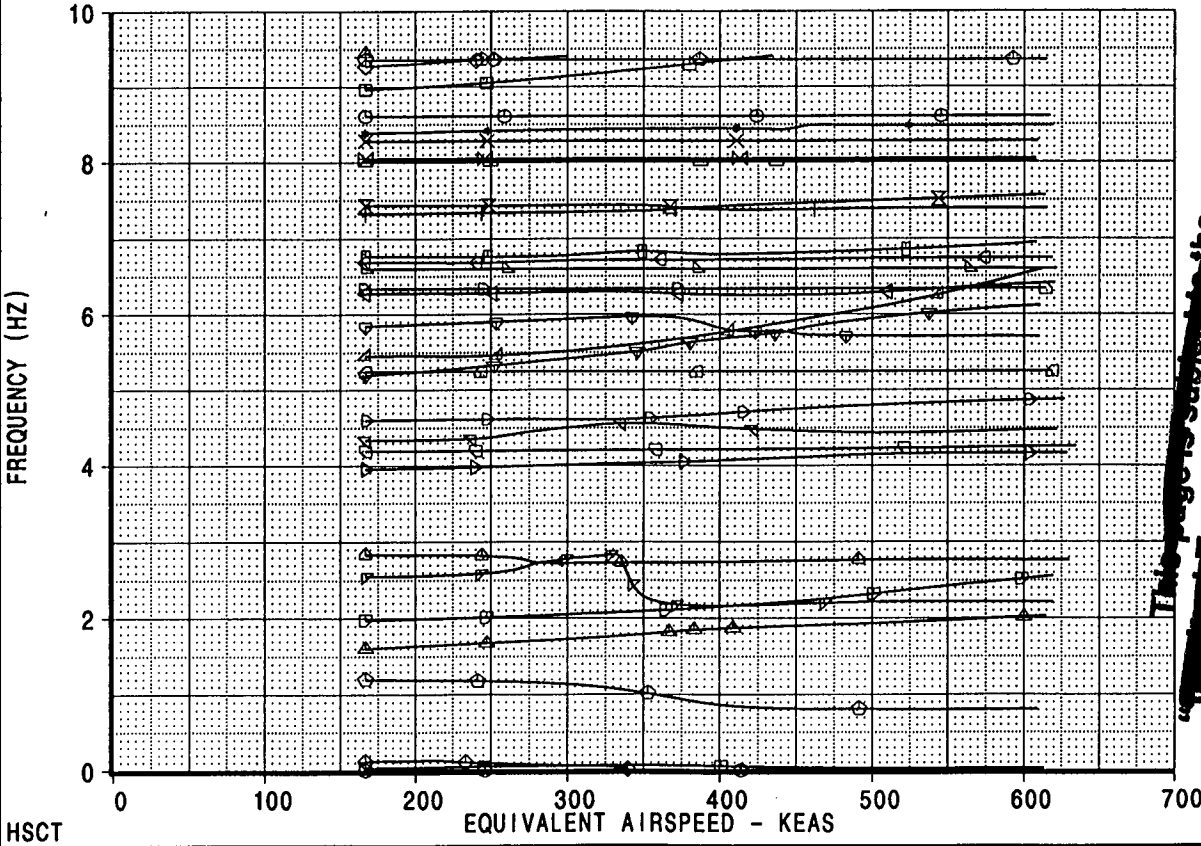

mode001
mode002
mode003
mode004
mode005
mode006
mode007
mode008
mode009
mode010
mode011
mode012
mode013
mode014
mode015
mode016
mode017
mode018
mode019
mode020
mode021
mode022
mode023
mode024
mode025
mode027
mode028
mode029
mode030
mode031
mode032
mode033

[A]: /acct/ksn8042/ASE/PLOTS/VGPLOTS/mach26.esb
[B]: /acct/ksn8042/ASE/PTC/M24/MT1/FLUTLP/COM/DOC1/CL3/IMPR/b865t5a6g5eC3x4_1_i1C1.esb
[C]: /acct/ksn8042/ASE/PTC/M24/MT1/FLUTLP/COM/DOC1/CL3/IMPR/b865t5a6g5eC3x4_1_i1_10hzC1.esb

HSCT

CALC	K.S.NAGARAJA	8Jun99	REVISED	DATE	CLOSED LOOP SOLUTION STRENGTH SIZED AIRPLANE DITS MODEL PTSD	HSCT FIG B.8
CHECK						
APPD.						
APPD.					BOEING	PAGE 64
PLOT						

APPENDIX C

Frequency Response Functions and Cumulative RMS values for Selected Conditions and Locations

WING SHEAR ETA=.100

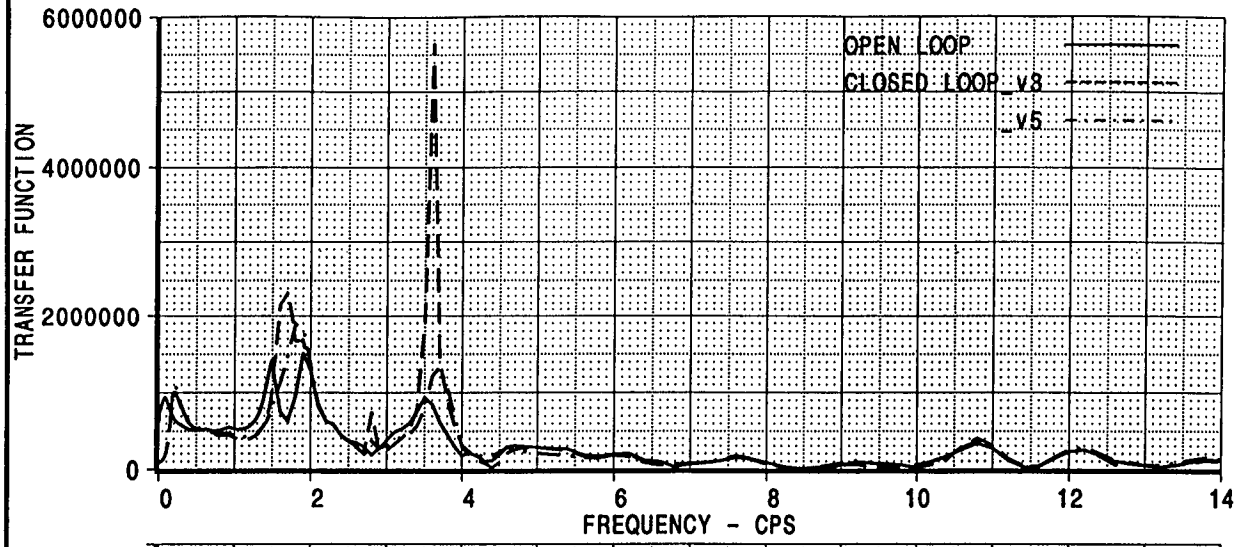

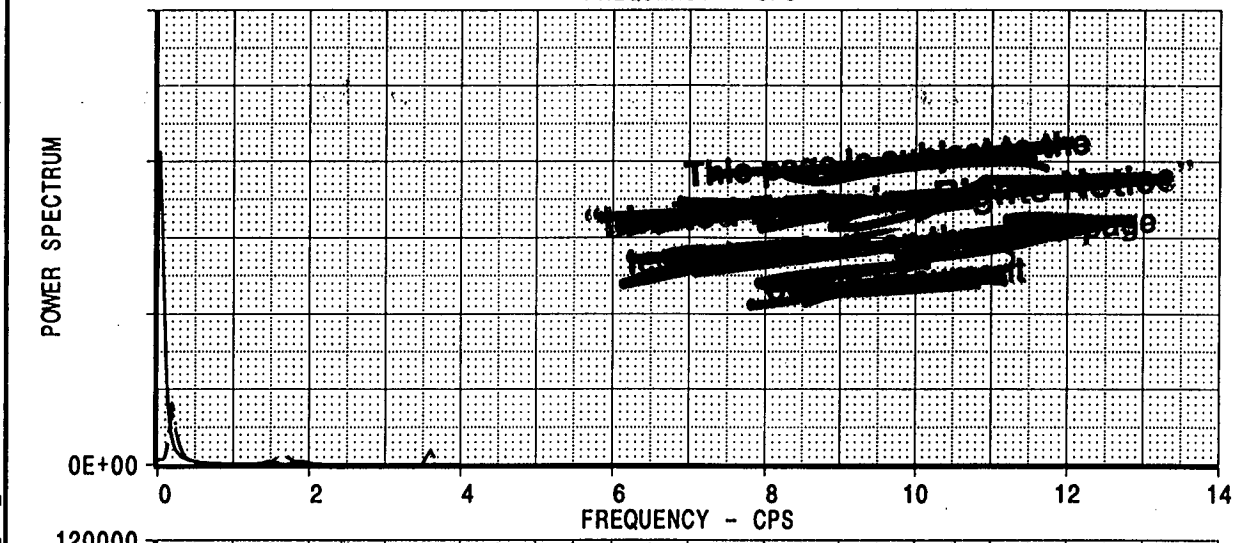

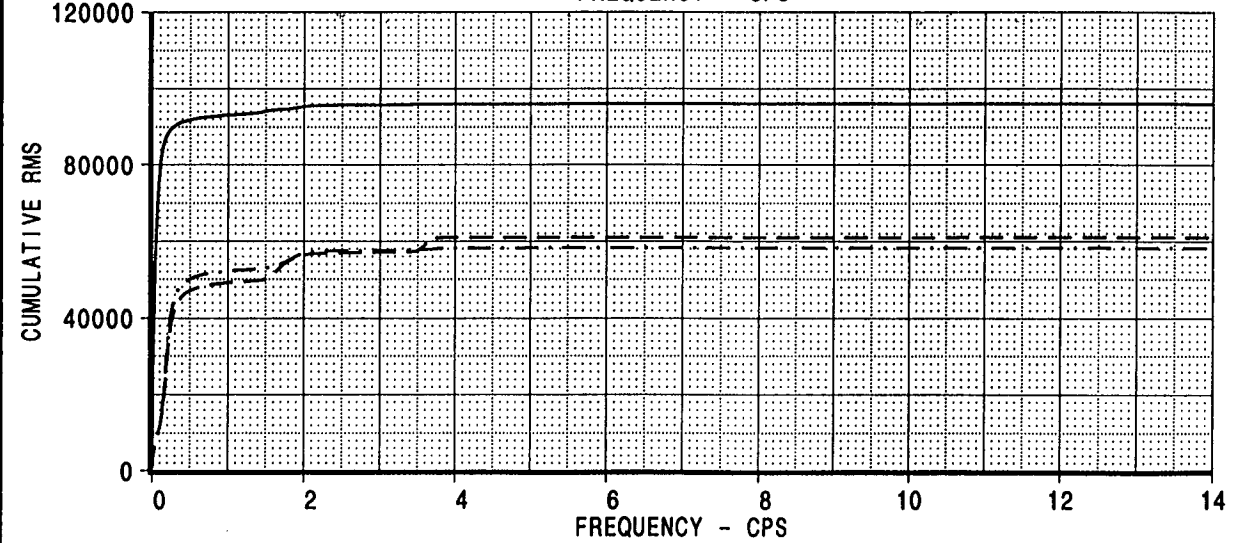

[A]: /acct/ksn8042/SOLVER/psd_gust_M1m0p65.esb
[B]: /acct/ksn8042/SOLVER/psd_gust_M1m0p65_fb.esb
[C]: /acct/ksn8042/SOLVER/psd_gust_M1m0p65_fb_v5.esb

CALC	K.S.NAGARAJA	23Jun99	REVISED	DATE	SYMMETRIC VERTICAL PSD GUST CASE MODEL=MTSD MASS=M1 MACH=0.65 ALT=35K COMPARISON OPEN VERSUS CLOSED LOOP	HSCT FIG C.1
CHECK						
APPD.						
APPD.					BOEING	PAGE 66

WING TORSION ETA=.100

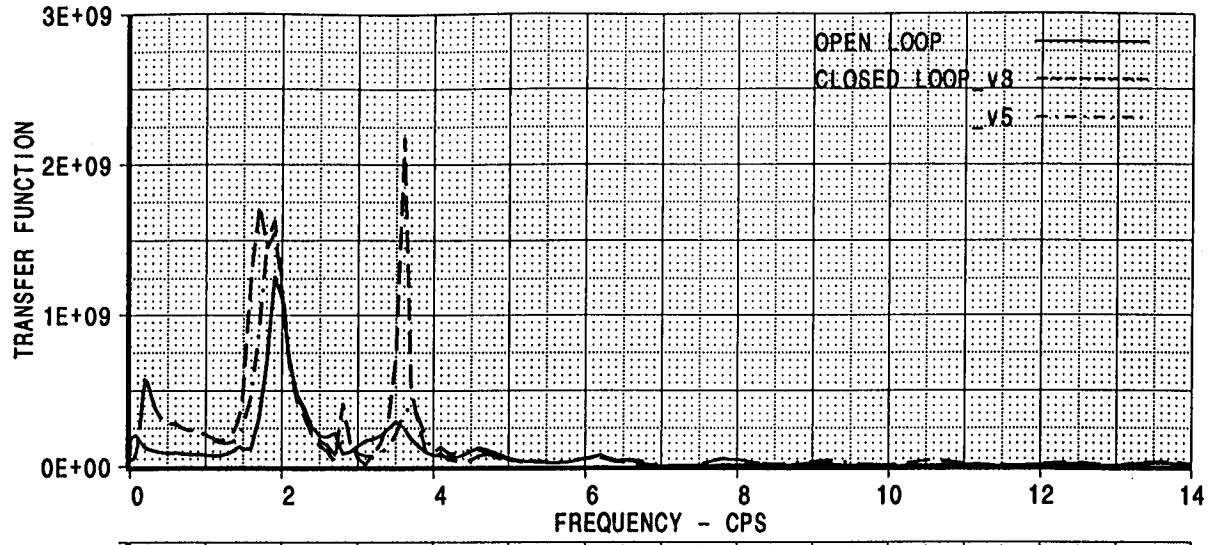

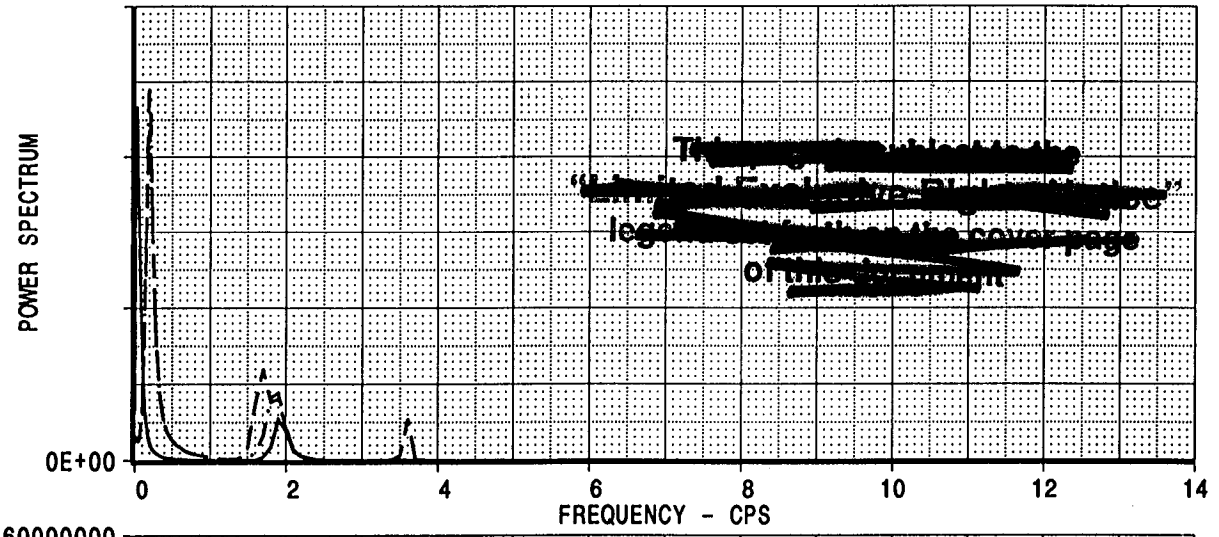

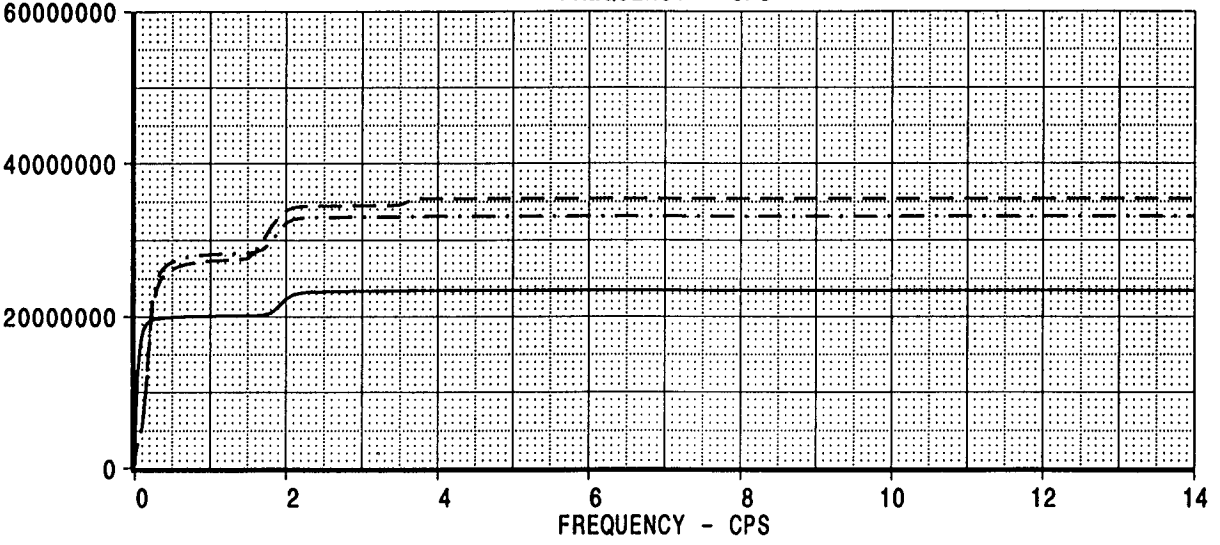

[A]: /acct/ksn8042/SOLVER/psd_gust_M1m0p65.esb
[B]: /acct/ksn8042/SOLVER/psd_gust_M1m0p65_fb.esb
[C]: /acct/ksn8042/SOLVER/psd_gust_M1m0p65_fb_v5.esb

CALC	K.S.NAGARAJA	23Jun99	REVISED	DATE	SYMMETRIC VERTICAL PSD GUST CASE MODEL=MTSD MASS=M1 MACH=0.65 ALT=35K COMPARISON OPEN VERSUS CLOSED LOOP	HSCT FIG C.2
CHECK						
APPD.						
APPD.					BOEING	PAGE 67

FUSELAGE MOMENT BS=650

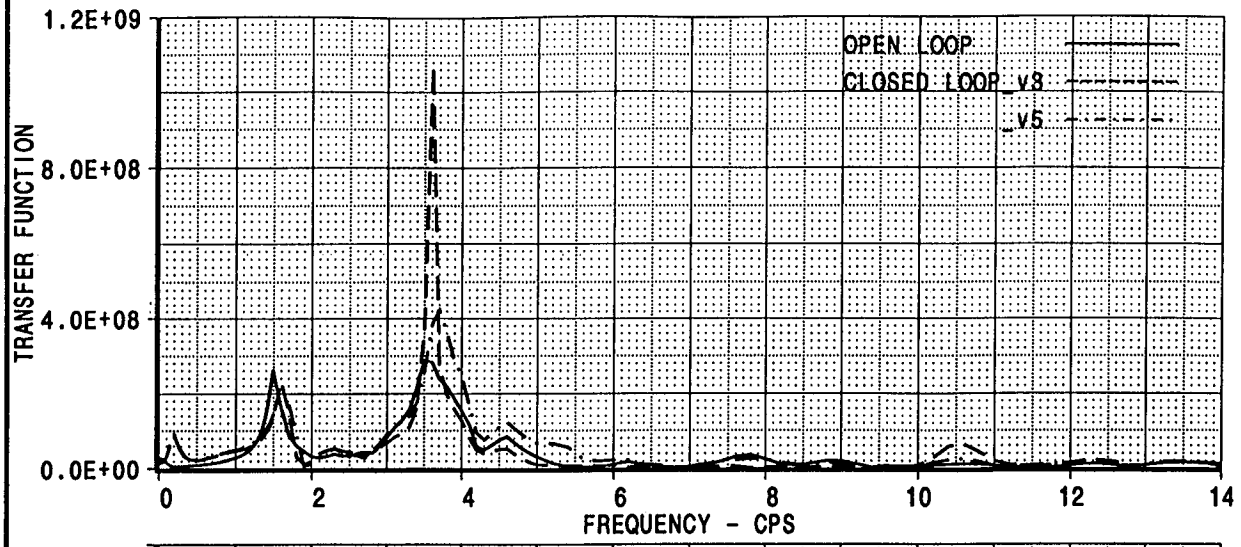

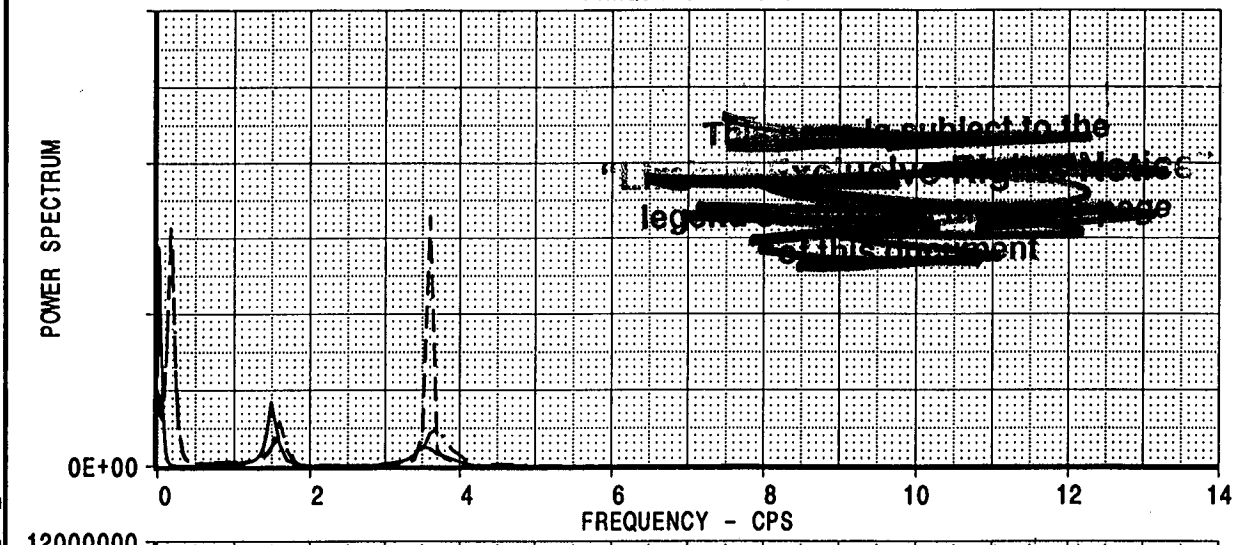

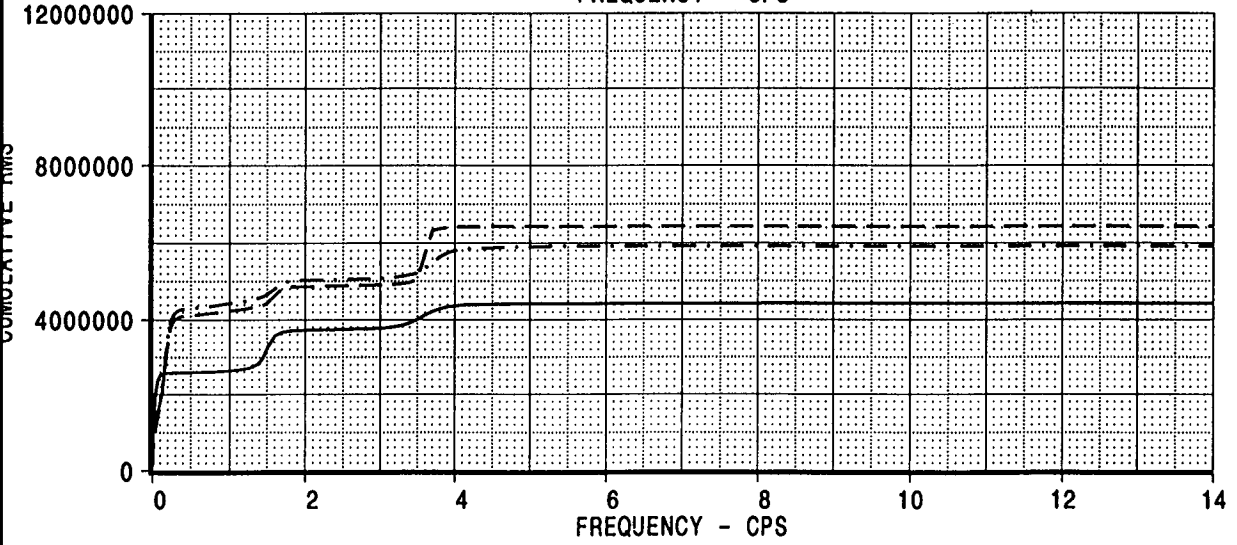

[A]: /acct/ksn8042/SOLVER/psd_gust_M1m0p65.esb
[B]: /acct/ksn8042/SOLVER/psd_gust_M1m0p65_fb.esb
[C]: /acct/ksn8042/SOLVER/psd_gust_M1m0p65_fb_v5.esb

CALC	K.S.NAGARAJA	23Jun99	REVISED	DATE	SYMMETRIC VERTICAL PSD GUST CASE	HSCT
CHECK					MODEL=MTSD MASS=M1 MACH=0.65 ALT=35K	
APPD.					COMPARISON OPEN VERSUS CLOSED LOOP	FIG C.3
APPD.					BOEING	PAGE 68

WING SHEAR ETA=.100

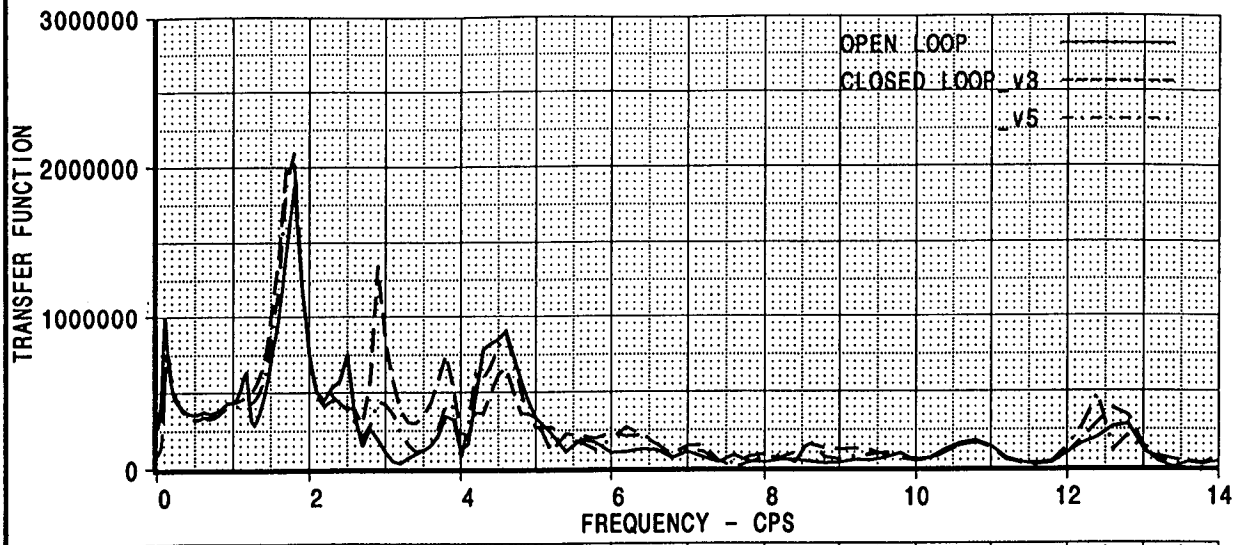

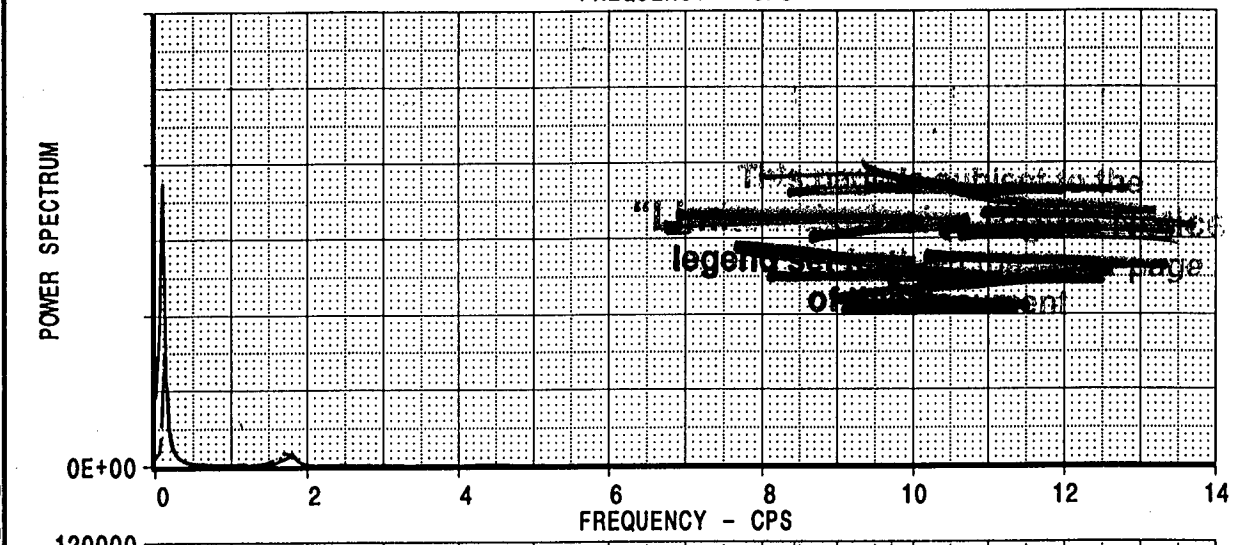

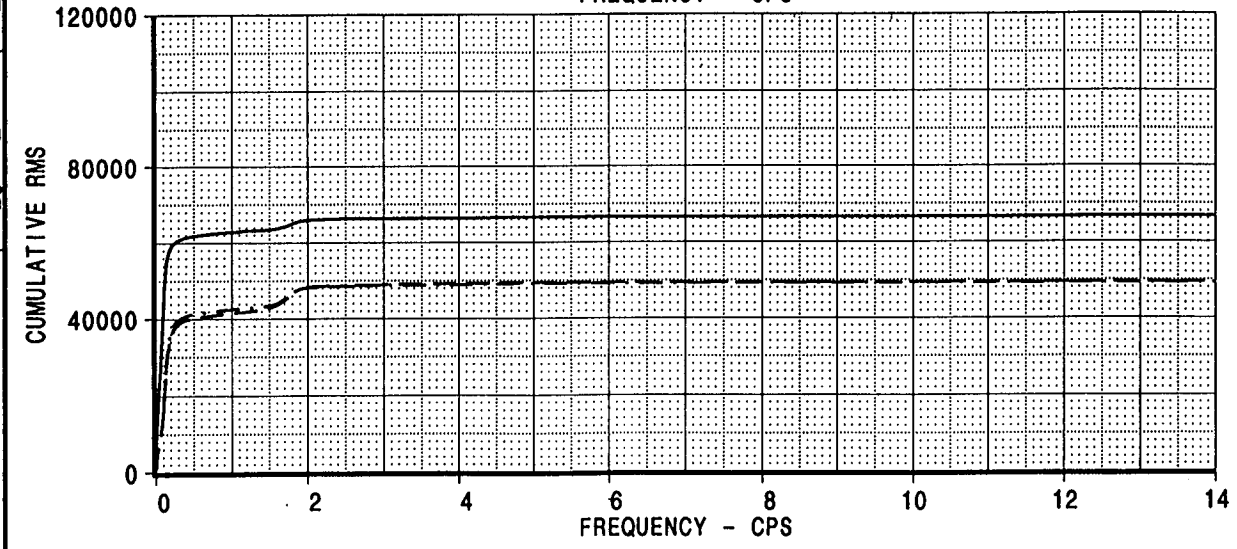

[A]: /acct/ksn8042/SOLVER/psd_gust_MT1m0p65.esb
[B]: /acct/ksn8042/SOLVER/psd_gust_MT1m0p65_fb.esb
[C]: /acct/ksn8042/SOLVER/psd_gust_MT1m0p65_fb_v5.esb

CALC	K.S.NAGARAJA	23Jun99	REVISED	DATE	SYMMETRIC VERTICAL PSD GUST CASE MODEL=MTSD MASS=MT1 MACH=0.65 ALT=35K COMPARISON OPEN VERSUS CLOSED LOOP	HSCT
CHECK						FIG C.4
APPD.						
APPD.					BOEING	PAGE 69

WING TORSION ETA=.100

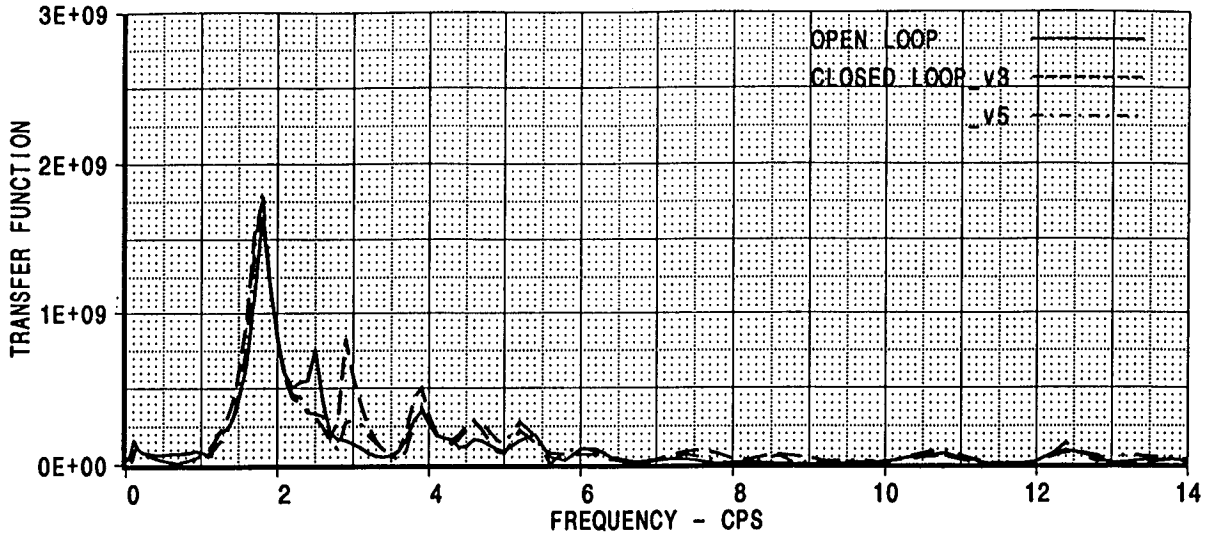

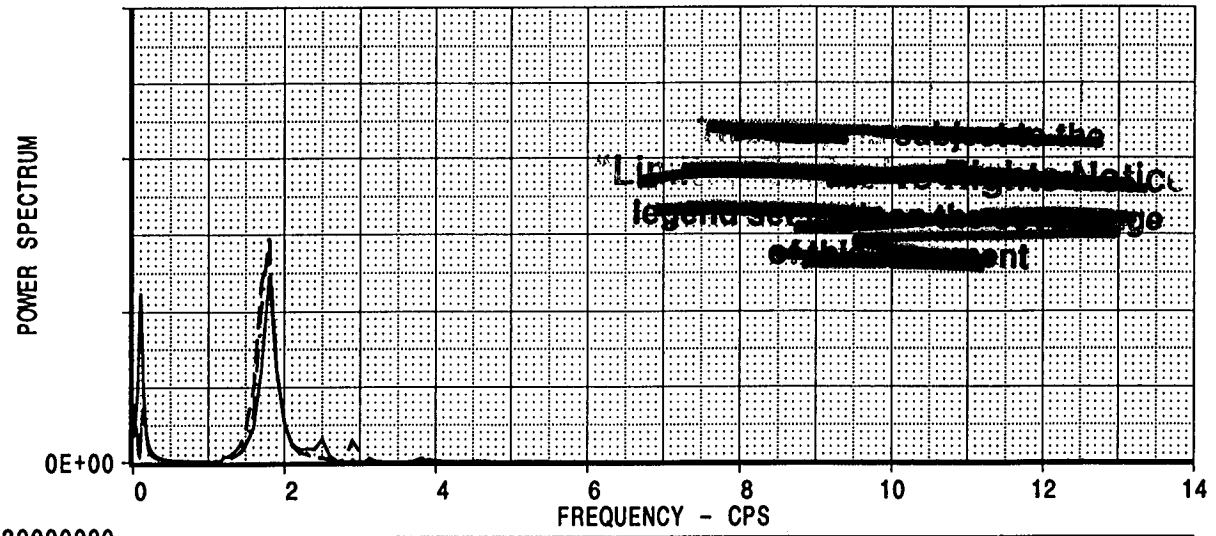

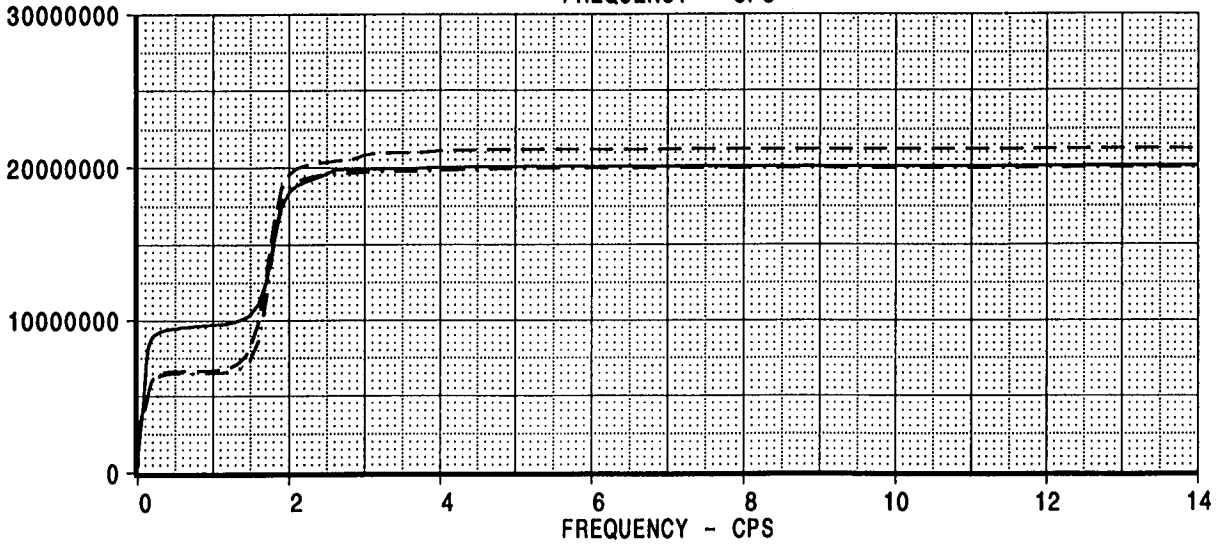

[A]: /acct/ksn8042/SOLVER/psd_gust_MT1m0p65.esb
[B]: /acct/ksn8042/SOLVER/psd_gust_MT1m0p65_fb.esb
[C]: /acct/ksn8042/SOLVER/psd_gust_MT1m0p65_fb_v5.esb

CALC	K.S.NAGARAJA	23Jun99	REVISED	DATE	SYMMETRIC VERTICAL PSD GUST CASE	HSCT
CHECK					MODEL=MTSD MASS=MT1 MACH=0.65 ALT=35K	FIG C.5
APPD.					COMPARISON OPEN VERSUS CLOSED LOOP	
APPD.					BOEING	PAGE 70

FUSELAGE MOMENT BS=650

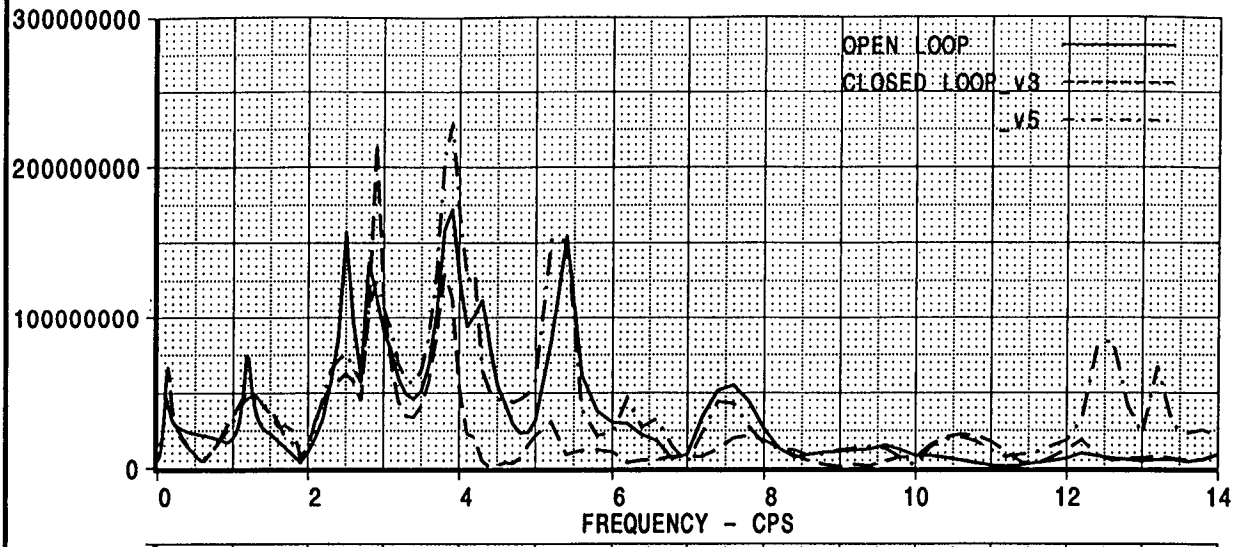

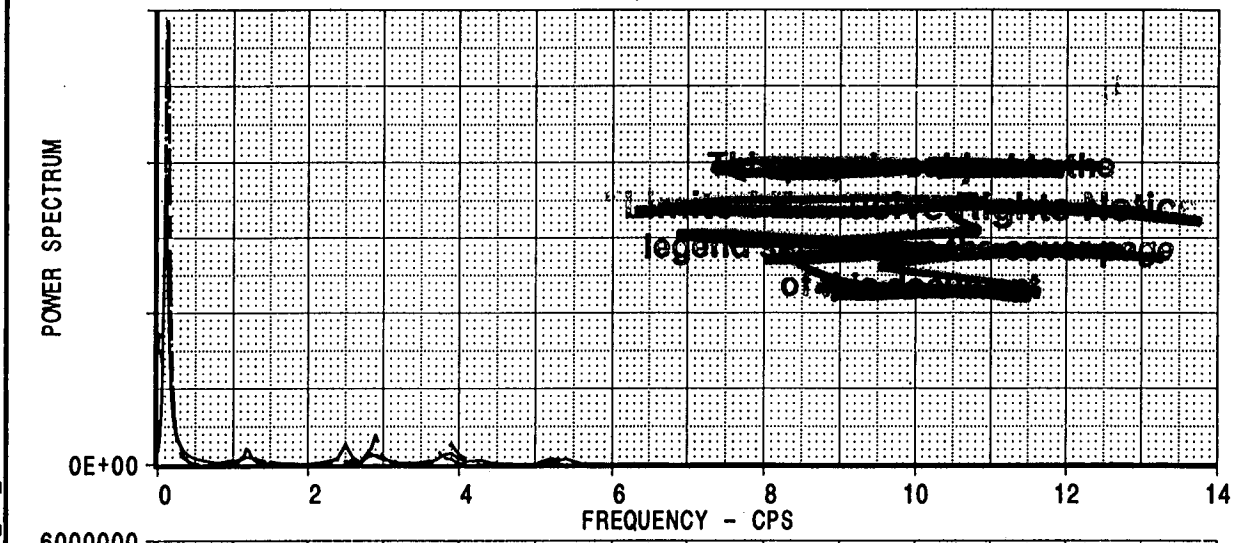

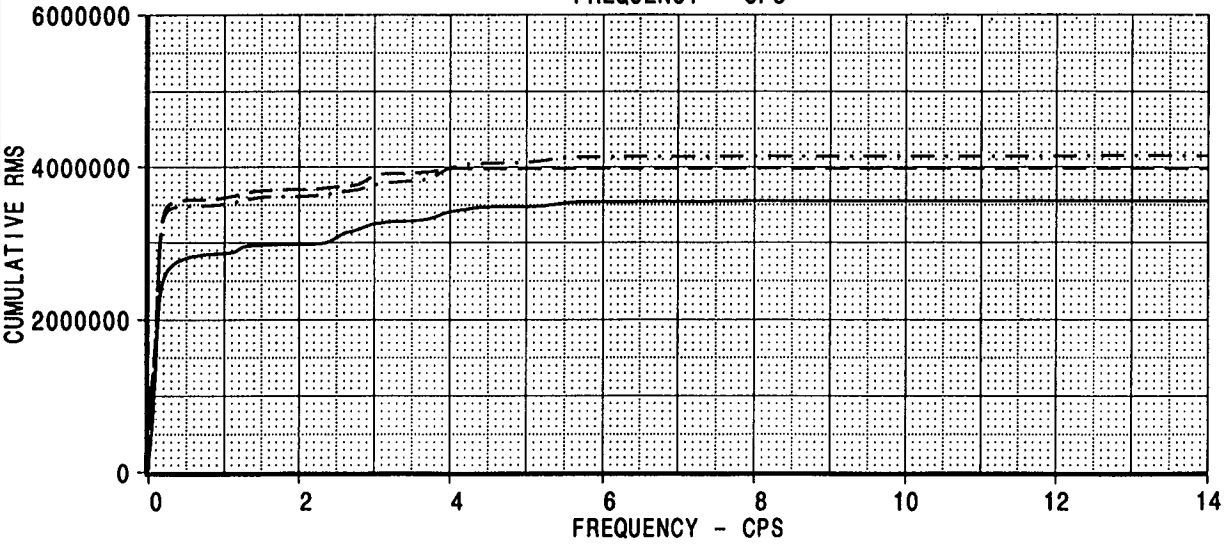

[A]: /acct/ksn8042/SOLVER/psd_gust_MT1m0p65.esb
[B]: /acct/ksn8042/SOLVER/psd_gust_MT1m0p65_fb.esb
[C]: /acct/ksn8042/SOLVER/psd_gust_MT1m0p65_fb_v5.esb

CALC	K.S.NAGARAJA	23Jun99	REVISED	DATE	SYMMETRIC VERTICAL PSD GUST CASE	HSCT
CHECK					MODEL=MTSD MASS=MT1 MACH=0.65 ALT=35K	FIG C.6
APPD.					COMPARISON OPEN VERSUS CLOSED LOOP	
APPD.					BOEING	PAGE 71

WING SHEAR ETA=.100

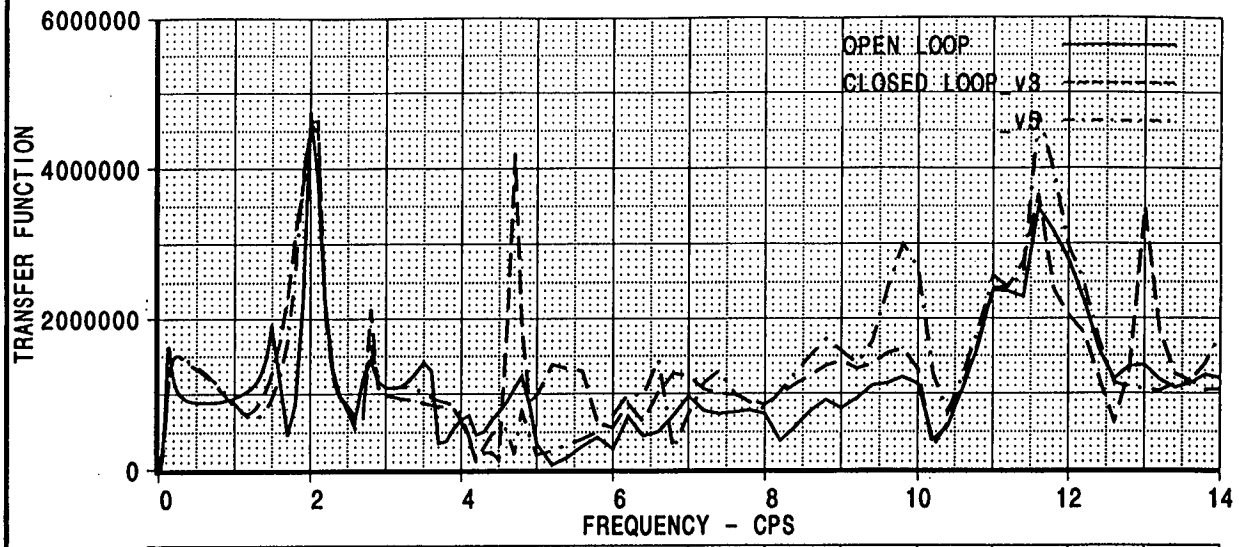

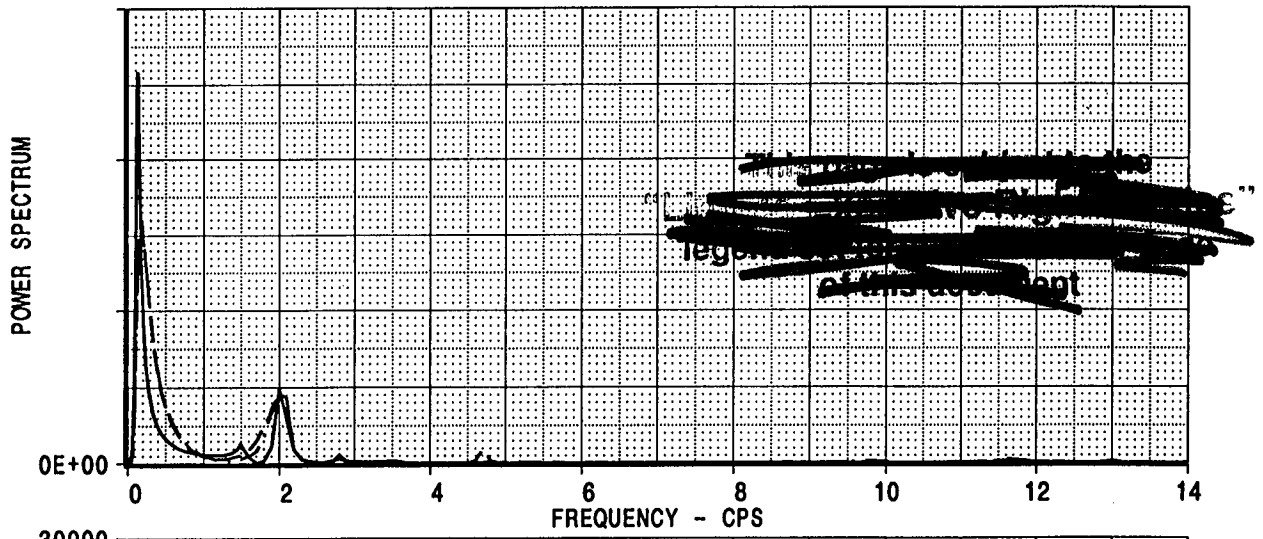

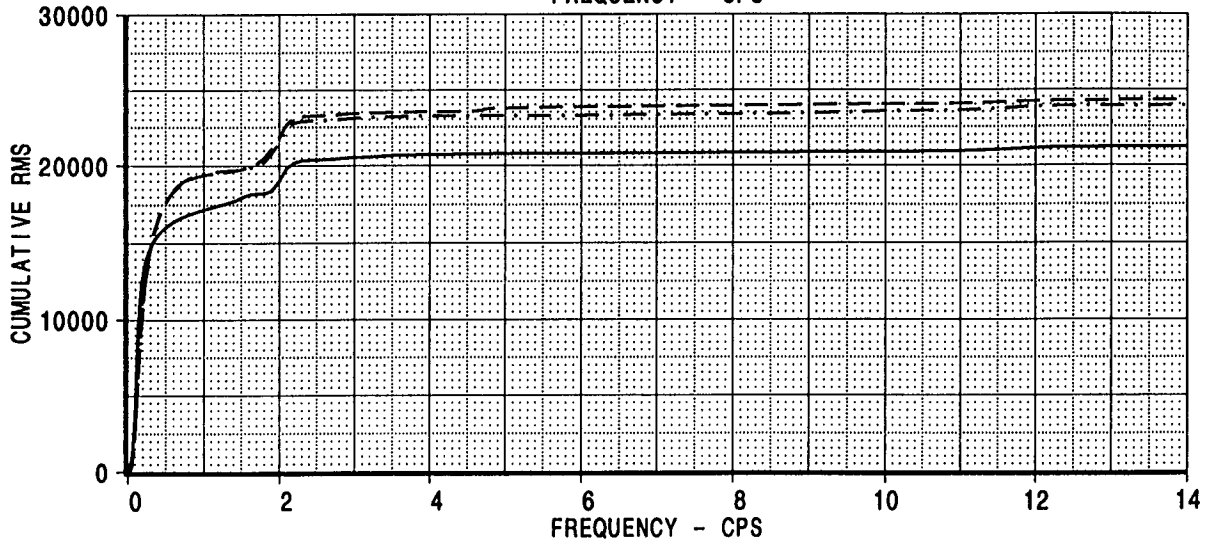

[A]: /acct/ksn8042/SOLVER/psd_gust_M1m2p40.esb
[B]: /acct/ksn8042/SOLVER/psd_gust_M1m2p40_fb.esb
[C]: /acct/ksn8042/SOLVER/psd_gust_M1m2p40_fb_v5.esb

CALC	K.S.NAGARAJA	23Jun99	REVISED	DATE	SYMMETRIC VERTICAL PSD GUST CASE	HSCT
CHECK					MODEL=MTSD MASS=M1 MACH=2.40 ALT=66K	FIG C.7
APPD.					COMPARISON OPEN VERSUS CLOSED LOOP	
APPD.					BOEING	PAGE 72

WING TORSION ETA=.100

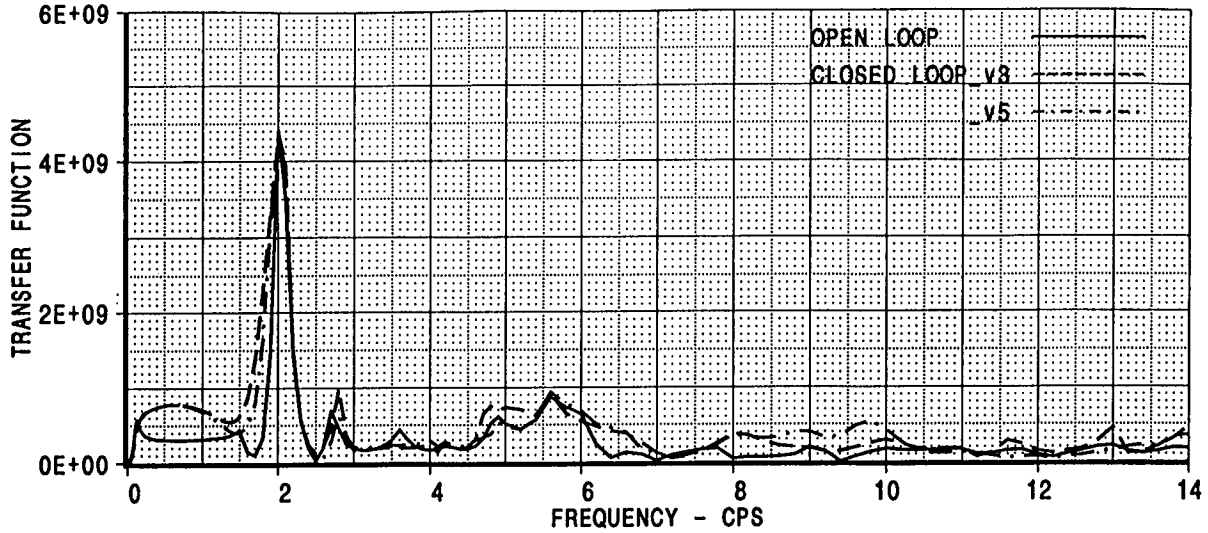

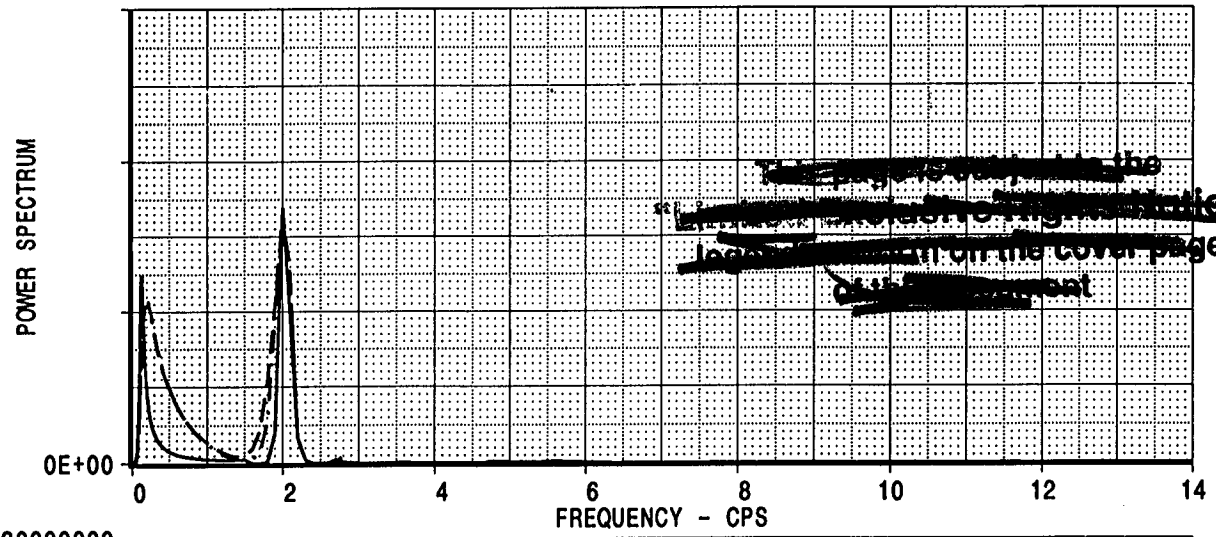

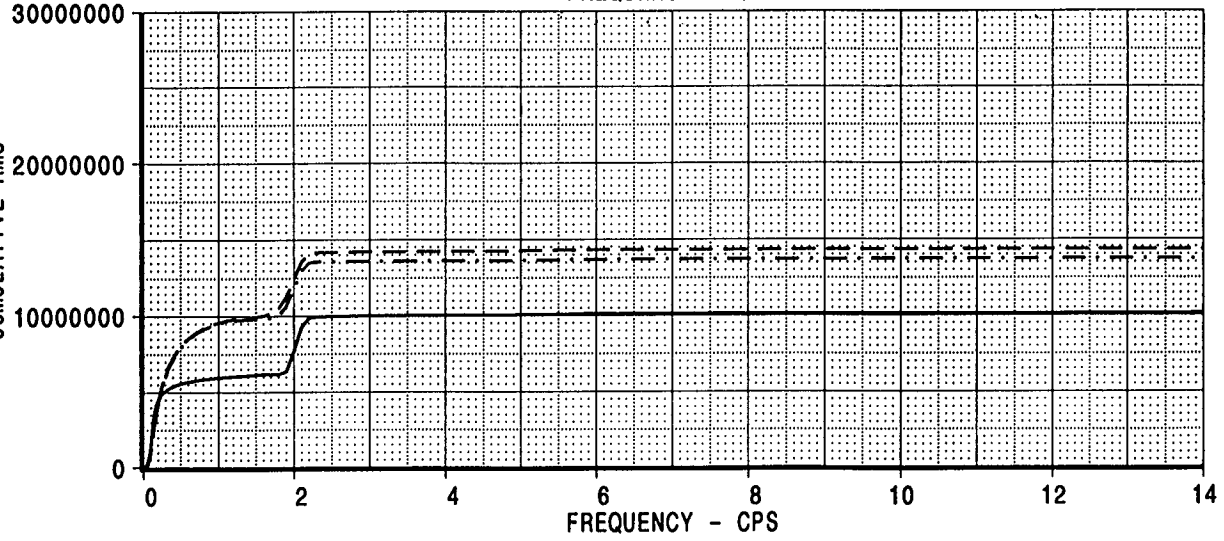

[redacted]

.A]: /acct/ksn8042/SOLVER/psd_gust_M1m2p40.esb
[B]: /acct/ksn8042/SOLVER/psd_gust_M1m2p40_fb.esb
[C]: /acct/ksn8042/SOLVER/psd_gust_M1m2p40_fb_v5.esb

CALC	K.S.NAGARAJA	23Jun99	REVISED	DATE	SYMMETRIC VERTICAL PSD GUST CASE	HSCT
CHECK					MODEL=MTSD MASS=M1 MACH=2.40 ALT=66K	FIG C.8
APPD.					COMPARISON OPEN VERSUS CLOSED LOOP	
APPD.					BOEING	PAGE 73

FUSELAGE MOMENT BS=650

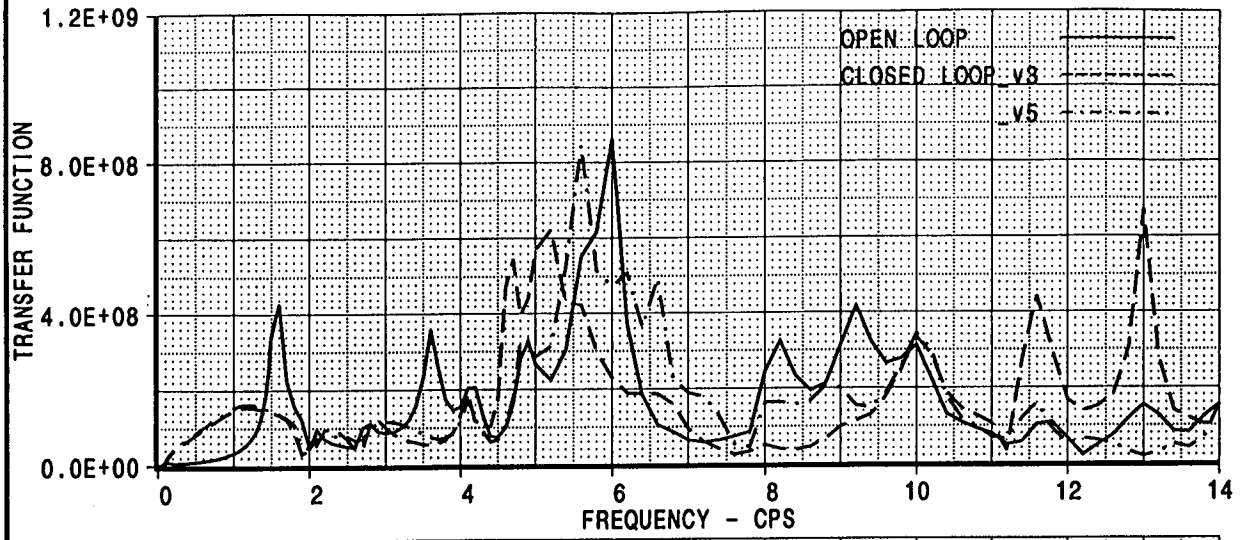

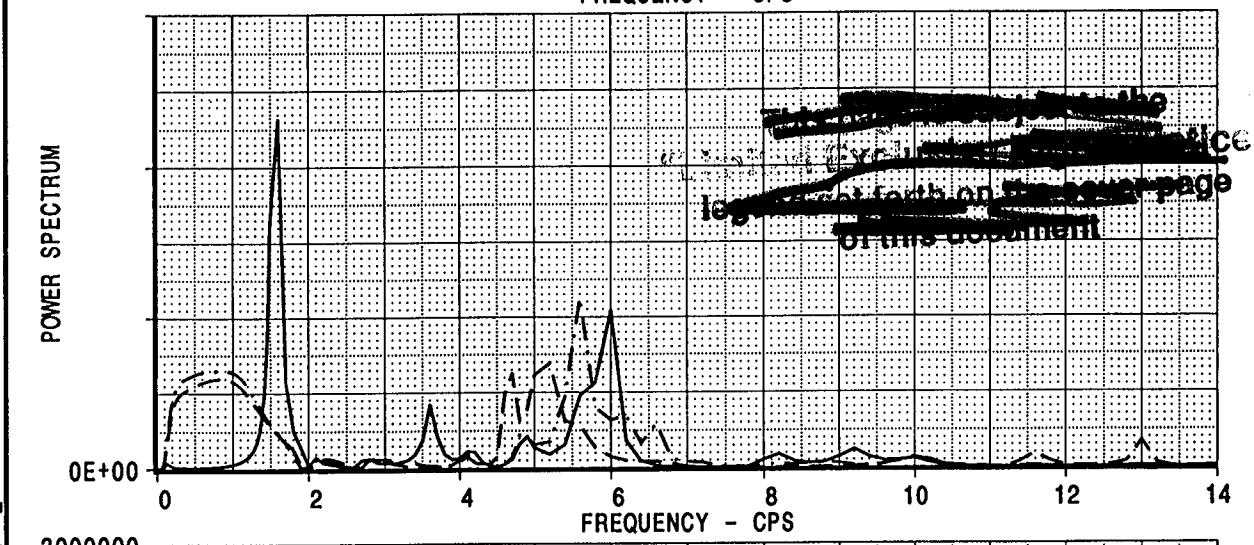

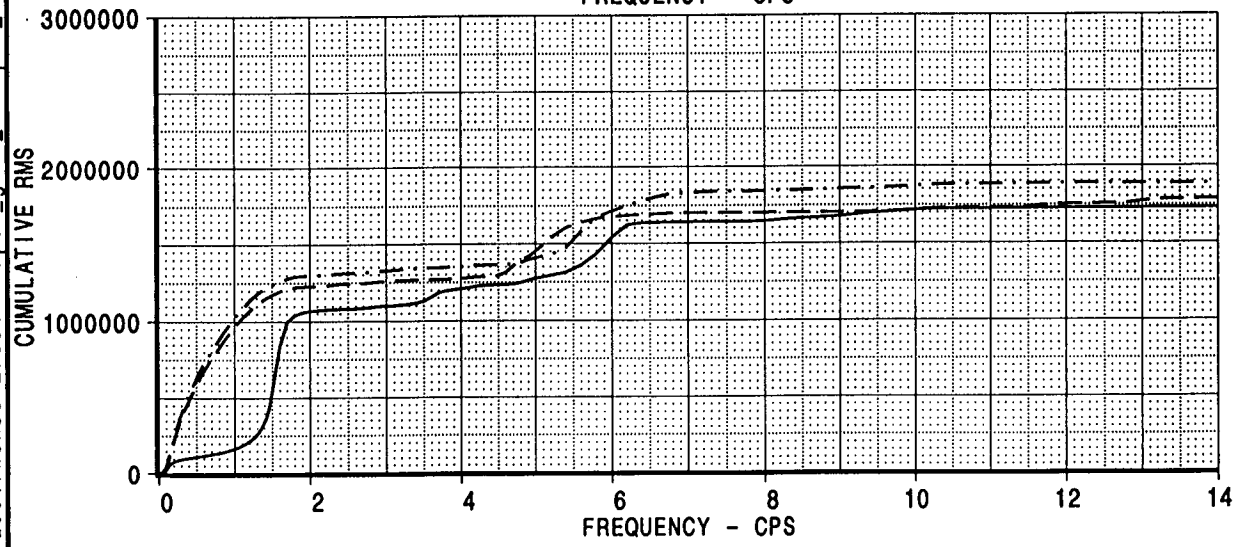

[A]: /acct/ksn8042/SOLVER/psd_gust_M1m2p40.esb
[B]: /acct/ksn8042/SOLVER/psd_gust_M1m2p40_fb.esb
[C]: /acct/ksn8042/SOLVER/psd_gust_M1m2p40_fb_v5.esb

CALC	K.S.NAGARAJA	23Jun99	REVISED	DATE	SYMMETRIC VERTICAL PSD GUST CASE	HSCT
CHECK					MODEL=MTSD MASS=M1 MACH=2.40 ALT=66K	FIG C.9
APPD.					COMPARISON OPEN VERSUS CLOSED LOOP	
APPD.					BOEING	PAGE 74

WING SHEAR ETA=.100

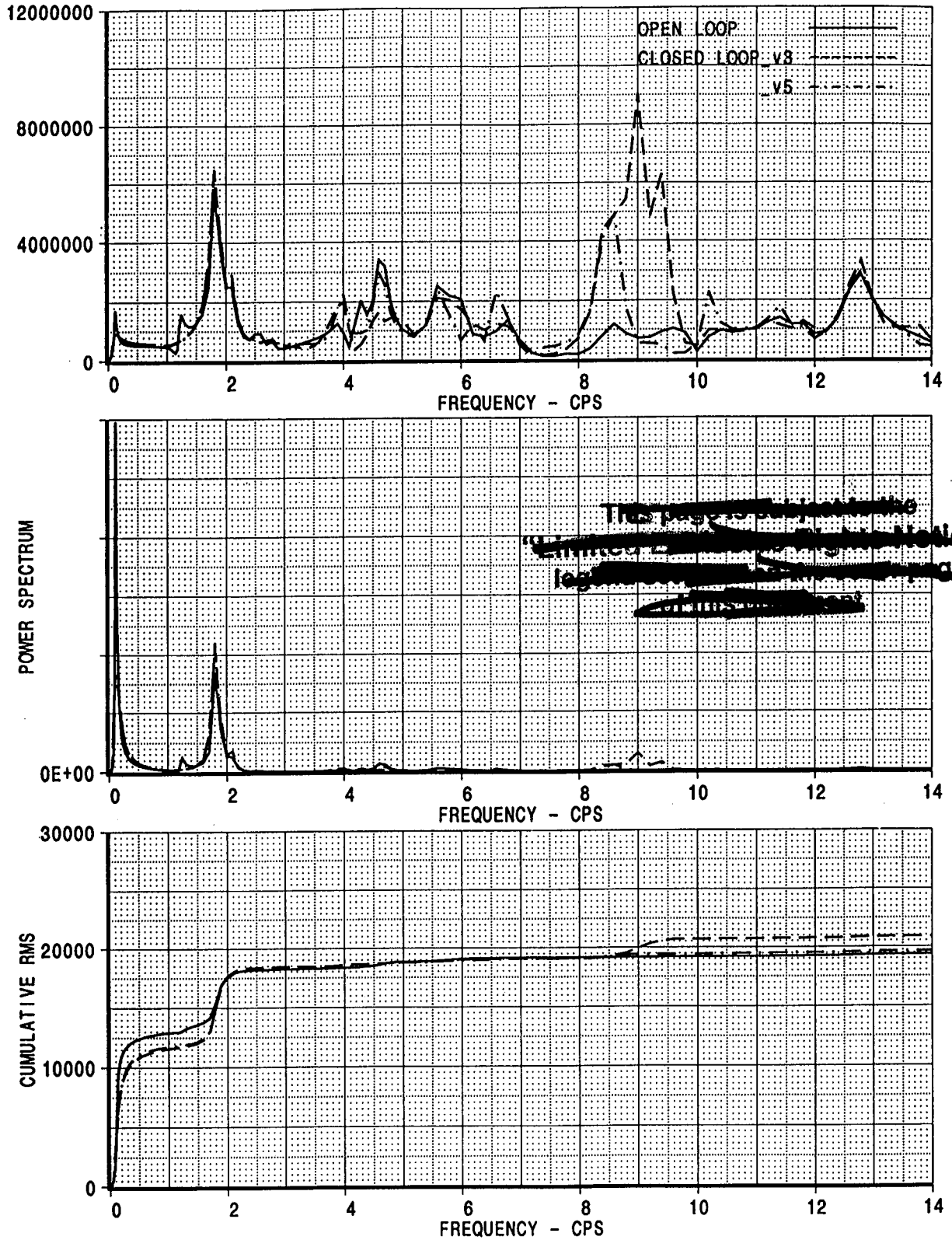

[A]: /acct/ksn8042/SOLVER/psd_gust_MT1m2p40.esb
[B]: /acct/ksn8042/SOLVER/psd_gust_MT1m2p40_fb.esb
[C]: /acct/ksn8042/SOLVER/psd_gust_MT1m2p40_fb_v5.esb

CALC	K.S.NAGARAJA	23Jun99	REVISED	DATE	SYMMETRIC VERTICAL PSD GUST CASE MODEL=MTSD MASS=MT1 MACH=2.40 ALT=66K COMPARISON OPEN VERSUS CLOSED LOOP	HSCT FIG C.10
CHECK						
APPD.						
APPD.					BOEING	PAGE 75

WING TORSION ETA=.100

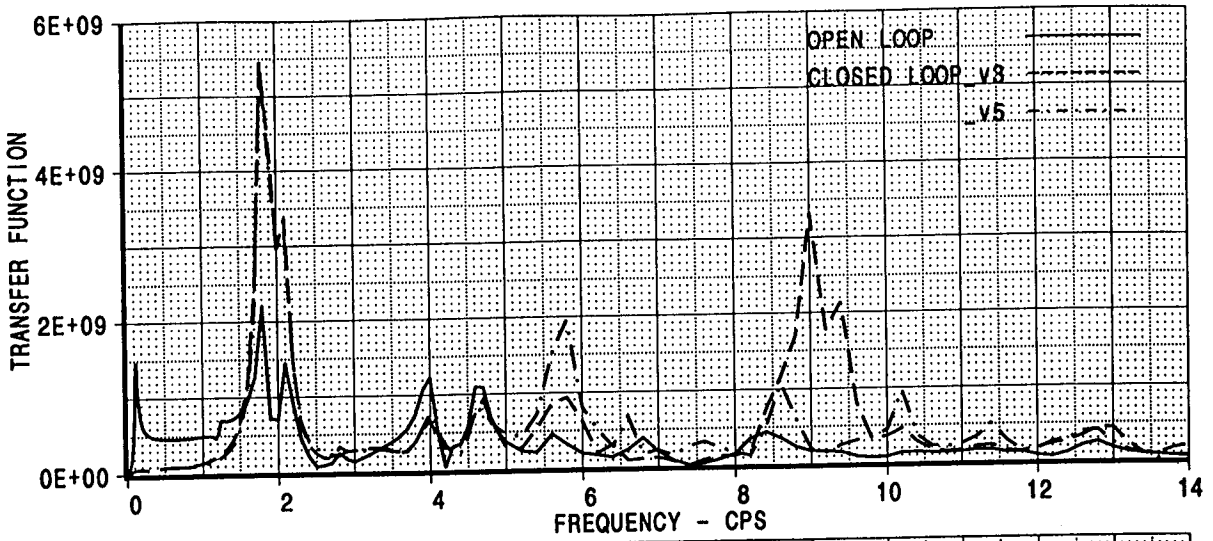

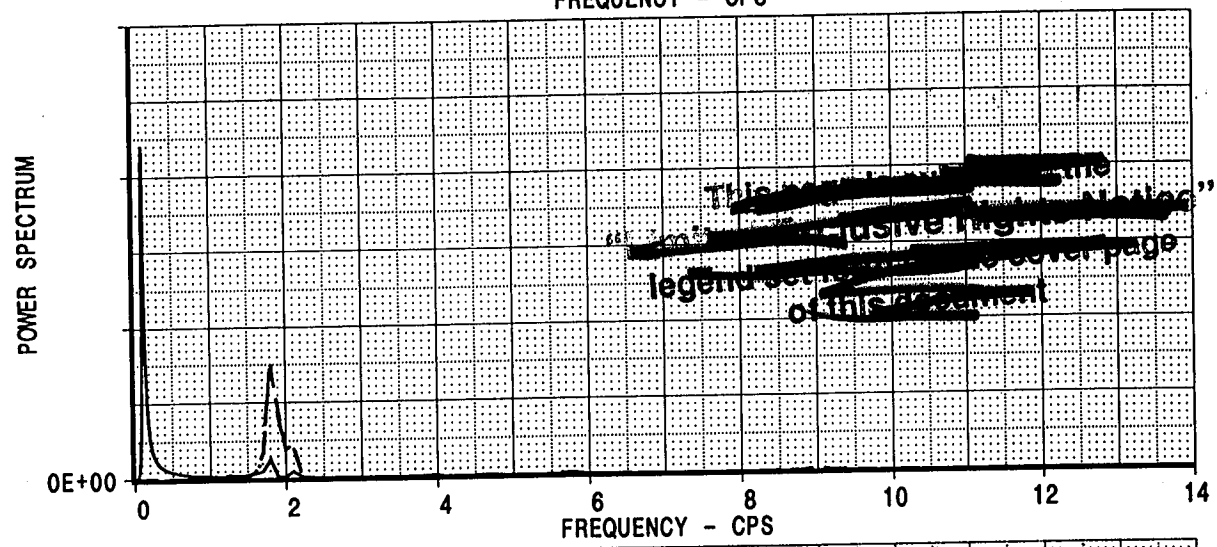

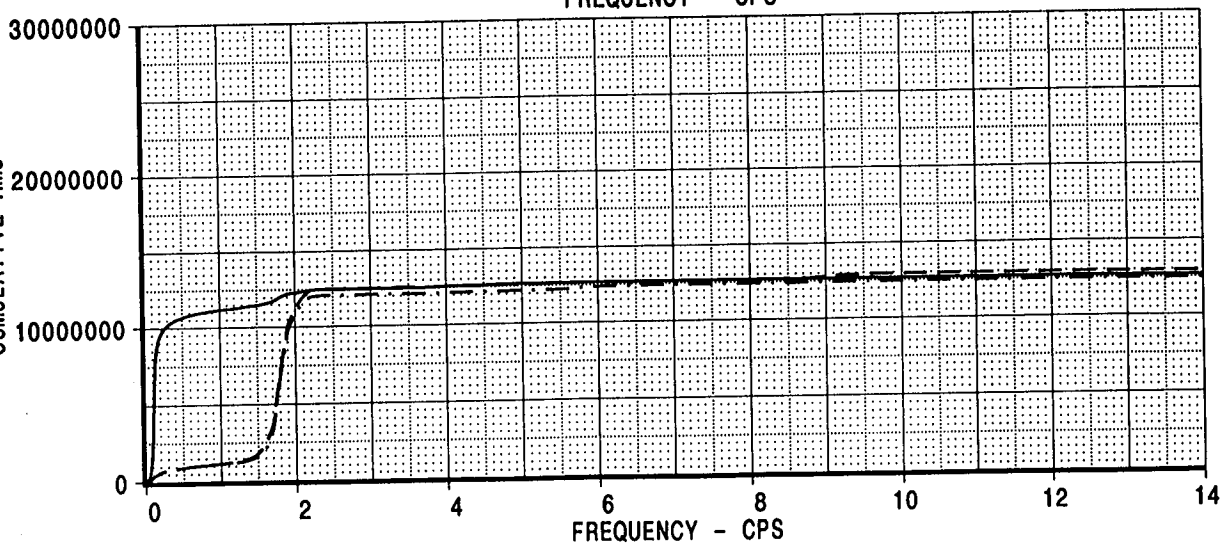

[A]: /acct/ksn8042/SOLVER/psd_gust_MT1m2p40.esb
[B]: /acct/ksn8042/SOLVER/psd_gust_MT1m2p40_fb.esb
[C]: /acct/ksn8042/SOLVER/psd_gust_MT1m2p40_fb_v5.esb

CALC	K.S.NAGARAJA	23Jun99	REVISED	DATE	SYMMETRIC VERTICAL PSD GUST CASE MODEL=MTSD MASS=MT1 MACH=2.40 ALT=66K COMPARISON OPEN VERSUS CLOSED LOOP	HSCT
CHECK						FIG C.11
APPD.						
APPD.					BOEING	PAGE 76

FUSELAGE MOMENT BS=650

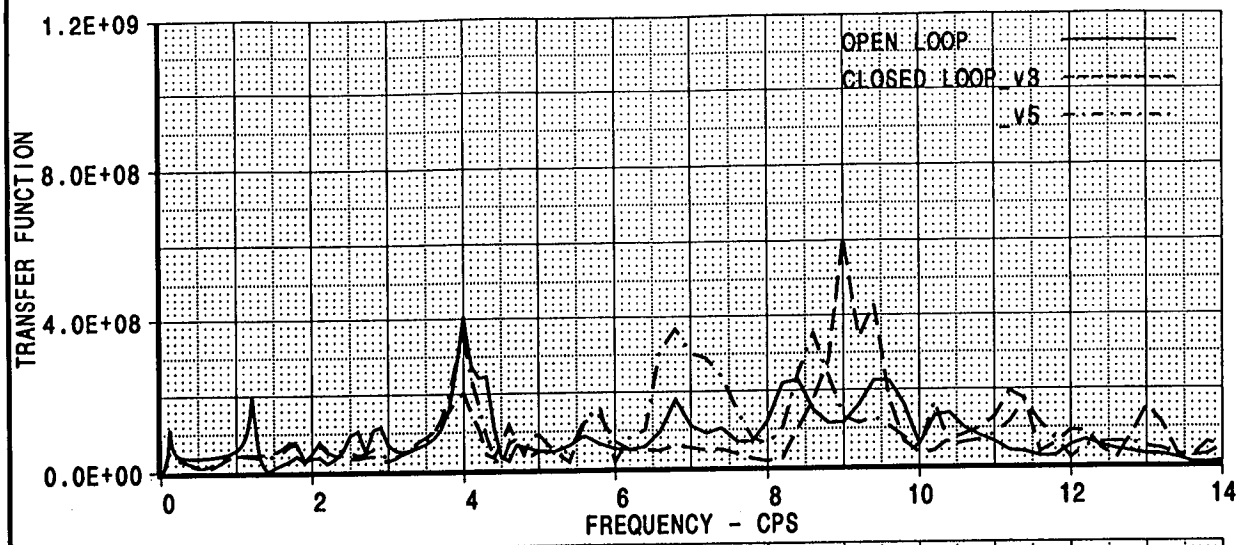

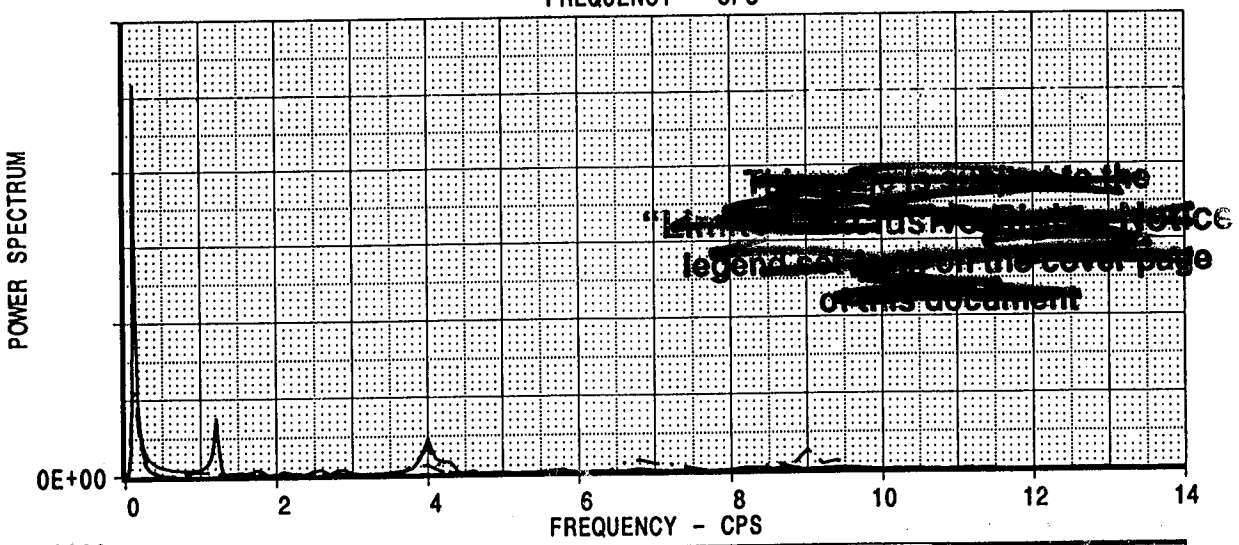

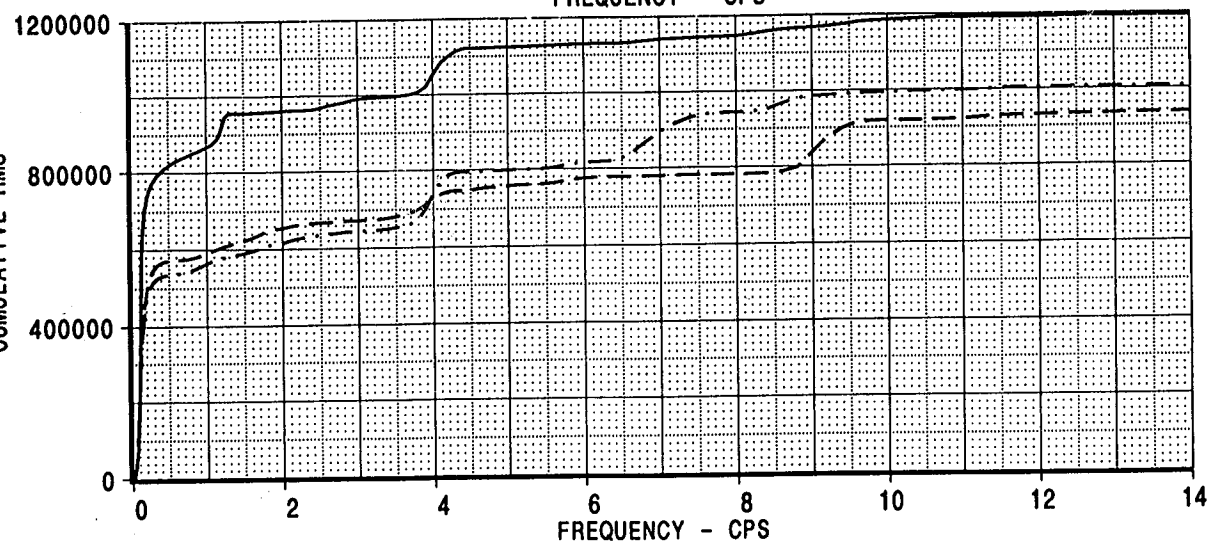

[A]: /acct/ksn8042/SOLVER/psd_gust_MT1m2p40.esb
[B]: /acct/ksn8042/SOLVER/psd_gust_MT1m2p40_fb.esb
[C]: /acct/ksn8042/SOLVER/psd_gust_MT1m2p40_fb_v5.esb

CALC	K.S.NAGARAJA	23Jun99	REVISED	DATE	SYMMETRIC VERTICAL PSD GUST CASE MODEL=MTSD MASS=MT1 MACH=2.40 ALT=66K COMPARISON OPEN VERSUS CLOSED LOOP	HSCT
CHECK						FIG C.12
APPD.						
APPD.					BOEING	PAGE 97